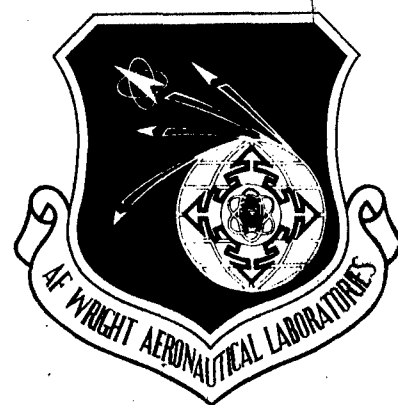


AFWL TR-84-4075

ADA149403

CHARACTERIZATION OF ACETYLENE- TERMINATED RESIN CURE STATES



**A. C. Lind
T. C. Sandreczki
R. L. Levy**

**McDonnell Douglas Research Laboratories
St. Louis, Missouri 63166**

**9 August 1984
Interim Report for Period March 1981 - May 1983**

Approved for public release; distribution unlimited

Best Available Copy

**MATERIALS LABORATORY
AIR FORCE WRIGHT AERONAUTICAL LABORATORIES
AIR FORCE SYSTEMS COMMAND
WRIGHT-PATTERSON AIR FORCE BASE, OHIO 45433**

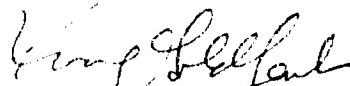
20040219041

NOTICE

When Government drawings, specifications, or other data are used for any purpose other than in connection with a definitely related Government procurement operation, the United States Government thereby incurs no responsibility nor any obligation whatsoever; and the fact that the government may have formulated, furnished, or in any way supplied the said drawings, specifications, or other data, is not to be regarded by implication or otherwise as in any manner licensing the holder or any other person or corporation, or conveying any rights or permission to manufacture use, or sell any patented invention that may in any way be related thereto.

This report has been reviewed by the Office of Public Affairs (ASD/PA) and is releasable to the National Technical Information Service (NTIS). At NTIS, it will be available to the general public, including foreign nations.

This technical report has been reviewed and is approved for publication.

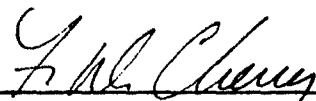


IVAN J. GOLDFARB
Project Scientist



R. L. VAN DEUSEN
Chief, Polymer Branch
Nonmetallic Materials Division

FOR THE COMMANDER



FRANKLIN D. CHERRY, Chief
Nonmetallic Materials Division

"If your address has changed, if you wish to be removed from our mailing list, or if the addressee is no longer employed by your organization please notify AFWAL/MEBP, W-PAFB, OH 45433 to help us maintain a current mailing list".

Copies of this report should not be returned unless return is required by security considerations, contractual obligations, or notice on a specific document.

UNCLASSIFIED

SECURITY CLASSIFICATION OF THIS PAGE

REPORT DOCUMENTATION PAGE

| | | | | | |
|--|-------|--|--|---|----------------------------------|
| 1a. REPORT SECURITY CLASSIFICATION UNCLASSIFIED | | | 1d. RESTRICTIVE MARKINGS | | |
| 2a. SECURITY CLASSIFICATION AUTHORITY | | | 3. DISTRIBUTION/AVAILABILITY OF REPORT Approved for public release; distribution unlimited | | |
| 2b. DECLASSIFICATION/DOWNGRADING SCHEDULE | | | | | |
| 4. PERFORMING ORGANIZATION REPORT NUMBER(S) MDC Q1212 | | | 5. MONITORING ORGANIZATION REPORT NUMBER(S) AFWAL-TR-84-4075 | | |
| 6a. NAME OF PERFORMING ORGANIZATION McDonnell Douglas Research Laboratories | | 6b. OFFICE SYMBOL (If applicable) | | 7a. NAME OF MONITORING ORGANIZATION AFWAL/MLBP | |
| 6c. ADDRESS (City, State and ZIP Code) P.O. Box 516 St. Louis, MO 63166 | | | 7b. ADDRESS (City, State and ZIP Code) Wright-Patterson Air Force Base, OH 45433 | | |
| 8a. NAME OF FUNDING/SPONSORING ORGANIZATION Department of the Air Force | | 8b. OFFICE SYMBOL (If applicable) | | 9. PROCUREMENT INSTRUMENT IDENTIFICATION NUMBER F33615-80-C-5170 | |
| 8c. ADDRESS (City, State and ZIP Code) Air Force Wright Aeronautical Laboratories Materials Laboratory Wright-Patterson Air Force Base, OH 45433 | | | 10. SOURCE OF FUNDING NOS. | | |
| 11. TITLE (Include Security Classification) CHARACTERIZATION OF ACETYLENE-TERMINATED RESIN CURE STATES | | | PROGRAM ELEMENT NO. 61102F | PROJECT NO. 2303 | TASK NO. Q3 |
| | | | WORK UNIT NO. 13 | | |
| 12. PERSONAL AUTHOR(S) Lind, Arthur C., Levy, Ram L., Sandreczki, Thomas C. | | | | | |
| 13a. TYPE OF REPORT Interim Technical | | 13b. TIME COVERED FROM 81 Mar to 83 May | | 14. DATE OF REPORT (Yr., Mo., Day) 09 August 1984 | |
| 15. PAGE COUNT 80 | | | | | |
| 16. SUPPLEMENTARY NOTATION | | | | | |
| 17. COSATI CODES | | | 18. SUBJECT TERMS (Continue on reverse if necessary and identify by block number) | | |
| FIELD | GROUP | SUB. GR. | | | |
| 11 | 01 | Adhesives | Acetylene-terminated sulfone | | |
| 11 | 04 | Composite | 4,4'-bis(3-ethynylphenoxy)diphenylsulfone | | |
| 19. ABSTRACT (Continue on reverse if necessary and identify by block number) | | | | | |
| <p>Acetylene-terminated oligomers are being considered for use in high-service-temperature adhesives and composites. It is thought that these resins cure via numerous pathways to produce different chemical structures such that the properties of the cured resin may be a strong function of the time-temperature cure schedule. Fourier transform infrared (FT-IR), nuclear magnetic resonance (NMR), and electron paramagnetic resonance (EPR) experiments were performed to characterize the cure states of 4,4'-bis(3-ethynylphenoxy)diphenylsulfone (ATS). Measurements were performed at selected times during isothermal cures at 403K, 423K, and 453K. Independent cure-state parameters were derived from IR absorbance changes, IR frequency shifts, ¹H NMR relaxation times, ¹³C NMR magic-angle spinning spectral areas, and EPR-determined concentrations of free radicals produced during polymerization. Preliminary postcure studies were performed.</p> | | | | | |
| 20. DISTRIBUTION/AVAILABILITY OF ABSTRACT UNCLASSIFIED/UNLIMITED <input checked="" type="checkbox"/> SAME AS RPT. <input type="checkbox"/> DTIC USERS <input type="checkbox"/> | | | 21. ABSTRACT SECURITY CLASSIFICATION Unclassified | | |
| 22a. NAME OF RESPONSIBLE INDIVIDUAL I. J. Goldfarb | | | 22b. TELEPHONE NUMBER (Include Area Code) 513-255-2340 | | 22c. OFFICE SYMBOL AFWAL/MLBP |

18. Subject Terms (continued)

Cure state

Reaction

Thermoset

Nuclear magnetic resonance

Electron paramagnetic resonance

Fourier-transform infrared

Polymerization

Free radical

Adhesive

Composite

FOREWORD

This Interim Technical Report covers work performed on Contract No. F33615-80-C-5170, Project No. 2303, entitled "Characterization of Acetylene Terminated Resin Cure States," during the period 3 March 1981 through 31 May 1983. This program is sponsored by the Air Force Aeronautical Laboratories, Materials Laboratory, Wright-Patterson Air Force Base, Ohio. Dr. Charles Lee is the Project Monitor. Personnel contributing to the program are Dr. Donald P. Ames, Program Manager, Dr. Arthur C. Lind, Principal Investigator, Dr. Ram L. Levy, Co-Investigator, and Dr. Thomas C. Sandreczki, Co-Investigator.

THIS DOCUMENT CONTAINED
BLANK PAGES THAT HAVE
BEEN DELETED

CONTENTS

| SECTION | PAGE |
|--|------|
| I INTRODUCTION | 1 |
| II EXPERIMENT | 2 |
| 1. MATERIAL AND CURE SCHEDULES | 2 |
| 2. SAMPLE PREPARATION | 2 |
| a. NMR Sample Preparation | 2 |
| b. EPR Sample Preparation | 3 |
| c. IR Sample Preparation | 4 |
| 3. SPECTROMETRIC TECHNIQUES | 5 |
| a. NMR Techniques | 5 |
| b. EPR Techniques | 6 |
| c. IR Techniques | 8 |
| III RESULTS | 10 |
| 1. ISOTHERMAL CURE RESULTS | 10 |
| a. NMR Isothermal Cure Results | 10 |
| b. EPR Isothermal Cure Results | 26 |
| c. IR Isothermal Cure Results | 36 |
| 2. POSTCURE | 51 |
| a. NMR Postcure Results | 51 |
| b. EPR Postcure Results | 54 |
| c. IR Postcure Results | 57 |
| IV CURE STATE PARAMETERS | 61 |
| 1. SELECTION OF SPECTROMETRIC CURE STATE PARAMETERS | 61 |
| 2. COMPARISON BETWEEN THE SPECTROMETRIC CURE STATE PARAMETERS AND THE MECHANICAL AND THERMAL PROPERTIES | 64 |
| V CONCLUSIONS | 71 |
| REFERENCES | 72 |

LIST OF ILLUSTRATIONS

| FIGURE | PAGE |
|--|------|
| 1. ^{13}C NMR Spectrum of Solid ATS Resin | 10 |
| 2. Low-Field ^{13}C NMR Resonance During 403 K (266°F) Cure | 12 |
| 3. Central-Field ^{13}C NMR Resonance During 403 K (266°F) Cure | 12 |
| 4. High-Field ^{13}C NMR Resonance During 403 K (266°F) Cure | 13 |
| 5. Low-Field ^{13}C NMR Resonance During 423 K (302°F) Cure | 13 |
| 6. Central-Field ^{13}C NMR Resonance During 423 K (302°F) Cure | 14 |
| 7. High-Field ^{13}C NMR Resonance During 423 K (302°F) Cure | 14 |
| 8. Low-Field ^{13}C NMR Resonance During 453 K (356°F) Cure | 15 |
| 9. Central Field ^{13}C NMR Resonance During 453 K (356°F) Cure | 15 |
| 10. High Field ^{13}C NMR Resonance During 453 K (356°F) Cure | 16 |
| 11. ^{13}C NMR Acetylene Intensity During Isothermal Cures | 17 |
| 12. Hydrogen ^1H NMR Free-Induction Decay Signal | 17 |
| 13. Gaussian Spin-Spin Relaxation Time During 403 K (266°F) Cure | 19 |
| 14. Gaussian Spin-Spin Relaxation Time During 423 K (302°F) Cure | 19 |
| 15. Gaussian Spin-Spin Relaxation Time During 453 K (356°F) Cure | 20 |
| 16. Spin-Lattice Relaxation Time During 403 K (266°F) Cure | 21 |
| 17. Spin-Lattice Relaxation Time During 423 K (302°F) Cure | 21 |
| 18. Spin-Lattice Relaxation Time During 453 K (356°F) Cure | 22 |
| 19. Change in Spin-Lattice Relaxation Time Caused by Aging in Air | 23 |
| 20. Spin-Lattice Relaxation Time Summary | 24 |
| 21. EPR Signal Intensities in Early Stages of Isothermal Cures | 28 |
| 22. EPR Signal Intensities During Isothermal Cures | 30 |
| 23. EPR Derivative Linewidths During Isothermal Cures | 32 |
| 24. EPR Derivative Linewidth During 453 K (356°F) Cure | 33 |
| 25. Change in EPR Signal Intensities of Solid Samples Caused by Aging in Air | 34 |
| 26. EPR Derivative Linewidth as a Function of EPR Signal Intensity | 35 |
| 27. Change in EPR Signal Intensity of a Powdered Sample Caused by Aging in Air | 36 |
| 28. Superimposed FT-IR Spectra of the 3295 cm^{-1} Acetylene-Band Region | 38 |
| 29. Superimposed FT-IR Spectra of the 941 cm^{-1} Acetylene-Band Region | 39 |

LIST OF ILLUSTRATIONS (Continued)

| FIGURE | PAGE |
|--|------|
| 30. Superimposed Difference FT-IR Spectra of the 400-1400 cm^{-1} Region | 40 |
| 31. Superimposed FT-IR Spectra of the 3295 cm^{-1} Acetylene-Band Region | 41 |
| 32. Superimposed FT-IR Spectra of the 550-750 cm^{-1} Region | 41 |
| 33. Superimposed FT-IR Spectra of the 750-950 cm^{-1} Region | 42 |
| 34. Schematic of Frequency-Shifted Band | 42 |
| 35. Frequency Shift of Aryl-Ether Band at 1250 cm^{-1} | 43 |
| 36. Frequency Shift of 1572 cm^{-1} Band | 43 |
| 37. Frequency Shift of 575 cm^{-1} Band | 44 |
| 38. IR-Band Ratios of Nonreactive Moieties During 403 K (266°F) Cure | 45 |
| 39. Superimposed FT-IR Spectra in the 2000-2400 cm^{-1} Region | 46 |
| 40. Superimposed Cumulative Difference FT-IR Spectra in the 2000-2400 cm^{-1} Region | 47 |
| 41. Superimposed Net Difference FT-IR Spectra in the 2000-2400 cm^{-1} Region | 47 |
| 42. Postulated Cure Reactions | 50 |
| 43. Degree of Cure Determined from the Average of 941 cm^{-1} and 3295 cm^{-1} IR Band Areas | 51 |
| 44. ^{13}C NMR Spectra of ATS Samples Cured at 423 K (302°F) and Postcured at Various Temperatuaries | 52 |
| 45. ^{13}C NMR Spectra of ATS Samples Cured at 453 K (356°F) and Postcured at Various Temperatures | 53 |
| 46. Radical Concentrations Before and After 523 K (482°F) Postcure | 54 |
| 47. Radical Concentrations Before and After 543 K (518°F) Postcure | 55 |
| 48. EPR Spectra During Curing and Postcuring | 56 |
| 49. Comparison of ^{13}C NMR and EPR Parameters | 62 |
| 50. Comparison of ^{13}C NMR and IR Parameters | 62 |
| 51. Comparison of EPR and IR Parameters | 63 |
| 52. Comparison of ^1H NMR and EPR Parameters | 63 |
| 53. Tensile Strength as a Function of ^{13}C NMR Parameter | 65 |
| 54. Tensile Strength as a Function of ^1H NMR Parameter | 65 |

LIST OF ILLUSTRATIONS (Continued)

| FIGURE | PAGE |
|--|------|
| 55. Tensile Strength as a Function of EPR Parameter | 66 |
| 56. Tensile Strength as a Function of IR Parameter | 66 |
| 57. Fracture Energy as a Function of ^{13}C NMR Parameter | 67 |
| 58. Fracture Energy as a Function of ^1H NMR Parameter | 67 |
| 59. Fracture Energy as a Function of EPR Parameter | 68 |
| 60. Fracture Energy as a Function of IR Parameter | 68 |
| 61. Glass Transition Temperatures as a Function of ^{13}C NMR Parameter | 69 |
| 62. Glass Transition Temperatures as a Function of ^1H NMR Parameter | 69 |
| 63. Glass Transition Temperatures as a Function of EPR Parameter | 70 |
| 64. Glass Transition Temperatures as a Function of IR Parameter | 70 |

LIST OF TABLES

| TABLE | PAGE |
|--|------|
| 1. Cure and Postcure Schedules | 3 |
| 2. Hydrogen ^1H NMR Measurements of Rockwell ATS Sample | 25 |
| 3. IR Band Areas for 403 K (266°F) Cure | 48 |
| 4. IR Band Areas for 423 K (302°F) Cure | 48 |
| 5. Comparison of DOC Values for 403 K (266°F) Cure | 49 |
| 6. Comparison of DOC Values for 453 K (356°F) Cure | 49 |
| 7. FT-IR Results of 453 K (356°F) Cure Followed by Postcures | 58 |
| 8. FT-IR Results of 423 K (320°F) Cure Followed by Postcures | 59 |
| 9. FT-IR 573 K (572°F) Postcure Results | 60 |

I. INTRODUCTION

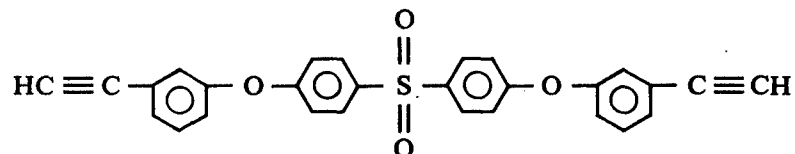
Acetylene terminated oligomers are being considered for use in high-service-temperature adhesives and composites.¹⁻² It is thought that these resins cure via numerous pathways² to produce different chemical structures such that the properties of the cured resin may be a strong function of the time-temperature schedule employed during curing. To better understand the acetylene terminated system, to enable the specification of appropriate cure schedules for achieving polymers with the desired properties, and to provide a means for assuring the quality of fabricated components containing these polymers, techniques are needed which use small samples to obtain accurate measurements of a set of parameters that uniquely determines the polymer properties. The objectives of this program are to

- (1) develop nuclear magnetic resonance (NMR), electron paramagnetic resonance (EPR), and Fourier-transform infrared (FT-IR) techniques for measuring parameters of acetylene-terminated sulfones (ATS) that have undergone a variety of cure schedules,
- (2) relate these parameters to the cure schedules, and
- (3) attempt a correlation of these parameters with the known mechanical properties.

II. EXPERIMENT

1. MATERIAL AND CURE SCHEDULES

The acetylene-terminated resin used in this study is based on the 4,4'-bis(3-ethynylphenoxy)diphenylsulfone (ATS) monomer. This ATS resin contains about 80% monomer and 20% higher-order oligomers having 95% meta configuration and 5% para configuration.³



The ATS resin was stored in a desiccator at 253 K (-4°F). Prior to curing, the samples were degassed (debulked) at 393 K (248°F) in vacuum for 15 min and backfilled with nitrogen. Isothermal curing measurements and postcure measurements were conducted in a nitrogen atmosphere.

Table 1 shows the isothermal and postcure temperature schedules used in this study. Spectral data for the isothermal cure studies were obtained at selected times during cures at 403 K (266°F), 423 K (302°F), and 453 K (356°F). Postcure spectral measurements were performed on samples that had been postcured for two hours at one of three different postcure temperatures, 523 K (482°F), 543 K (518°F), and 573 K (573°F), after incomplete cures at one of the three previously mentioned isothermal cure temperatures.

2. SAMPLE PREPARATION

a. NMR Sample Preparation

^{13}C NMR: Samples for carbon-13 nuclear magnetic resonance (^{13}C NMR) measurements were prepared and cured in silicone rubber molds. The inside dimensions of the molds were 0.71 cm (0.28 in.) diameter by 1.66 cm (0.655 in.) length with wall thickness of 0.11 cm (0.045 in.). A sample was prepared by adding ~ 1.3 g (0.04 oz) of ATS to a mold, inserting the mold into a tightly fitting hole in an aluminum block preheated to 393 K (248°F), outgassing at 393 K (248°F) for 15 min in a vacuum oven, and backflushing the sample with cool nitrogen gas during rapid (< 1 min) cooling to room temperature.

Sample curing was similarly performed in the silicone rubber mold. The mold containing the sample was inserted into a nitrogen-purged preheated

TABLE 1.
CURE AND POSTURE SCHEDULES

| Cure conditions | | Postcure conditions | | | |
|-------------------------|---|---------------------|----------------------------|----------------------------|----------------------------|
| Temperature [K (°F)] | Time (min) | No postcure | 2 h at 523 K (482°F) | 2 h at 543 K (518°F) | 2 h at 573 K (572°F) |
| 403 (266) | Selected times between 0 and 20 000 | X | | | |
| | 180 | X | X | X | X |
| | 420 | X | X | X | X |
| | 2300 | X | X | X | X |
| 423 (302) | Selected times between 0 and 2000 | X | | | |
| | 75 | X | X | X | X |
| | 170 | X | X | X | X |
| | 320 | X | X | X | X |
| 453 (356) | Selected times between 0 and 200 | X | | | |
| | 0 | X | X | X | X |
| | 20 | X | X | X | X |
| | 55 | X | X | X | X |

aluminum block in a well-regulated forced-air oven. After the appropriate cure or postcure time, the mold was removed from the aluminum block and flushed with nitrogen gas to cause rapid (< 1 min) sample cooling. These samples were stored in stoppered glass vials in a freezer at 253 K (-4°F) when not being measured in the ^{13}C NMR spectrometer.

^1H NMR: Samples for hydrogen nuclear magnetic resonance (^1H NMR) measurements were prepared in sealed glass tubes. About 0.1 gm (0.003 oz) of ATS was placed in a 5-mm-o.d. (0.20-in.-o.d.) Pyrex NMR tube. The sample was vacuum degassed at 393 K (248°C) for 15 min, backfilled with dry nitrogen, and sealed. Isothermal cures and postcures of these samples were achieved by placing these tubes into oil-filled wells in preheated aluminum blocks for appropriate times. The low thermal mass of these samples permitted rapid heating and cooling. The samples were stored in a freezer at 253 K (-4°F) when not being measured in the ^1H NMR spectrometer.

b. EPR Sample Preparation

ATS resin received from AFML was stored in a desiccator at 253 K (-4°F). Samples were prepared by warming the material to ambient temperature,

pulverizing the desired quantity, and placing the powder in 5-mm-o.d. Pyrex sample tubes. The samples were degassed for 15 min at 393 K (248°F), back-filled with nitrogen gas, and sealed. They were stored at 253 K (-4°F) until used in EPR experiments.

The samples were cured isothermally at 403 K (266°F), 423 K (302°F), or 453 K (356°F) by placing them in an aluminum block containing ~ 6 mm holes filled with silicone oil. The block was brought to cure temperature prior to sample insertion and was maintained at cure temperature in a calibrated, forced convection oven. Samples came to within 1 K of the cure temperature within 1 min using this system. Thermal lag effects were also minimized by using a series of two or three samples for each isothermal cure experiment. In this way, each sample could be removed from the oven fewer times during its cure cycle, thus minimizing the time spent during heat-up and cool-down.

For the postcuring experiments, samples were heated in a copper tube through which a gentle stream of nitrogen purge gas flowed. In this way, sample tube breakage from thermal expansion of the ATS did not result in exposure of the sample to air at the postcure temperature. Following post-curing the copper tube was cooled to ambient temperature prior to sample removal. The sample was then placed in a new EPR sample tube, degassed, backfilled with nitrogen, and sealed.

The samples were rapidly brought to the postcure temperature by the above technique, because the copper tube was heated prior to sample insertion and was not cooled until postcuring was completed.

c. IR Sample Preparation

ATS specimens suitable for sequential curing and recording of FT-IR spectra after each cure interval were prepared by two different methods: the thin-film KBr plate method and the bulk-cure KBr pellet method.

A thin ATS resin film was deposited between two KBr plates, by heating the plates to 90-100°C and allowing 2 mg of resin to melt onto one of the plates, the perimeter of which contained strips of 0.13-mm shim metal spacer. Placing the second KBr plate over the first and securing them with clamps produced a uniform film of ATS resin having a spectrum with absorbance of less than 1.35 for the strong 1249 cm^{-1} IR band. Thin-film specimens were then cured in a nitrogen atmosphere while confined between the KBr plates. A relatively thick ATS film (0.4 mm) positioned between two KBr plates was prepared in a similar

manner to permit recording of FT-IR spectra in the 1900-2500 cm^{-1} spectral region where very weak acetylene bands appear.

Since the thin-film method is not compatible with recording of IR spectra of cured specimens of different geometries, the KBr pellet method was developed for IR studies of bulk specimens. Bulk specimens weighing about 0.5 g were isothermally cured in nitrogen-purged test tubes inserted into oil-filled wells in a preheated aluminum block as described in Section 2a. The test tube was removed from the heated block after each cure interval and allowed to cool to room temperature. Then 5-15 mg of resin were removed from the bulk for preparation of KBr pellets (discs) following standard procedures.⁴

Specimens for IR study of the effect of post-cure heating were of the same origin as the ones used for NMR measurements. Their preparation is described in Section 2a.

3. SPECTROMETRIC TECHNIQUES

a. NMR Techniques

^{13}C NMR: Solid state ^{13}C NMR spectra of the ATS resins were obtained on a JEOL FX60QS spectrometer operating at 15 MHz using magic-angle spinning⁵ with cross-polarization and high-power decoupling.⁶ The magic-angle spinner bodies were fabricated from Kel-F; as a result they produced no ^{13}C spectral lines that would interfere with those of the samples. The spinner was usually spun at a rate of 2.4 kHz, which was sufficient to reduce the area beneath the sideband peaks to less than 5%. The cross-polarization was accomplished using a Hartmann-Hahn double resonance at approximately 50 kHz. Cross-polarization contact times between 1 and 10 ms were investigated, and 4 ms was found to be optimum. The high-power hydrogen decoupling field was 1.2 mT. Usually, the samples from 3000 pulse sequences were averaged before Fourier transforming the data to obtain the spectra.

The solid-state ^{13}C NMR spectra of the ATS resin consisted of three well-resolved lines whose assignments were determined by comparison with solution spectra of the uncured ATS resin⁷ (which consisted of 12 well-resolved lines). The low-field line is assigned to the aryl carbons adjacent to the oxygens, the high-field line to the acetylenic carbons, and the mid-field line to the remaining aryl carbons. Parameters were derived from these spectra by measuring the areas beneath the lines at various stages of cure or by measuring the areas beneath the lines in the difference spectra obtained by subtracting

spectra at different stages of cure, as had been done in a study of acetylene-terminated polyimide resins.⁸

¹H NMR: The pulsed ¹H NMR measurements were performed on a MDRL-designed, single-coil spectrometer operating at 100 MHz. An external fluorine lock sample at 94 MHz was used to control the magnet (Varian V-4014) so that small signals could be signal averaged for a long time without attendant drift. The 100-MHz and 94-MHz rf signals were derived from a frequency synthesizer (Hewlett Packard HP5100), and the 8 mT pulsed rf magnetic field was generated using a programmable digital pulser and a 100-W linear amplifier (Electronic Navigation Industries 3100L). The dead time of the receiver was < 6 μ s. A transient recorder (Biomation 826) in conjunction with a signal averager (Nicolet 1070) was used to acquire and store the signals, and a computer (Digital Equipment PDP-8) was used to analyze the signals.

Two different types of pulsed ¹H NMR experiments were performed:

- (1) a single 90° pulse experiment to determine the relative amounts of rigid and mobile phases and their spin-spin relaxation times T_2 , and
- (2) a 180°, τ , 90° pulse experiment to determine the spin-lattice relaxation times T_1 .

b. EPR Techniques

EPR spectra were recorded at selected times during the curing reaction using a Varian E-102 Century series EPR spectrometer interfaced with the Varian E-900 data acquisition system. The latter enabled signal averaging and spectral scaling, integration, subtraction, and simulation.

Free radical concentrations were determined by comparing the ATS signal with that of a reference sample. In one series of experiments, the ATS samples were cured in 4-mm-o.d. sample tubes which were then inserted into a 5-mm-o.d. tube containing a reference composed of a polyurethane doped with the free radical di-tert-butylnitroxide (DBNO). The observed spectrum from this sample/reference combination was a superposition of the separate ATS and DBNO spectra. Using the data manipulation software, the DBNO and ATS spectra were separated and integrated to yield their relative intensities. This method had the advantage that the relative intensities of the ATS and reference signals were not affected by small changes in spectrometer parameters such as microwave cavity Q and sensitivity. A disadvantage, however, was that

the relative intensities depended upon reproducible placement of the sample and reference in the cavity. This was normally not a problem unless the position of the Dewar cavity insert was changed.

Because of the above difficulty, a second technique was also employed for determining radical concentration. Instead placing both samples in the cavity together, we observed the sample and reference separately. Any variations in spectrometer parameters were minimized by recording the reference spectrum along with each sample or group of samples observed within a short time period ($\lesssim 30$ min). Reproducible placement of sample and reference was achieved by using long samples that extended from the bottom of the cavity to beyond the top of the cavity where the microwave intensities were small. The samples were about 5 cm long.

The reference used in this method was a strong pitch sample having a Lorentzian line shape and a radical concentration of 2.46×10^{15} spins per cm length.

Spectral intensities were calculated either by direct numerical integration or by using the expression:

$$I \propto hw^2 \quad (1)$$

when comparing spectra having the same line shapes. In this expression I is the integrated intensity, h is the peak-to-peak amplitude of the recorded derivative spectrum, and w is the peak-to-peak linewidth.

When performing direct integration, error in signal intensity due to improper signal phasing is potentially present. Incorrect phasing occurred because the spectrometer was operated at low power to avoid saturation and distortion of the ATS signal (ATS saturated easily). At these low power levels, the spectra contained small amounts of dispersion signals and slightly reduced absorption signals. The integral of the former did not contribute to the integrated signal intensity, so that the overall intensity of the incorrectly phased EPR signal was reduced accordingly. It was to avoid the difficulties of direct integration that the integration procedure using Equation (1) was employed.

In Equation (1) it is essential for the spectra being compared to have the same spectral line shapes. Thus, two Lorentzian or two Gaussian lines can be compared, but a Lorentzian and a Gaussian line cannot be compared with each

other. For example, if the intensities of a Lorentzian line and a Gaussian line having the same h and w (and I) values were determined by direct integration, the true integrated intensity of the Lorentzian would be a factor of 3.5 times greater than that of the Gaussian. The ATS lineshapes corresponding to $> 20\%$ cure are approximately Gaussian in shape. Since the strong pitch produced a Lorentzian signal it was not possible to determine the intensity of ATS relative to the reference simply by comparing the values of I calculated using Equation (1). Instead, these values of I were compared to intensities obtained by direct integration of the reference and selected ATS spectra having very little dispersion signal content. In this manner, the I values for the reference lineshape and ATS lineshapes were calibrated using their true intensity values, enabling Equation (1) to be used for the remaining ATS samples.

c. IR Techniques

The transmission IR spectra of ATS specimens were obtained either on a Digilab FTS-20V FT-IR spectrometer or on a Nicolet 7199 spectrometer. Both spectrometers yielded identical spectra for a given specimen and, therefore, the spectra obtained were interchangeable. Nevertheless, any sequence of spectra resulting from a particular series of experiments were recorded on the same spectrometer. Approximately 75% of the spectra were recorded on the Digilab FTS-20V spectrometer.

The raw single beam spectra from both instruments were recorded in digital form on a magnetic tape using a Kennedy Model 9700 recorder and transferred to a CDC Cyber mainframe computer for interactive processing via a Tektronix 4010 CRT terminal. The software for extensive off-line processing of spectral data on a mainframe computer was developed at MDRL. Spectra were recorded either at 300 scans (signal averaged) at a resolution of 1 cm^{-1} or 100 scans at a resolution of 2 cm^{-1} . For determination of band areas or band intensities, both conditions yielded the same results. However, for measurement of small cure-induced frequency shifts, spectra obtained from 300 scans at a resolution of 1 cm^{-1} produced greater accuracy and were therefore used. Transmission spectra were recorded at room temperature before curing and after each isothermal cure or postcure stage of a given curing sequence.

Difference spectroscopy was used because it is a sensitive method for detecting and measuring minor cure-induced changes in polymers. Difference

spectra, providing net changes in ATS after curing for a given increment of time, were obtained by digital absorbance subtraction as follows:

$$\Delta A(\nu) = A_2(\nu) - kA_1(\nu) \quad (2)$$

where $\Delta A(\nu)$ is the net absorbance change at frequency ν , k is an adjustable scaling factor to correct for changes in the thickness of the specimen, and $A_2(\nu)$ and $A_1(\nu)$ are the absorbances of the ATS specimen at frequency ν for the two different cure states. The difference spectrum consists of a plot of $\Delta A(\nu)$ as a function of the frequency ν .

III. RESULTS

1. ISOTHERMAL CURE RESULTS

a. NMR Isothermal Results

¹³C NMR: Figure 1 shows the ¹³C NMR spectrum of solid, uncured, debulked ATS resin. This spectrum was obtained using a cross-polarization contact time of 4 ms. Also shown in Figure 1 is the structure of the ATS monomer along with the spectral assignments that were obtained from solution ¹³C NMR spectra.⁷ The solution spectra are well resolved because the molecular motion present in the liquid averages conformational chemical shifts so that single sharp spectral lines occur for nonequivalent carbons. In the solid spectra these conformational differences are not averaged, and broad spectral lines result. Because this sample contains higher order oligomers, there are a larger number of nonequivalent carbons than in a pure monomer and additional spectral broadening occurs.

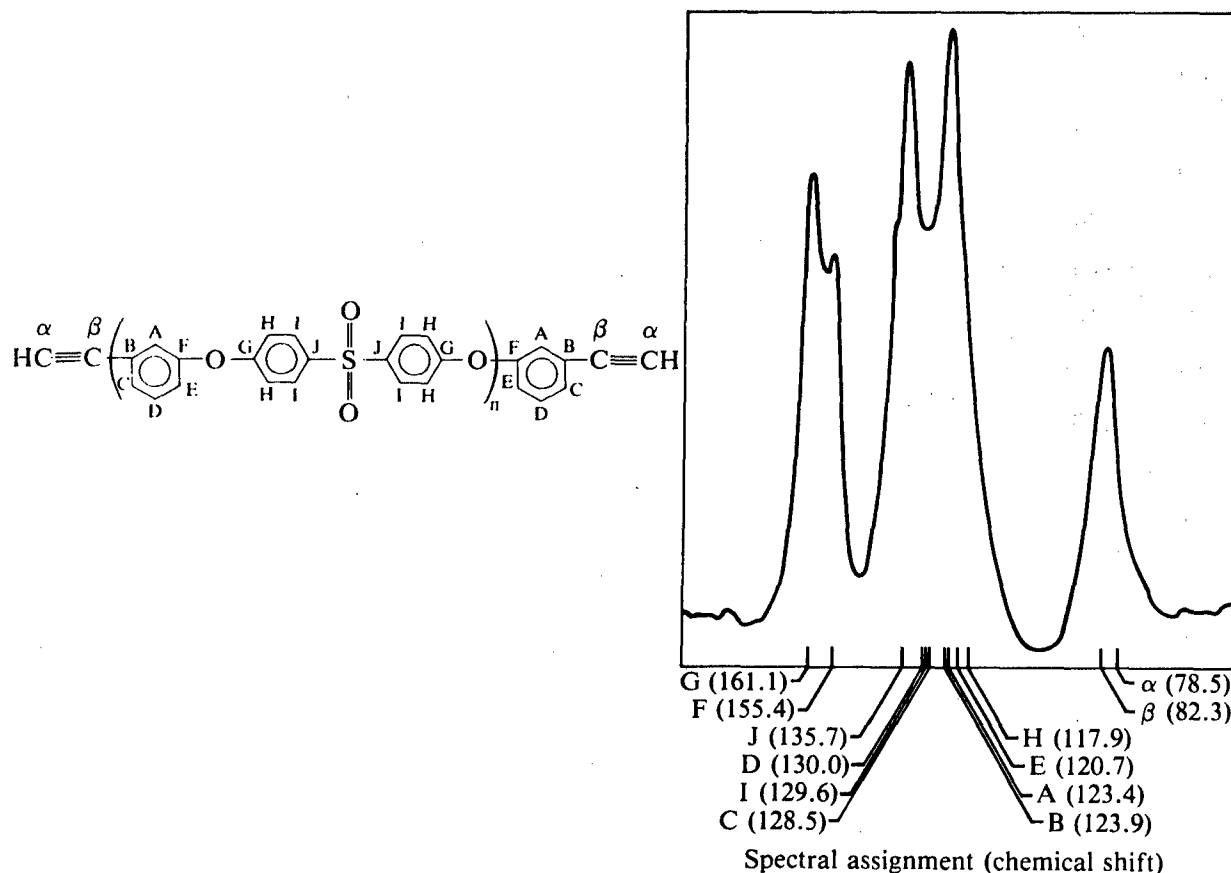


Figure 1. ¹³C NMR spectrum of solid, uncured, debulked ATS resin, whose structure is shown in the inset. The chemical shifts of the spectral lines observed in the ¹³C NMR spectrum of the resin dissolved in CDCl₃ are shown along with the spectral assignments.

^{13}C NMR spectra of the type shown in Figure 1 were obtained on ATS samples in various stages of cure. The spectra were analyzed by two procedures:

- (1) subtracting spectra obtained from samples at different stages of cure, and
- (2) obtaining the areas beneath the three well-resolved resonance peaks and expressing the three areas as a fraction of the total area beneath all three peaks.

While the first procedure yielded difference spectra that characterized the changes taking place during curing, the second procedure generated more useful cure-state parameters. The reason is that the second procedure required only a single spectrum of the ATS sample being characterized, while the first procedure required a reference spectrum whose amplitude and chemical shift had to be manually adjusted to obtain valid difference spectra. The amplitude adjustment corrected for gain changes and differences in sample size, while the chemical shift adjustment corrected for shifts caused by spectrometer drift or slight sample position changes in the magnet. While these adjustments could be performed in an objective manner for research applications, they were not suited to routine measurement of cure-state parameters. Therefore, only area ratios were measured in this study.

At selected times during the isothermal cures, the samples were removed from the oven; and ^{13}C NMR spectra were obtained at room temperature for two different cross-polarization contact times, 1 and 4 ms. From these spectra, the fractional areas beneath the three well-resolved peaks were determined. The results (Figures 2-10) show that cure occurs faster at higher temperatures and that there are three significant similarities at all three cure temperatures.

First, the fractional area beneath the low-field peak (aryl carbons adjacent to the oxygens) increases with increasing contact time, while the fractional area beneath the central peak (remaining aryl carbons) decreases with increasing contact time, and the fractional area beneath the high-field peak (acetylenic carbons) is insensitive to increasing contact time. During the contact time, spin polarization is resonantly coupled from ^1H nuclei to ^{13}C nuclei; spin polarization is also lost due to a number of relaxation processes. Thus, the optimum contact time for ^{13}C nuclei is different for

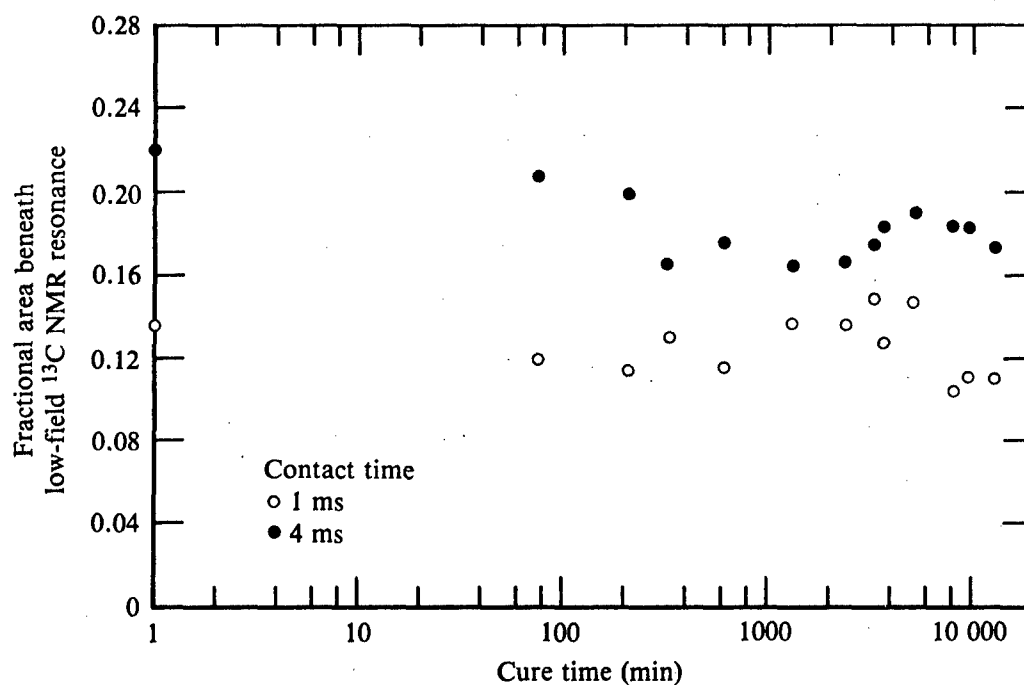


Figure 2. Fractional area beneath low-field ^{13}C NMR resonance during ATS cure at 403 K (266°F) for two different contact times.

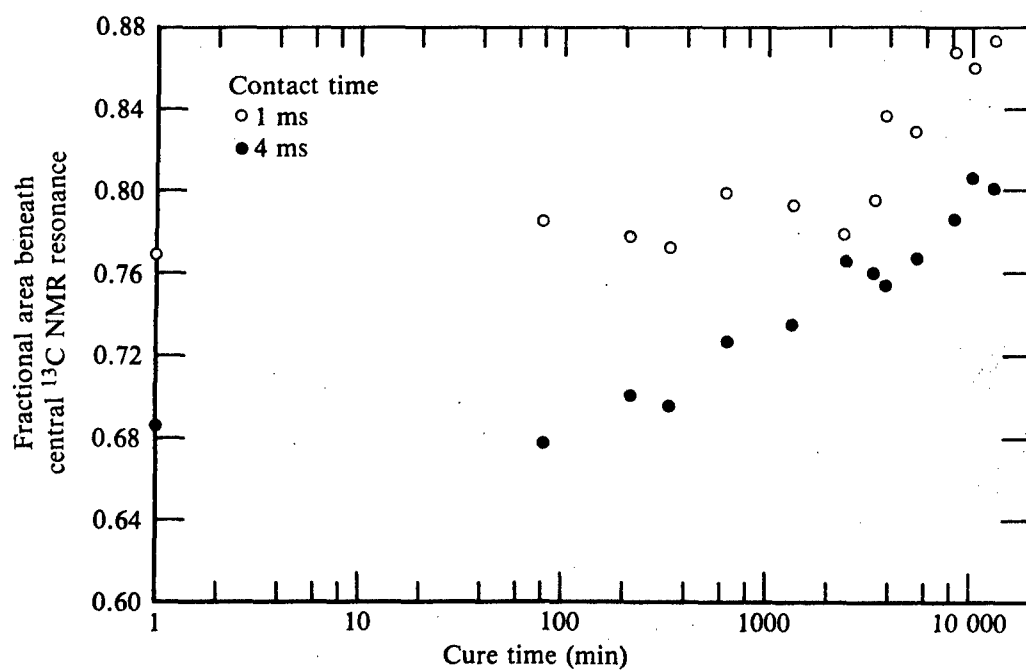


Figure 3. Fractional area beneath central-field ^{13}C NMR resonance during ATS cure at 403 K (266°F) for two different contact times.

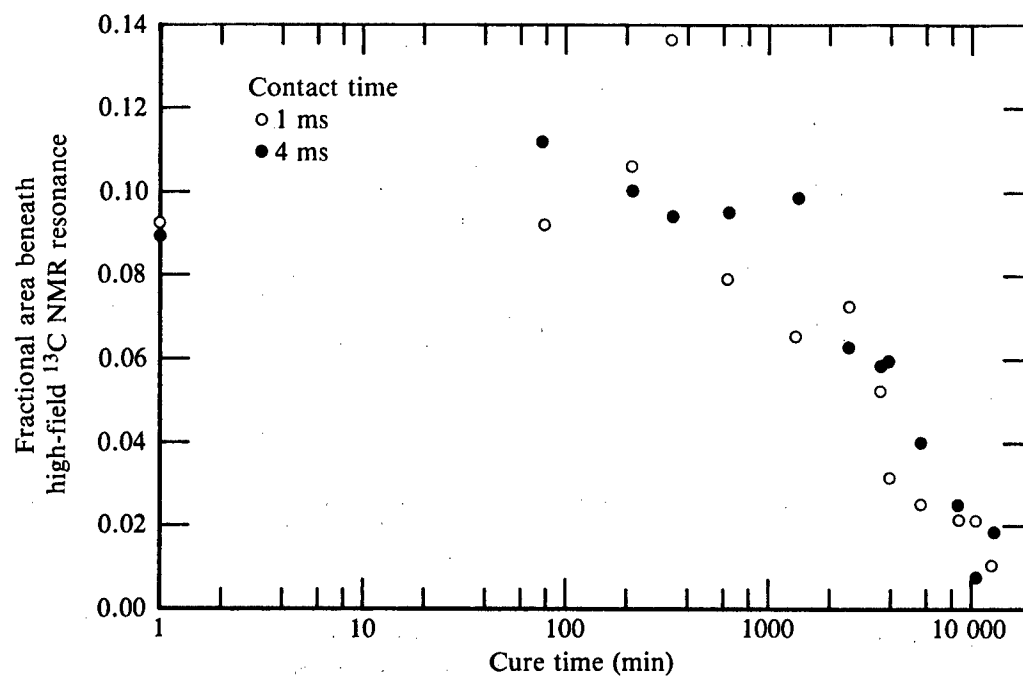


Figure 4. Fractional area beneath high-field ^{13}C NMR resonance ($-\text{C}=\text{CH}$) during ATS cure at 403 K (266°F) for two different contact times.

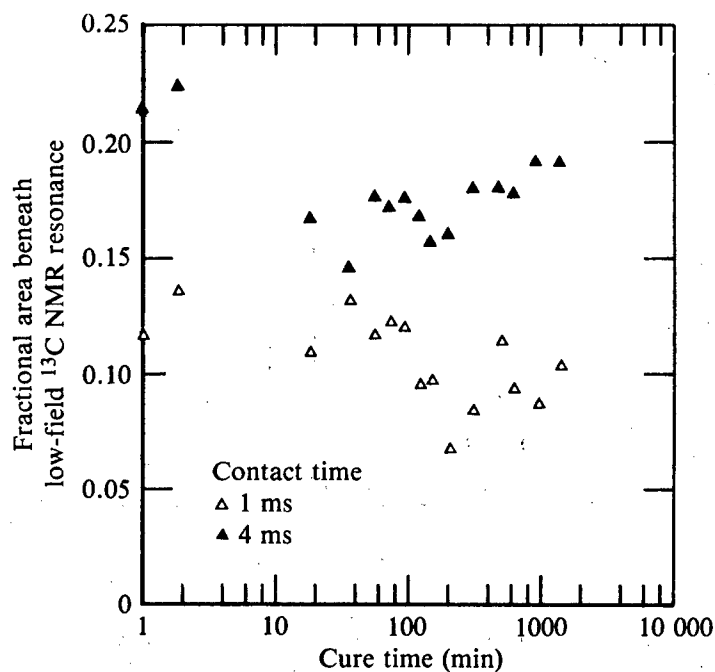


Figure 5. Fractional area beneath low-field ^{13}C NMR resonance as a function of ATS cure time at 423 K (302°F) for two different contact times.

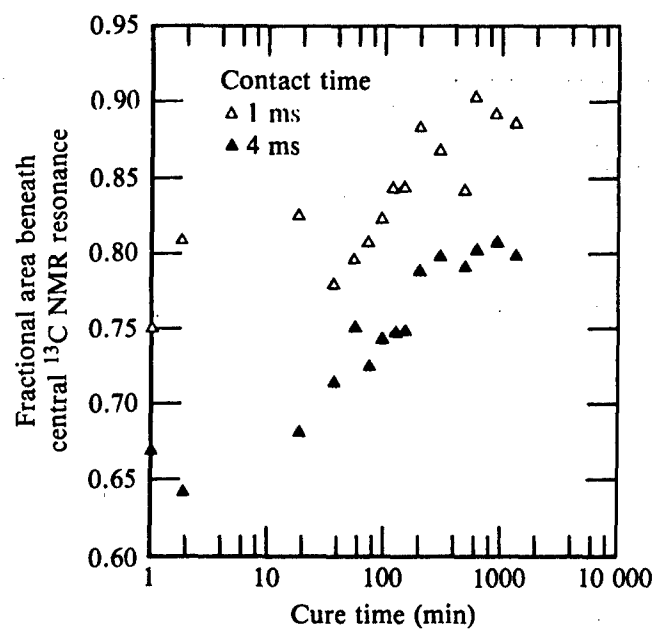


Figure 6. Fractional area beneath central-field ^{13}C NMR resonance as a function of ATS cure time at 423 K (302°F) for two different contact times.

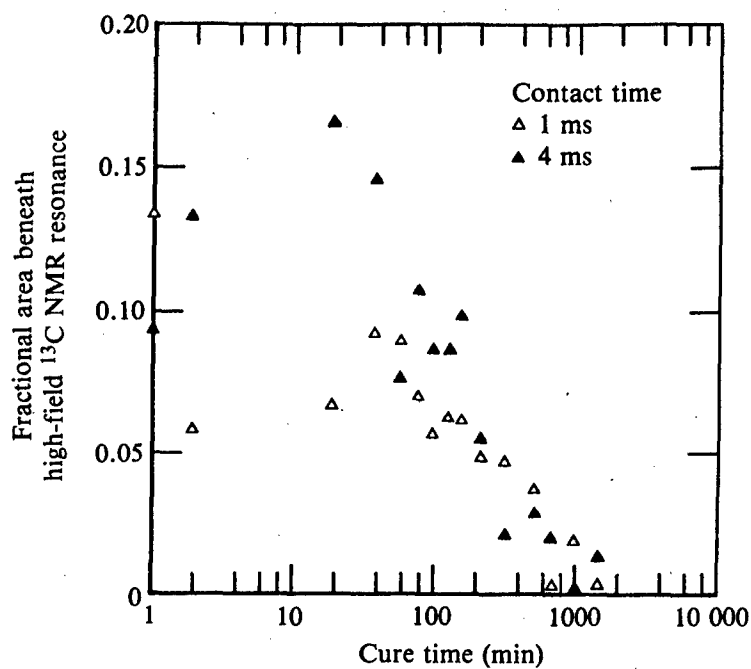


Figure 7. Fractional area beneath high-field ^{13}C NMR resonance ($-\text{C}\equiv\text{CH}$) as a function of ATS cure time at 423 K (302°F) for two different contact times.

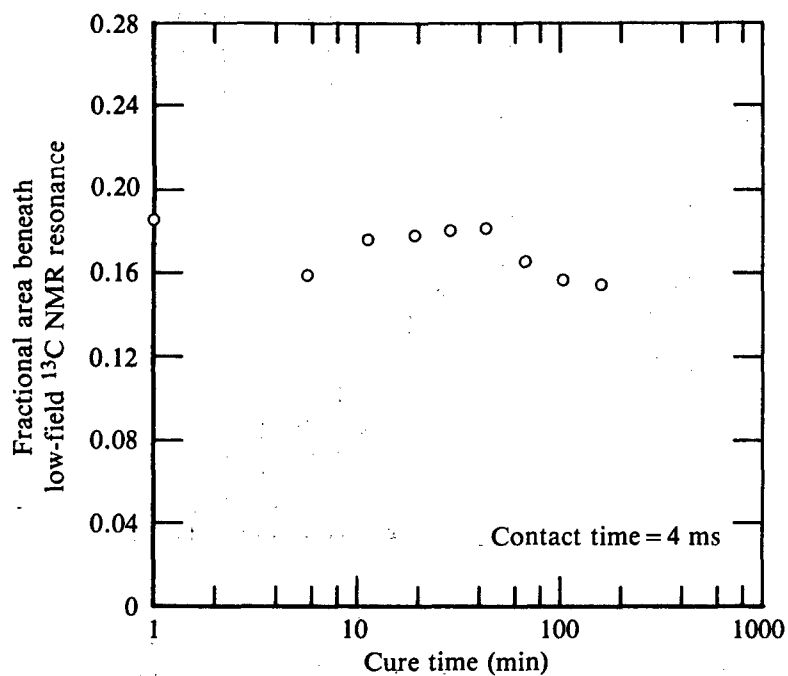


Figure 8. Fractional area beneath low-field ^{13}C NMR resonance during ATS cure at 453 K (356°F).

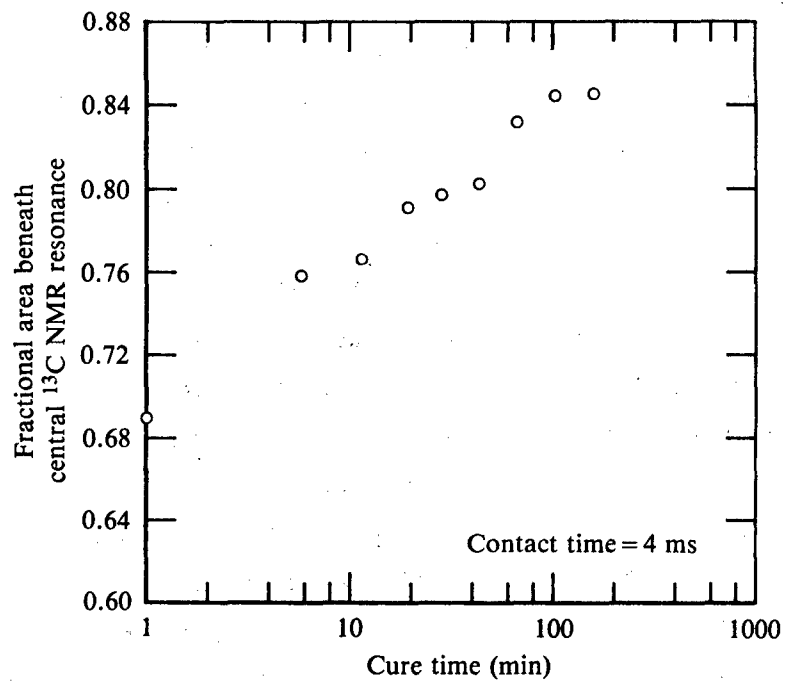


Figure 9. Fractional area beneath central-field ^{13}C NMR resonance during ATS cure at 453 K (356°F).

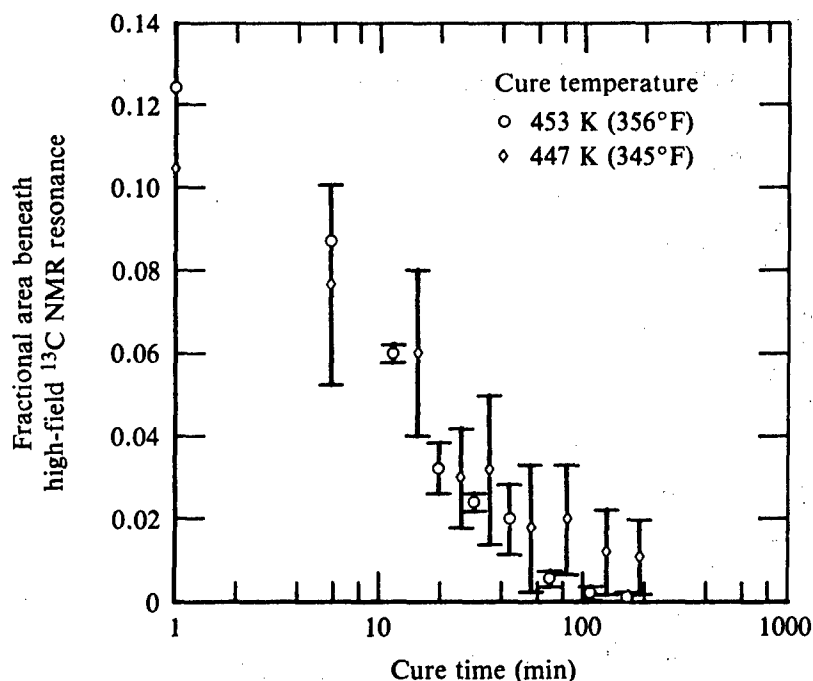


Figure 10. Fractional area beneath the high-field ^{13}C NMR resonance ($-\text{C}\equiv\text{CH}$) during ATS cure at 453 K (356°F) and 477 K (345°F). Error bars were obtained from the differences between data for 1 and 4 ms contact times.

different nuclear environments, and one contact time had to be chosen. Measurements taken at shorter and longer contact times showed that at 4 ms the results were relatively insensitive to small changes in contact time, so this contact time produced the most reliable results. Fortunately the acetylenic carbon resonance was insensitive to contact time changes.

Second, the fractional area beneath the low-field peak does not change significantly during the cure, indicating the number of aryl carbons adjacent to oxygens neither increases nor decreases during cure.

Third, the fractional area beneath the central-field peak increases while the fractional area beneath the high-field peak decreases during cure. This suggests that acetylenic carbons are reacting to form a conjugated polyene having either a linear or trisubstituted benzene structure.

Upon reviewing the data shown in Figures 2-10, the area beneath the acetylene (high-field) ^{13}C NMR resonance was found to be the most suitable for a cure-state parameter. It was not as dependent upon contact time as were the areas beneath the other two resonances, and it experienced the greatest change during curing. It also has the advantage of being approximately proportional to the number of unreacted acetylene groups in the sample. This cure-state parameter is plotted in Figure 11 for the three isothermal cures.

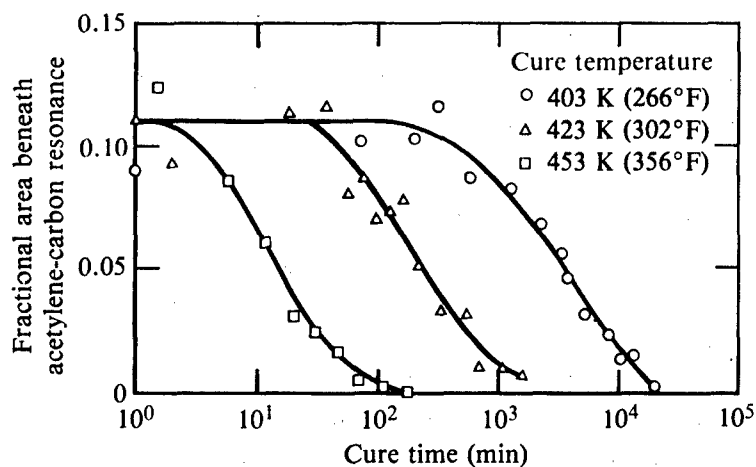
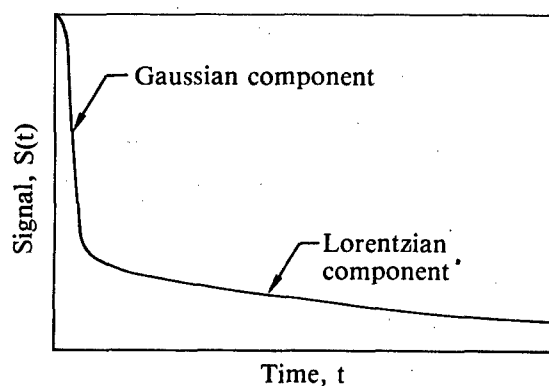


Figure 11. ^{13}C NMR acetylene intensity during isothermal cures.

^1H NMR: Pulsed ^1H NMR experiments showed that the room-temperature hydrogen free-induction decay signal following a single 90° pulse consisted of a Gaussian and Lorentzian component, viz.,

$$S(t) = A_G \exp[-(t/T_{2G})^2] + A_L \exp[-t/T_{2L}] , \quad (3)$$

as shown in Figure 12. The amplitude of the Gaussian component, A_G , is proportional to the number of hydrogens in the rigid portion of the resin, and the amplitude of the Lorentzian component, A_L , is proportional to the number of hydrogens in the mobile portion of the resin.



Signal = Gaussian component (rigid) + Lorentzian component (mobile)

$$S(t) = A_G \exp \left[-(t/T_{2G})^2 \right] + A_L \exp \left[-t/T_{2L} \right]$$

Figure 12. Hydrogen NMR free-induction decay signal.

The ratio A_L/A_G was expected to be a meaningful cure-state parameter. Before curing, the room-temperature value of A_L/A_G was equal to 0.024; after 1327 min of cure at 423 K (302°F) it was 0.003. This result implies that mobile regions having low crosslink density exist within the sample and that they decrease during cure.

We attempted to measure the sizes of these mobile regions using the Goldman-Shen pulse sequence.⁹ This technique measures the time required for nuclear spin polarization to diffuse through mobile regions to the rigid regions of the polymer. The measured time and the spin diffusion constant (determined from the measured time along with the spin-spin relaxation time, T_{2L} , in the mobile region) are sufficient to calculate the size of the mobile region.¹⁰⁻¹²

A prerequisite for successful application of this technique is the existence of two components in the free-induction decay of the NMR signal of the polymer. Two components were observed, although the amplitude of the mobile component was very small. The component resulting from the rigid portion of the polymer must have a spin-spin relaxation time, T_{2G} , at least three times smaller than that resulting from the mobile portion of the polymer, T_{2L} . This proved to be the case, but the rigid component dominated the free-induction decay signal of the ATS, and it was difficult to observe the diffusion of nuclear spin polarization from the mobile regions to the rigid regions of the ATS. In an effort to enhance molecular motion in the more mobile regions of the polymer and increase their amplitude, A_L , the sample's temperature was increased. As the temperature increased, the spin-spin relaxation time of the rigid component increased, but no second component with an amplitude sufficiently large to accurately measure was observed. As a result, the size of the mobile regions in ATS could not be measured.

The Gaussian spin-spin relaxation time, T_{2G} , was found to decrease with increasing cure time, as shown in Figure 13 for 403 K (266°F) isothermal cures in both nitrogen and air. A decrease in T_{2G} is generally an indication of increased rigidity. Beyond about 125 min of curing, T_{2G} did not decrease as rapidly as it did earlier in the cure; but it still decreased measurably, indicating that the polymer was becoming more rigid. Figures 14-15 show similar decreases in T_{2G} for isothermal cures at 423 K (302°F) and 453 K (356°F) in nitrogen and air atmospheres. In all cases the decrease in T_{2G} caused by curing is small, so it is not a particularly sensitive cure-state

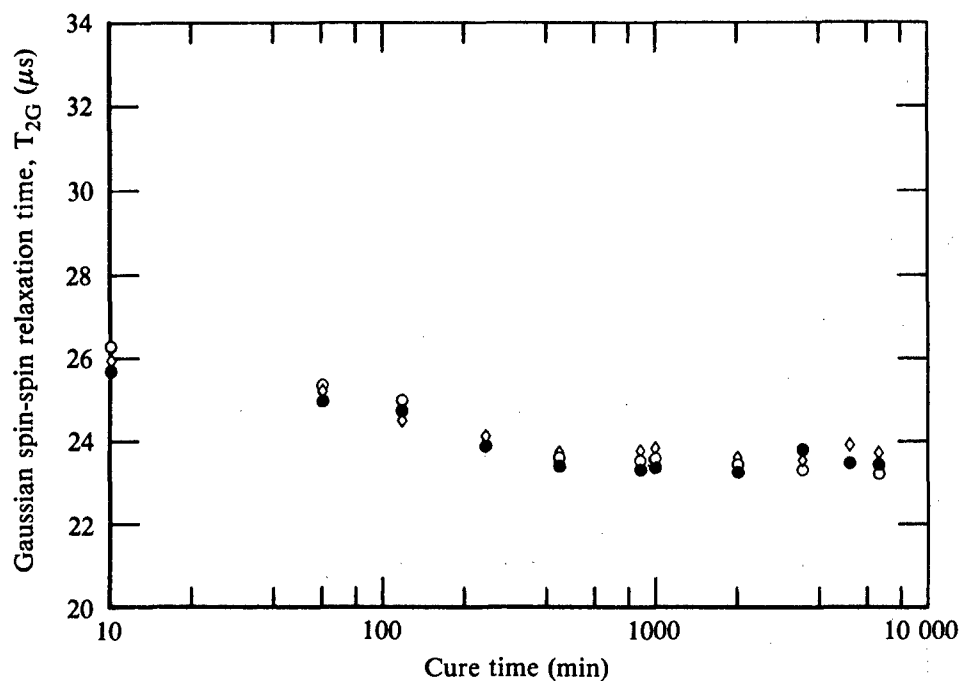


Figure 13. Gaussian spin-spin relaxation time at various times during the 403 K (266°F) isothermal cure of two ATS samples in a nitrogen atmosphere (\circ , \bullet) and one ATS sample in air (\diamond).

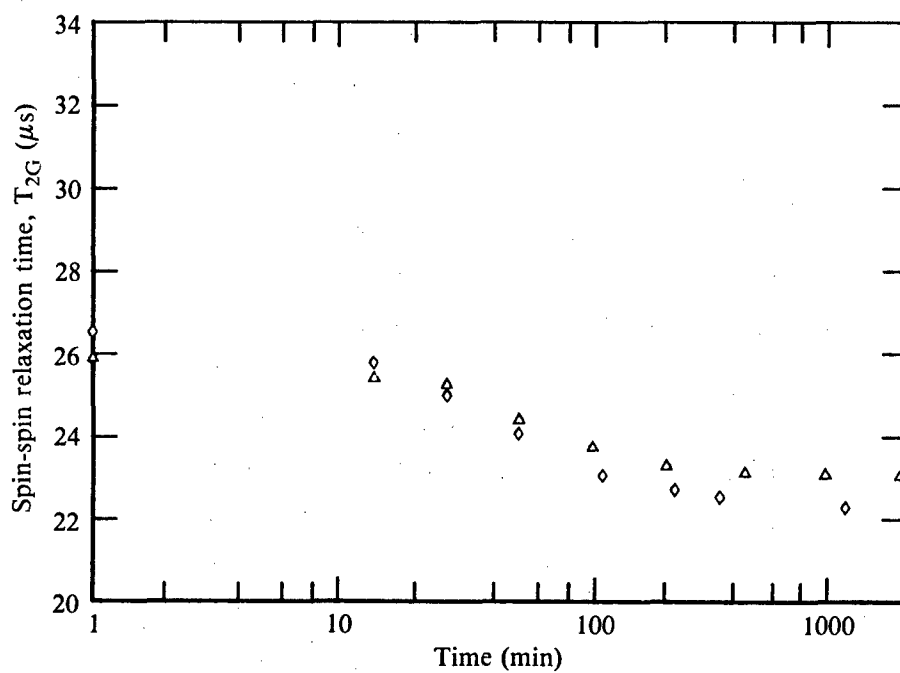


Figure 14. Gaussian spin-spin relaxation time, T_{2G} , at various times during the 423 K (302°F) isothermal cure of an ATS sample in (Δ) nitrogen atmosphere and (\diamond) air.

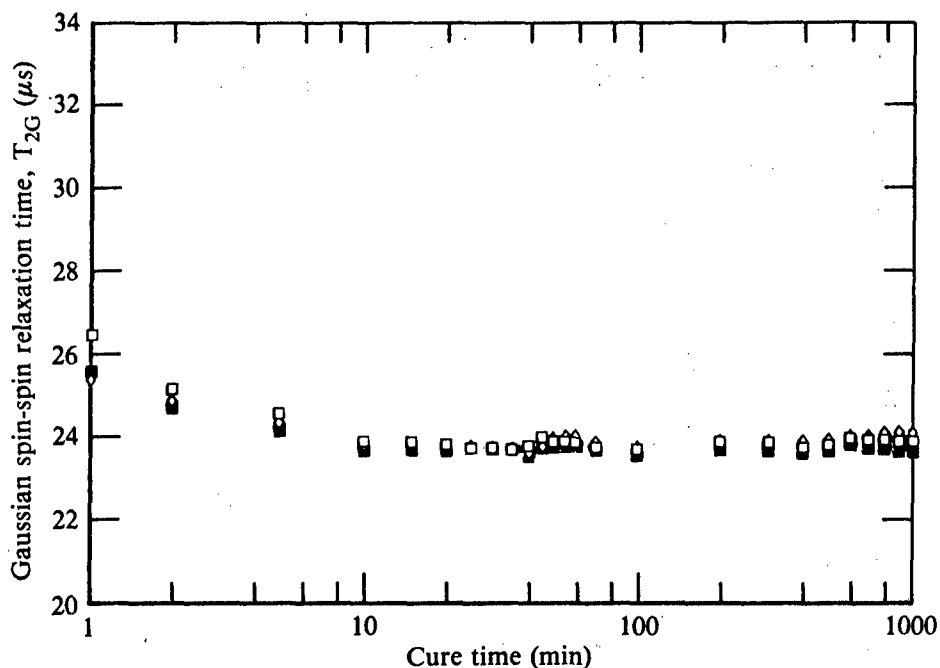


Figure 15. Gaussian spin-spin relaxation time at various times during the 453 K (356°F) isothermal cure of two ATS samples in a nitrogen atmosphere (□, ■) and one ATS sample in air (◊).

parameter. Also, there is no significant difference between the T_{2G} results for the cures in nitrogen and air.

The spin-lattice relaxation time, T_1 , was measured at room temperature by observing the recovery of the NMR signal after a 180° spin-inverting pulse. The Lorentzian signal recovered slightly faster than the Gaussian signal, indicating the two signals may have originated in spatially separated regions. Because the two relaxation times were nearly equal, only a single spin-lattice relaxation time, T_1 , was measured. The spin-lattice relaxation times during the three different isothermal cures in nitrogen and air atmospheres are shown in Figures 16-18. In all cases the spin-lattice relaxation times of the samples in air are less than those for the samples in nitrogen because the oxygen in air is paramagnetic and causes more rapid spin-lattice relaxation.

Generally, as a polymer becomes more rigid, T_1 increases. This behavior was observed during the initial stages of curing, but during the intermediate stages of curing T_1 decreased rapidly. This rapid decrease is thought to be the result of free radicals produced during polymerization, which cause rapid spin-lattice relaxation. This assumption is supported by the EPR results pre-

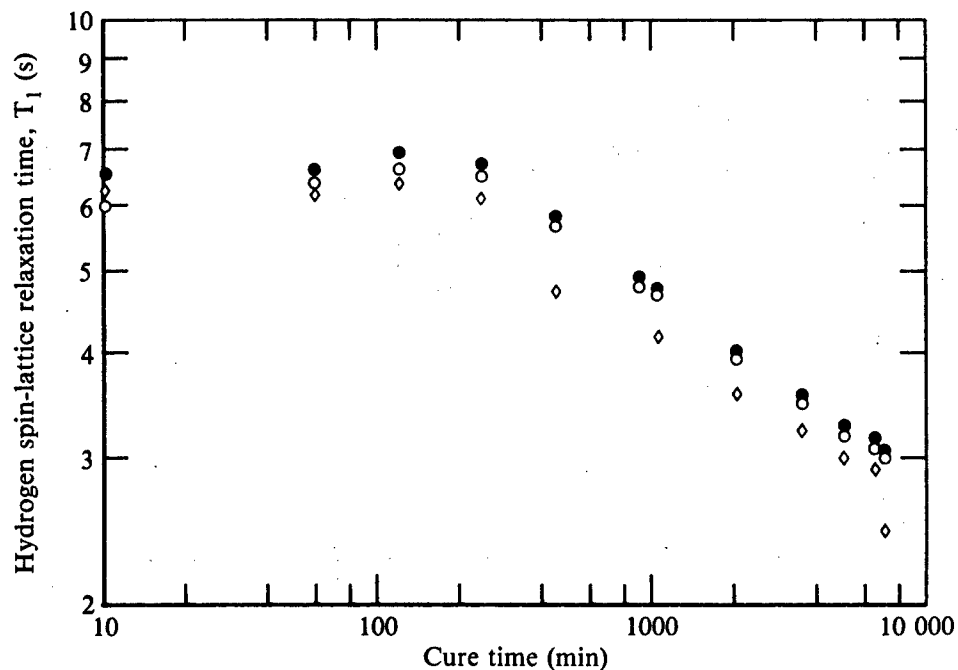


Figure 16. Spin-lattice relaxation time, T_1 , at various times during the 403 K (266°F) isothermal cure of two ATS samples in a nitrogen atmosphere (○,●) and one ATS sample in air (◇).

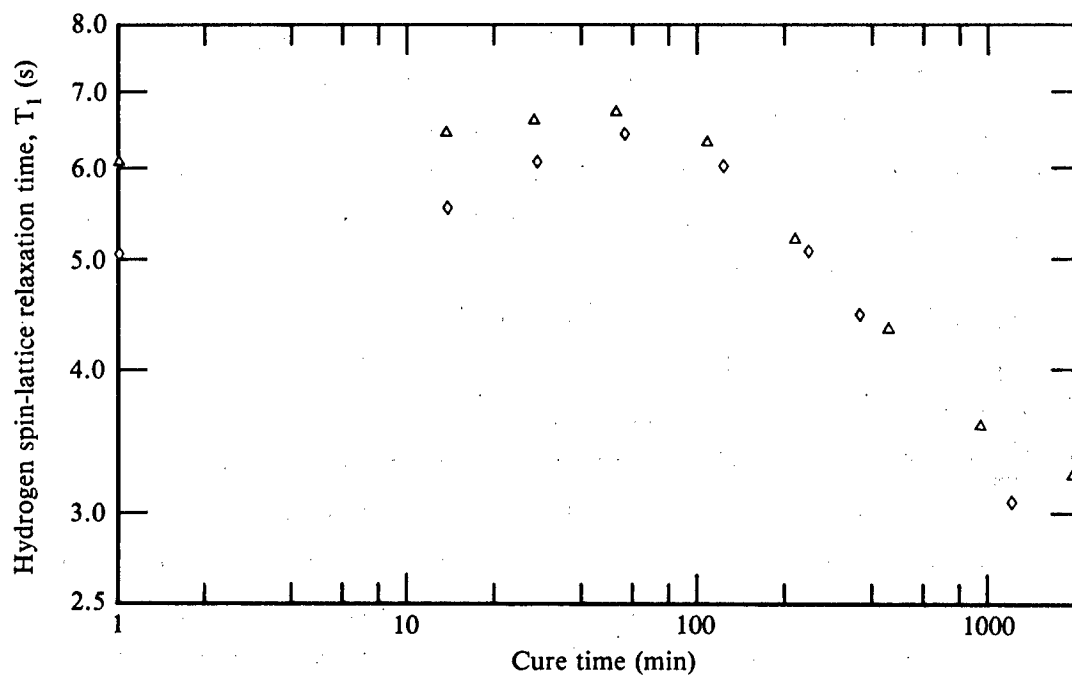


Figure 17. Spin-lattice relaxation time, T_1 , at various times during the 423 K (302°F) isothermal cure of ATS samples in air (◇) and in nitrogen (△).

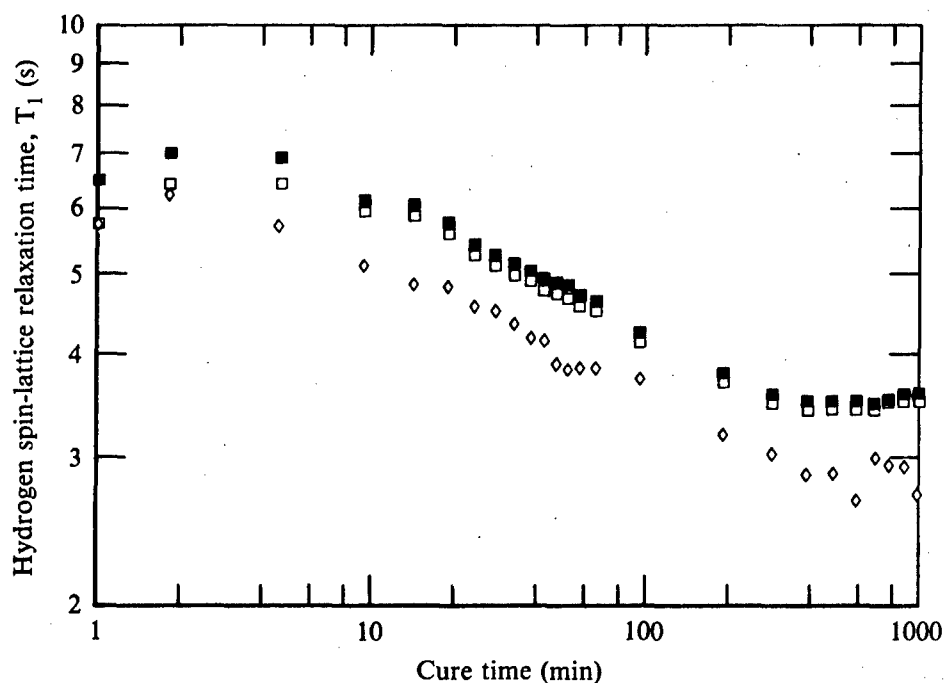


Figure 18. Spin-lattice relaxation time, T_1 , at various times during the 453 K (356°F) isothermal cure of two ATS samples in a nitrogen atmosphere (□, ■) and one ATS sample in air (◇).

sented in the following section, which show a rapid increase in free radical concentration at the same time T_1 decreases rapidly.

In the last stages of curing, T_1 increases again. This increase is thought to be the result of free radical decomposition. Again, this assumption is supported by the EPR results which follow.

ATS samples that had been isothermally cured and stored in a nitrogen atmosphere were opened to permit air to contact the samples. These samples had received the following cures:

- (1) isothermal cure at 403 K (266°F) for 7000 min,
- (2) isothermal cure at 423 K (302°F) for 2500 min, and
- (3) isothermal cure at 453 K (356°F) for 1000 min.

The spin-lattice relaxation times for these samples did not change during a 60-day storage at room temperature in a nitrogen atmosphere. The spin-lattice relaxation times of these samples as a function of the square root of the time following admitting air are shown in Figure 19. This figure shows that the diffusion of oxygen into the samples significantly reduces the spin-lattice relaxation times of all three samples.

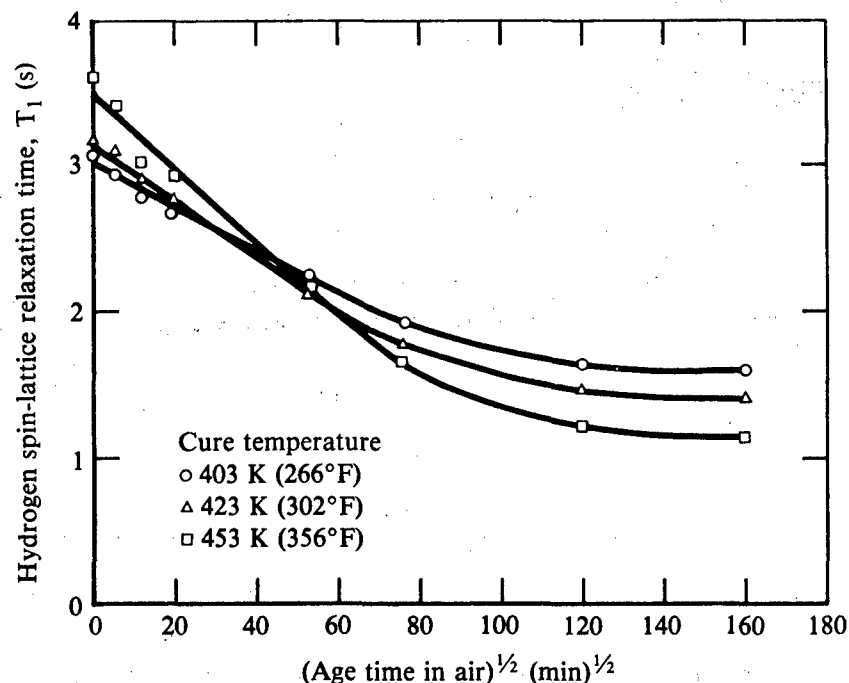


Figure 19. Change in room-temperature spin-lattice relaxation times of cured ATS samples following the breaking of the seals on the nitrogen-filled sample tubes to allow air to enter.

Figure 20 shows the spin-lattice relaxation time history for ATS samples during their cure at 403 K (266°F), 423 K (302°F), and 453 K (356°F) and aging under different conditions. Before curing T_1 was 6.1 ± 0.3 s, and during curing T_1 decreased significantly to about 3 s. This decrease is the result of the free radicals formed during cure. If it were not for these radicals, an increase in T_1 would have been observed because of the decrease in molecular mobility during cure. Following > 90% degree of cure, the samples were aged at room temperature for 90 days (1.3×10^5 min) with no change in T_1 . At this time the sample tubes were opened to admit air. During the time the samples were exposed to air, the T_1 's of the samples decreased significantly but not all by the same amount, so that the sample with the largest T_1 in nitrogen later had the smallest T_1 in air. A decrease in T_1 was expected for all samples because oxygen is paramagnetic and can cause spin-lattice relaxation. Removal of oxygen was expected to increase the T_1 's of the samples back to the values they had before admitting the air. But, after heating the samples to 383 K (230°F) 16 h in vacuum, backfilling with nitrogen, and sealing, the T_1 's increased to greater than their original values. The EPR

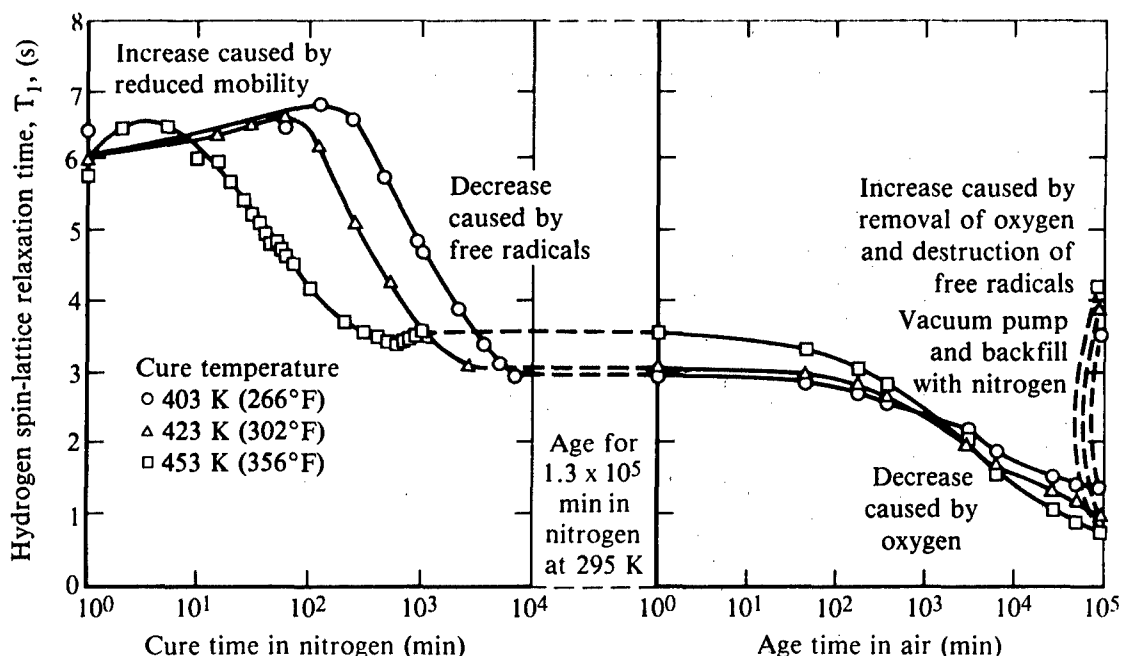


Figure 20. Spin-lattice relaxation time during isothermal cure and subsequent aging.

results presented in the next section show that this greater-than-expected increase in T_1 was the result of a loss of free radicals during exposure to air.

Because of these aging effects, it is necessary to either keep the samples in nitrogen prior to measurement or devise a procedure for correcting these errors. Because the spin-lattice relaxation time is sensitive to both molecular motion and free-radical concentration, while the EPR intensity is more sensitive to free-radical concentration, we thought it would be possible to combine the results of these two measurements to yield a parameter that characterizes molecular motion of the ATS. However, results to be presented in Section IV.1 show that the spin-lattice relaxation time measurements and the EPR measurements are not independent.

Samples that had been used for EPR studies and other samples that had been used for mechanical studies were measured to ensure that consistent results would be obtained. Three EPR samples that had been stored in a nitrogen atmosphere at 253 K (-4°F) for more than 60 days had NMR spin-lattice relaxation times that were in agreement with our previous measurements. A few of the ATS samples that had been cured by Rockwell International and used in mechanical measurements were sent to us by Chuk L. Leung.¹³ These samples had been cured in nitrogen but had been stored in air for between 30 and 60 days.

The T_2 values of these samples agreed with our previous results. The T_1 values of these samples, as measured in an air atmosphere, were much smaller than the values previously obtained from samples cured and measured in a nitrogen atmosphere. The Rockwell samples were heated in 5-mm NMR tubes to 393 K (248°F) for 18 h in vacuum, backfilled with nitrogen, and sealed. This procedure caused the values of T_1 to increase, apparently because of the removal of the paramagnetic oxygen which causes rapid spin-lattice relaxation. As an example, the T_1 of the Rockwell samples cured at 453 K (356°F) increased from 2.3 s to 4.3 s after oxygen removal. The values of T_1 after oxygen removal are in fair agreement with our previously obtained T_1 values. These results are summarized in Table 2. The predicted degree of cure based on T_1 measurements in nitrogen are within 4% of those given by Rockwell.

TABLE 2.
RESULTS OF HYDROGEN NMR MEASUREMENTS ON ROCKWELL
ATS SAMPLES

| Rockwell International sample data | | | NMR results for as-received sample in air | | NMR results for sample in nitrogen atmosphere | |
|------------------------------------|-----------------|---------------------|---|-----------|---|--------------------------------|
| Cure temperature [K(°F)] | Cure time (min) | Degree of cure* (%) | T_1 (s) | T_1 (s) | Predicted cure time (min) | Predicted degree of cure** (%) |
| 403 (266) | 7200 | 90 | 1.3 | 3.5 | 3500 | 88 |
| 423 (302) | 960 | 93 | 1.4 | 3.8 | 870 | 92 |
| 453 (356) | 60 | 91 | 2.3 | 4.3 | 100 | 95 |

* This degree of cure, measured by Rockwell International is based on curing exotherms below 600 K (1112°F), and excludes the exotherm at 630K, (1166°F).

** Based on Rockwell International's degree of cure.

Temperature-dependent T_2 measurements were made on the Rockwell samples to determine if differences in curing temperature could cause different high-temperature T_2 behavior. Based on our NMR studies of epoxy resins having different crosslink densities, it was anticipated that samples cured at lower temperatures would experience a larger increase in T_2 with increasing temperatures than those cured at higher temperatures. Unfortunately, the ATS samples cured at 403 K (266°F), 423 K (302°F), and 453 K (356°F) experienced almost identical increases in T_2 as the temperature was increased. Specifically, T_2 increased from $24.0 \pm 0.8 \mu\text{s}$ at 300 K (81°F) to $30.9 \pm 0.7 \mu\text{s}$ at 503 K (466°F)

for all samples. These measurements were made as rapidly as possible; but at these elevated temperatures significant curing occurred, which may have prevented the anticipated results from being obtained.

b. EPR Isothermal Cure Results

Prior to collecting EPR data as a function of cure time, baseline data were collected on the uncured ATS resin received from AFML. It was determined that some radicals were present in the uncured resin and that the concentration of radicals was about 1% of that obtained after ~ 90% cure. The signal observed from the uncured resin was similar to that observed after curing, but had some subtle differences in line shape and linewidth, as discussed later in this report. When the resin was dissolved in toluene and examined by EPR, a single line having a width of ~ 1.0 mT was obtained. No resolvable hyperfine components could be distinguished; however, the presence of unresolved hyperfine components could be inferred from the overall broadness of the spectral line. It is likely that the radicals observed both before and after curing are delocalized into a conjugated double bond system, which would explain the radical stability and the unresolved spectrum.

After the baseline measurements, EPR spectra were collected at selected times during isothermal curing. The typical spectrum consisted of a single EPR line having a near-Gaussian shape and a width of about ~ 1.0 to 1.5 mT. The growth in the signal's intensity occurred on the same time scale as that of the curing process, as determined by changes in NMR and IR spectra, sample viscosity, and DSC measurements. Thus, radical production was intimately associated with the curing process.

Intensities and radical concentrations were calculated as described in Section II 3.b. The best results were obtained using the strong pitch reference sample and Equation (1) for intensity calculation. Signal intensity data are plotted as a function of cure time in Figures 21 and 22. There are three distinct regions of interest in the curves shown in these figures. First, at early stages of cure, there is an induction period during which net radical production appears to be inhibited. Second, there is a region in which radical concentration increases approximately linearly with $\log(t)$, where t is cure time. This region is also observed in the IR and NMR data. Finally, after the curve maximum is a third region in which radical concentration decreases with time. Typically, the radicals lasted many hours at 453 K (356°F) and a few months at 403 K (266°F) if kept in an inert atmosphere.

Samples cured at 453 K (356°F) produced radicals at the fastest rate but had the smallest maximum radical concentration, whereas samples cured at 403 K (266°F) produced free radicals the most slowly but had the highest maximum radical concentration. Thus, the samples cured at 453 K, 423 K and 403 K had maximum free radical concentrations of $\sim 25 \times 10^{17}$, $\sim 31 \times 10^{17}$, and $\sim 38 \times 10^{17}$ spins/g respectively.

The induction period observed early in the cure cycle was ~ 20 min at 453 K, ~ 75 min at 423 K, and ~ 300 min at 403 K (see Figure 21). One would ordinarily expect the free radical generation reaction(s) to proceed at a maximum rate at the beginning of the cure cycle if the observed radicals were produced directly from unreacted acetylene, whose concentration is highest at the beginning of the cure cycle. The fact that there is an induction period at the initial stages of cure would therefore imply either that free radical decay reactions are particularly effective during this period or that free radicals are produced by means of an intermediate product that must itself increase in concentration during the induction period. In the latter case, appreciable radical formation would not occur until the concentration of intermediate had become sufficiently high, the exact amount depending on the ratio of the reaction rates for the formation of intermediate and radical.

Several instrumental/experimental artifacts could potentially contribute to the observed induction period early in the cure cycle. These include

- (1) a lower cavity Q because of higher dielectric lossiness of the sample at early stages of reaction,
- (2) saturation of the EPR signal because of longer relaxation times when radical concentrations are low, and
- (3) a difference in spectral line shape below $\sim 20\%$ cure that would affect the intensity values calculated using Equation (1).

The first possibility can be discounted because an induction period was observed even when using the "internal" reference, DBNO in polyurethane; in this case the intensity of the sample relative to the reference did not depend on cavity Q. The second and third possibilities can also be discounted because quantitative considerations indicate these effects are inadequate to produce the required deviations from linearity observed during the induction period in Figure 21. The induction period therefore appears to be a real effect associated with ATS curing.

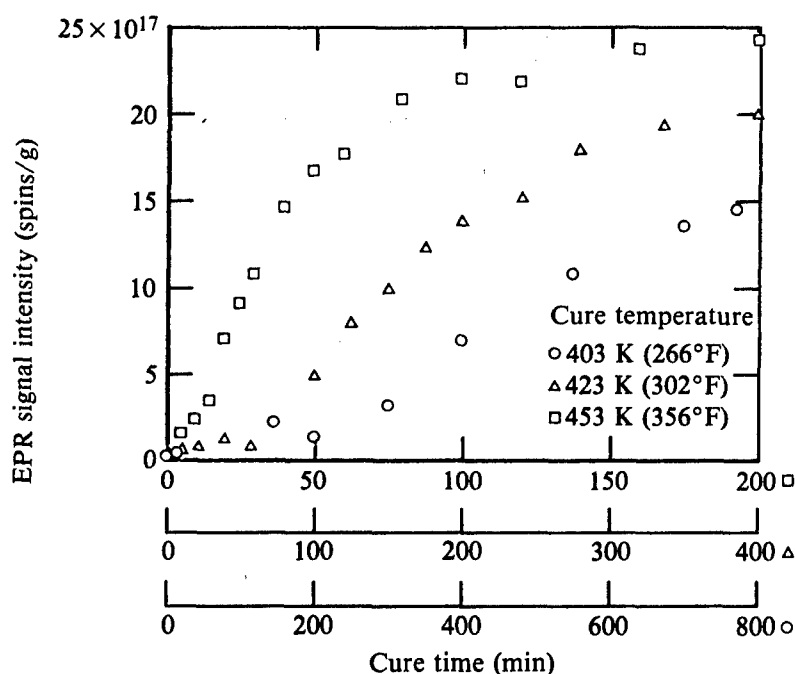


Figure 21. EPR signal intensities as a function of cure time at early stages of cure. The presence of an induction period at short cure times indicates inhibited net radical production, possibly due to a limited amount of impurity that destroys radical and is itself consumed in the process.

We cannot conclusively distinguish between the presence of radical-consuming reactions that are particularly effective at early stages of cure and consecutive reactions involving formation of radicals via a nonparamagnetic intermediate. However, there is evidence that favors the former possibility. The curves in Figure 21 can be extrapolated to a common y-axis intercept at approximately -8×10^{17} spins/g for each cure temperature. If the induction period were due to consecutive reactions involving a nonparamagnetic intermediate, the value of the intercept would be determined by the relative rates of the reactions for formation of intermediate and radical. Since the activation energies for these reactions need not be the same, the ratio of the rate constants should be a function of temperature, making the above intercepts different for different cure temperatures (although the observed differences may be small). This is contrary to the observed common intercept at -8×10^{17} spins/g for all three cure temperatures.

Therefore, the preferred explanation is that free radicals are being consumed during the induction period. This enhanced free radical consumption may be caused by

- (1) the initial presence of a finite amount of a radical-consuming species that is consumed or rendered ineffective as the cure progresses, or

- (2) a greater mobility of the free radicals in the uncured resin, which allows decay reactions to occur, followed by immobilization and reduced reactivity of the radicals at the end of the induction period.

The first decay mechanism seems more likely than the second for the following reasons. Preliminary results indicate that the liquid-like consistency of the resin at its cure temperature extends to times longer than the induction period. In addition, as mentioned above, the curves in Figure 21 can be extrapolated to a common intercept at -8×10^{17} spin/g (extrapolation of the 453 K data is subject to error, however). This indicates that $\sim 8 \times 10^{17}$ radicals/g are destroyed during the induction period at each temperature. Thus, the presence of the same concentration of radical-consuming species at all temperatures would be expected. Finally, the shapes of the curves in the region of the induction period are consistent with a radical decay mechanism involving eventual consumption of the scavenger species.

By conducting experiments employing purified ATS resin, it may be possible to verify or eliminate the possibility of radical scavengers present in the as-received ATS resin.

As shown in Figure 22, following the induction period is the region in which radical concentration increases linearly with $\log(t)$. In this region the time scale for growth of radical concentration is similar to the time scale for acetylene reaction as observed by NMR and IR. The linear portions of the curves in Figure 22 can be replotted in the form $I \propto (1 - e^{-kt})$, which is the functional dependence one would expect physically for a first-order rate-determining reaction for radical formation. This may imply that the isothermal reaction rate primarily depends on the concentration of a single component (e.g., acetylene moiety).

If it is assumed that the amount of radical observed is proportional to the amount of acetylene consumed and that the proportionality constant does not depend on reaction temperature, it is possible to determine the activation energy for radical formation (and therefore acetylene reaction) by comparing the slopes of the curves in Figure 22 at constant radical concentration. When this is done at a radical concentration of 7.3×10^{17} spins/g, the activation energy for radical production is 88 kJ/mol, which is in satisfactory agreement with reported activation energy values of 92-100 kJ/mol.^{2,14,15} On the other hand, if it is assumed that radical concentration is not proportional to

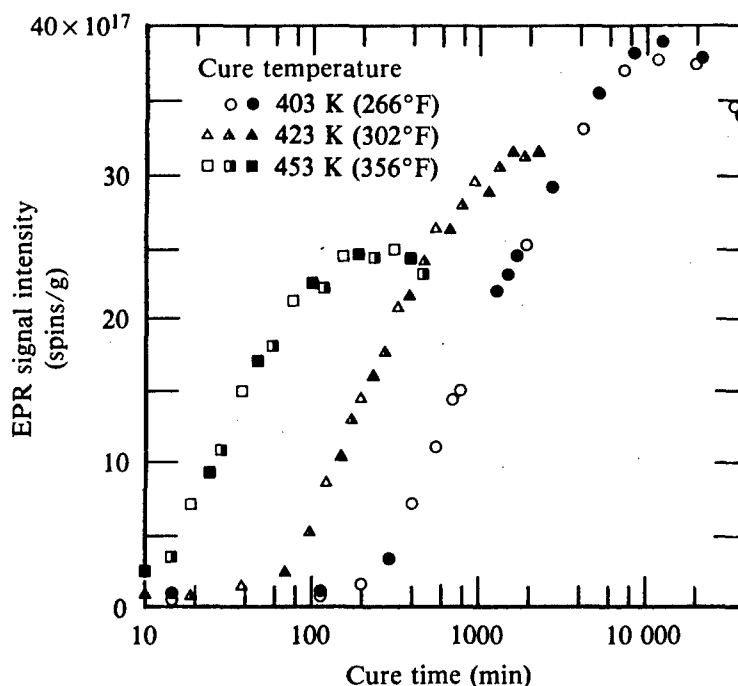


Figure 22. EPR signal intensities (spin/g) as a function of cure time. Differences in maximum intensity for samples cured at different temperatures may be due to differences in polyene-chain lengths, radical stabilities, and/or polymerization/radical-decay mechanisms at different temperatures.

acetylene reacted and the slopes of the curves shown in Figure 22 are evaluated at data points corresponding to particular degrees of cure as determined by NMR or IR, the temperature dependence of the rate constant yields activation energies of ~ 170 kJ/mol and ~ 130 kJ/mol, respectively. These results suggest that in the linear regions of the plots in Figure 22 the radical concentration is truly a measure of the extent of reaction, i.e., a measure of the amount of reactant consumed.

Following the region where radical concentration increases linearly with $\log(t)$, the radical concentration reaches a maximum, the intensity value of which depends on cure temperature. These results can be explained either in terms of radical decay that is more effective relative to radical production at high temperatures than at low temperatures, or in terms of different chain lengths for the polymers formed at different cure temperatures. The results of Pickard et al.² indicate that polymer chain length does not depend strongly on cure temperature, which would argue in favor of the former explanation for differences in maximum intensity. In the absence of the decay reaction, one might therefore expect the ultimate free radical concentration to be the same for all three cure temperatures. Extension of cure schedules to times longer

than those corresponding to concentration maxima, followed by quantitative analysis of the resulting intensity/time curves should more conclusively determine the correct explanation for the differences in maximum intensities corresponding to different cure temperatures.

The intensity/time results discussed above can be summarized as follows. There is an induction period early in the cure cycle which indicates either that enhanced radical decomposition occurs during this part of the cure process or that an intermediate is required prior to formation of the observed stable free radical species. By quantitatively evaluating the EPR intensity curves corresponding to this portion of the cure cycle and/or by examining purified ATS resin, it may be possible to distinguish between these possibilities.

Later in the cure cycle, radicals are produced approximately linearly with $\log(t)$, where t is time of cure. In this region of the cure cycle, the radical concentration also follows the functional form $I \propto (1 - e^{-kt})$ where I is EPR signal intensity. Evaluation of the temperature dependence of the rate constants in this portion of the cure cycle yields an activation energy of ~ 88 kJ/mol when the curves are evaluated at points corresponding to the same radical concentration.

The last region of the cure cycle is that in which the radical concentration decreases with increasing cure time. The rates of radical decomposition relative to the rates of radical production may be responsible for the different maximum intensities observed for samples cured at different temperatures. Alternatively, different polymer chain lengths in the cured ATS may account for this difference in intensity. By extending cure times such that significant radical decomposition occurs, it should be possible to evaluate the rates of radical decay at the different cure temperatures and thus determine which of the above possibilities is correct.

In addition to spectral intensities, spectral linewidth changes were measured as a function of cure time. The results are shown in Figure 23. The curves resemble those of integrated signal intensity as a function of $\log(t)$, where t is cure time. The scatter in this figure reflects the difficulty in directly measuring the spectral linewidths; however, the scatter can be reduced by calculating the linewidths from the ratio of integrated intensity to amplitude:

$$\Delta \propto (I/A)^{1/2}, \quad (4)$$

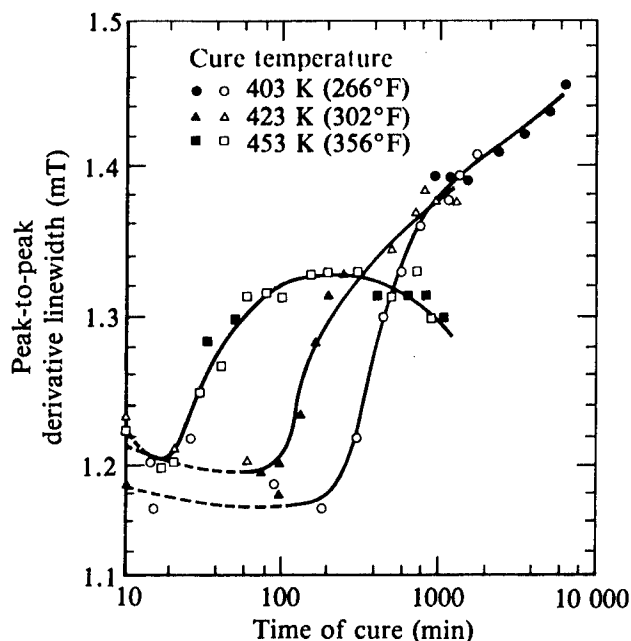


Figure 23. EPR derivative linewidths as a function of cure time. Curves are similar to EPR intensity curves shown in Figure 22, which is expected if linewidth is due to electron-electron dipolar interactions. Open and closed symbols indicate different samples.

where Δ is the peak-to-peak derivative linewidth, I is the integrated intensity, and A is the measured amplitude of the derivative line. Although I and A are sensitive to variations in spectrometer sensitivity and sample placement, their ratio is not.

At early stages of cure [for example, at less than 20 min of curing at 453 K (356°F)] the spectral linewidth is dominated by a broad line, $\Delta = 1.2$ mT, that is present in the sample even before curing (see Figure 24). After 20 min of curing at 453 K (356°F), the signal associated with the curing reaction(s) dominates the observed spectrum, producing a linewidth of 1.07 mT. As curing progresses, the linewidth again increases to a value of 1.21 mT. Using computer subtraction, the initial broad component can be removed from the spectrum at early stages of cure. When this is done, the signal associated with curing decreases monotonically to a value of ~ 1.06 mT as the cure time decreases to zero. Thus, it seems that the observed spectrum is actually a superposition of component spectra due to different radicals in the sample, one of which is present before curing. The initial radical may contain information regarding the pre-cure history of the ATS resin.

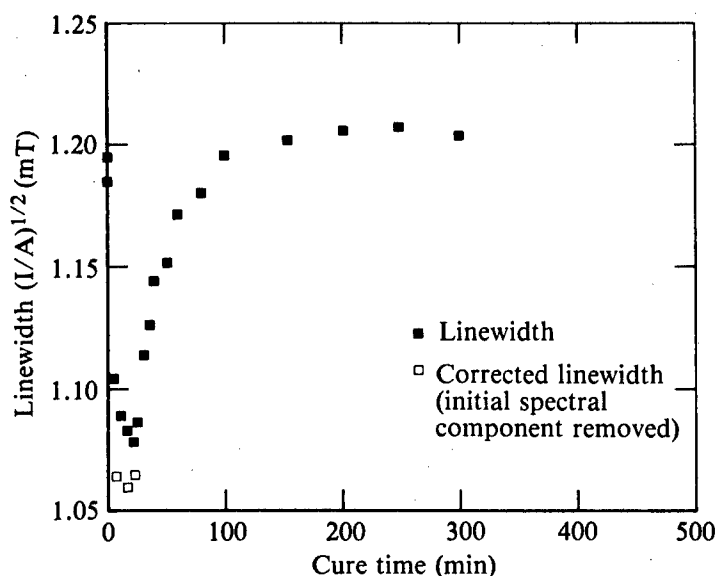


Figure 24. EPR derivative linewidth as a function of cure time for a sample cured at 453 K (356°F). In addition to the signal generated by curing, there is a background signal observed at short cure times (≤ 20 min) having a linewidth of ~ 1.2 mT. The signal generated by curing monotonically increases from 1.06 mT to 1.20 mT as curing progresses.

The fact that the curves in Figures 22 and 23 have a similar appearance can be explained in terms of the interactions that cause line broadening in the samples. These interactions are dipolar with magnitudes that are a function of $1/r^3$, where r is an average radical-radical separation. Since $1/r^3$ is linearly dependent on sample concentration, a linear increase in linewidth with radical concentration is expected. Thus, intensity and linewidth should increase in a similar manner (as is observed) as curing progresses. Linewidth has at least one advantage over spectral intensity as a cure-state parameter: no reference is needed to determine the former, i.e., linewidth is relatively insensitive to spectrometer sensitivity and to sample placement in the EPR cavity.

Following isothermal curing in an inert atmosphere, some samples were exposed to air at 253 K (-40°F) for up to 84 days. The total integrated intensities of the samples typically decreased by an average of $\sim 15\%$ within 10 days, 30% in 20 days, and 35 to 55% in 84 days. The linewidths decreased as well, typical values being decreases of $\sim 3.5\%$ in 10 days and $\sim 7\%$ in 20 days. Results are shown in Figure 25. From these results, it can be concluded that the presence of air (oxygen) enhances the rate of free-radical decay in these samples. No obvious changes in shape associated with peroxy

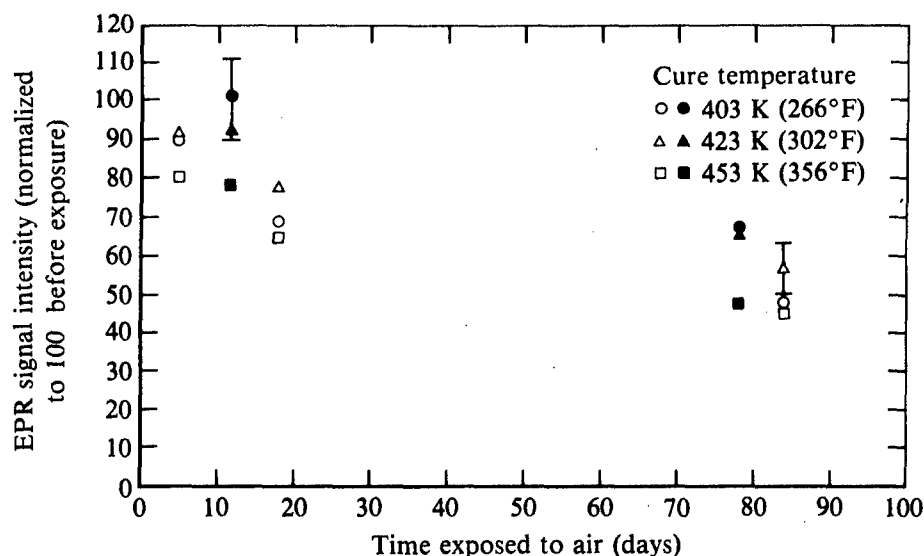


Figure 25. EPR signal intensities of solid samples as a function of exposure time to air at 253 K (-4°F). The intensity decreases by 50% in ~ 80 days. Different symbols indicate different samples; initial intensity equals 100 in all cases.

formation have been observed.

Figure 26 shows a comparison of change in linewidth with change in integrated signal intensity resulting from exposure to air. Although linewidth is related to total signal intensity, it is possible for different samples to have nearly identical intensities yet significantly different linewidths; this inconsistency suggests that linewidth changes due to exposure to air are not determined exclusively by the concentration of paramagnetic centers present in the sample. The reason for these results is not clear at this time and could be a potential subject of further investigation.

In an attempt to compare data from samples prepared by Rockwell with our own data, we examined two of Rockwell's samples by EPR. The samples had been cured at 403 K (266°F) and 453 K (356°F) for 7200 and 60 min, respectively. The relative free-radical concentrations were determined by comparing their EPR signals with those of samples having known intensities.

The data points of both Rockwell samples were below the curves for our samples, which seemed to indicate that the free-radical concentrations of the Rockwell samples were too low for the cure times specified. This apparent lower radical concentration may have been caused by differences in sample geometry and/or filling factor between our samples and those submitted by Rockwell. It also undoubtedly due to exposure of the Rockwell samples to air which would have destroyed some of the radicals formed during curing.

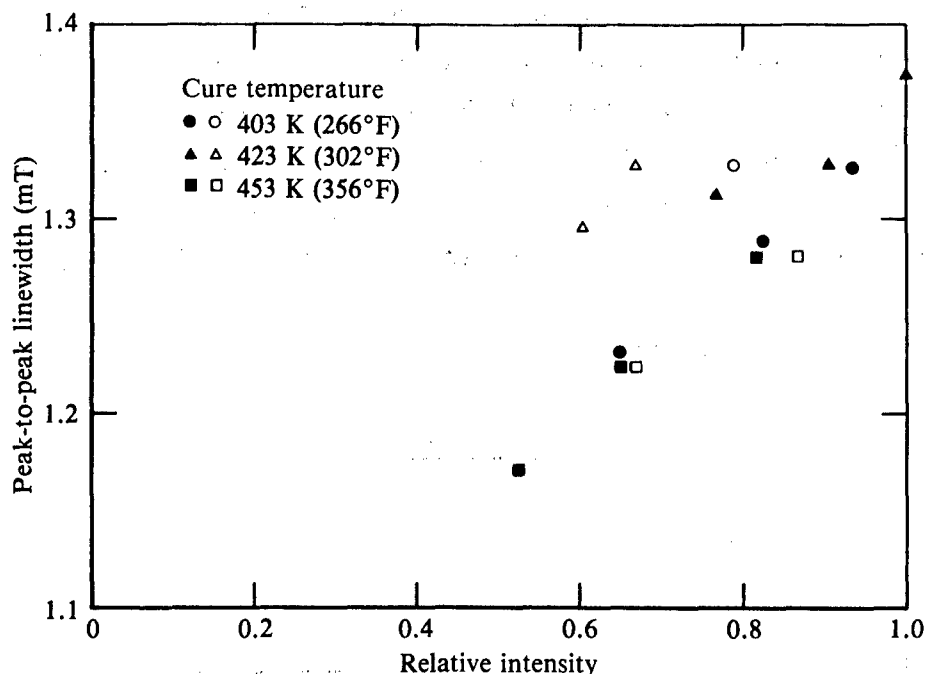


Figure 26. EPR derivative linewidth as a function of EPR signal intensity. For all samples, the linewidth decreases linearly with decreasing intensity, which is consistent with an electron-electron dipolar-broadening mechanism.

From the EPR intensities, the cure times for the Rockwell samples would have been predicted to be 2200 min for the sample cured at 403K (266°F) for 7200 min, and 50 min for the sample cured at 453 K (350°F) for 60 min. The predicted cure times correspond to 85% cure and 90% cure respectively. The actual degrees of cure for the samples were 90% and 91%, respectively, as determined by Rockwell [using DSC and excluding the exotherm at 630 K (1166°F)].

By using correct sample geometry, which can easily be accomplished using pulverized samples, and preventing exposure to air, we expect reliable cure state data to be collected in the future from samples fabricated/cured elsewhere. To further evaluate our ability to reliably examine ATS samples of arbitrary geometry (such as those submitted from outside this laboratory), an experiment was performed in which the EPR spectrum of a cured ATS sample was examined both prior to and following pulverization in an inert atmosphere. The signal intensities of the solid and pulverized samples, after correcting for density differences, were within 3.2% of each other, demonstrating that EPR can be used to characterize samples of arbitrary geometry.

For comparison, a sample was pulverized in air and then examined by EPR as a function of exposure time to air at 298 K (77°F) (Figure 27). It was found that signal intensity losses of nearly 20% can be expected for exposure times as short as 1 h, with losses of 55% after approximately two days. These results can be contrasted with those obtained from solid samples exposed to air at 253 K (-4°F). In the latter case exposure times of ~3 months were required for ~50% decrease in signal intensity, as described above.

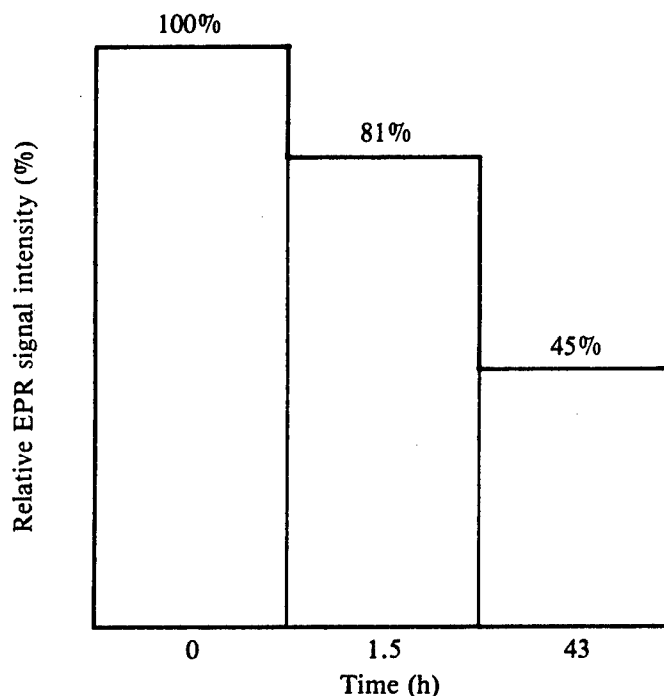


Figure 27. EPR signal intensity of a powdered sample as a function of exposure time to air. Note that the intensity has decreased more than 50% in less than 2 days.

c. IR Isothermal Cure Results

Infrared spectroscopy, which is widely used in polymer characterization studies, is particularly suitable for measurement of chemical changes taking place in the course of polymerization. In this study, FT-IR spectroscopy was used mainly to derive parameters for characterization of ATS cure states based on measurement of spectral changes induced by cure. The search for sensitive cure-state parameters also produced valuable information on the nature of some cure reactions. The search for spectral changes suitable for use as cure-state parameters encompassed detailed examination of all the cure-induced changes in individual IR bands and their relationship to the other bands of the spectrum.

IR parameters suitable for characterization of the cure states were derived from three distinctly different sets of spectral changes which were monitored as a function of the degree of cure:

- (1) measurement of the changes in band intensities (or band areas) of the acetylene bands,
- (2) measurement of the changes in ratios of bands representing various nonreactive moieties, and
- (3) determination of cure-induced frequency shifts.

IR Bands of the Main ATS Functional Groups

The main functional groups of ATS and the corresponding IR bands arising from their vibrations are:

- (1) Acetylene group--622, 941, 2108, and 3295 cm^{-1} .
- (2) Sulfone group--576, 1105, and 1151 cm^{-1} .
- (3) Aryl ether link--1249 cm^{-1} .
- (4) Benzene rings (carbons)--1485 and 1580 cm^{-1} .
- (5) Benzene rings (hydrogens)--794, 833, and 3040-3120 cm^{-1} .

The two main acetylene bands at 941 and 3295 cm^{-1} can be assigned with confidence to the following vibrations: the 3295 cm^{-1} band to the C-H stretch of the acetylenic H atom, and the 941 cm^{-1} band to the bending of the entire acetylene group relative to the benzene ring, based on the assignment made by Bloor et al.¹⁶

The weak acetylene band at 622 cm^{-1} can be assigned to bending vibrations of the acetylenic H, whereas the very weak band at 2108 cm^{-1} originates in the stretch vibrations of the acetylene carbons. Cure-state parameters were derived only from measurement of the changes in the two main acetylene bands, while the very weak band at 2108 cm^{-1} was used to detect the formation of enyne linkages.

The strong IR band at 1249 cm^{-1} which can be assigned to the stretch vibration of the aryl ether moiety was used to study the utility of cure-induced frequency shifts as cure-state parameters. Some of the changes in the bands originating in the vibrations of the benzene ring hydrogens (mainly the aromatic C-H stretch) were used as evidence supporting the intramolecular cyclization (IMC) mechanism.¹⁷

Cure-Induced Changes in the IR Spectrum of ATS

Acetylene Group: The absorbance decreases of the IR bands which originate in the vibrations of the acetylene group are the most pronounced spectral changes observed in the early stages of ATS cure, as shown in Figures 28 and 29. However, the frequency shifts of the aryl-ether band at 1249 cm^{-1} provide the greatest spectral change during the later stages of cure, as shown in Figure 30. Figures 28 and 29 show three-dimensional plots of the 3295 cm^{-1} and 941 cm^{-1} acetylene-band regions of the ATS IR spectra as function of cure time. Figure 31 illustrates the proportionality of the consumed acetylene to the degree of cure (for the 3295 cm^{-1} band).

The overall spectral differences between early and late stages of cure for two other regions of the ATS spectrum are shown in Figures 32 and 33 by shading.

Frequency Shifts: Difference spectroscopy is a powerful method for detecting minor spectral changes in polymers. Difference spectra which represent the

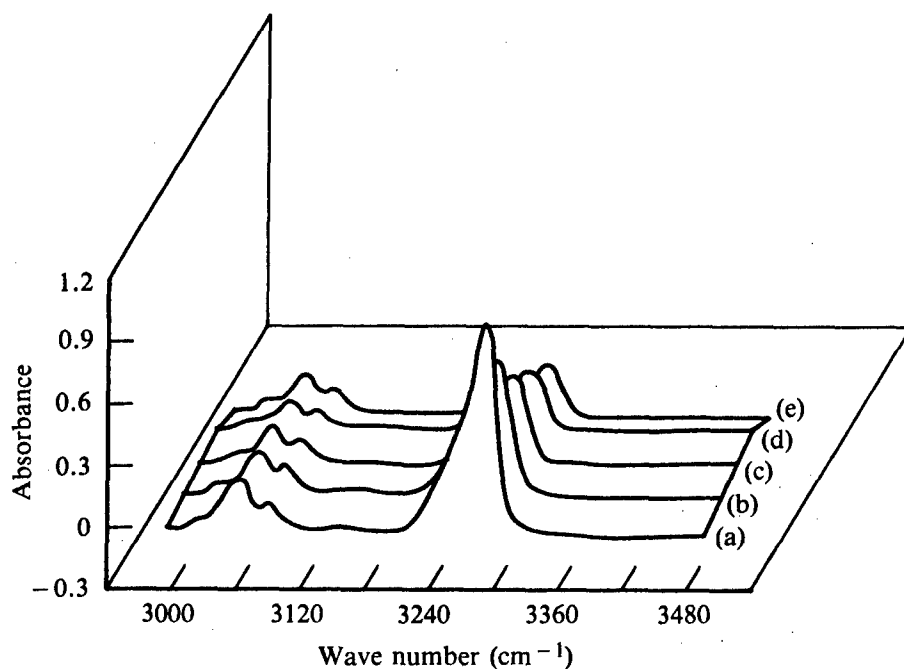


Figure 28. Superimposed FT-IR spectra of the 3295 cm^{-1} acetylene-band region of ATS at different stages of cure at 423 K (302°F); (a) 0 min cure, (b) 40 min cure, (c) 70 min cure, (d) 100 min cure, and (e) 150 min cure.

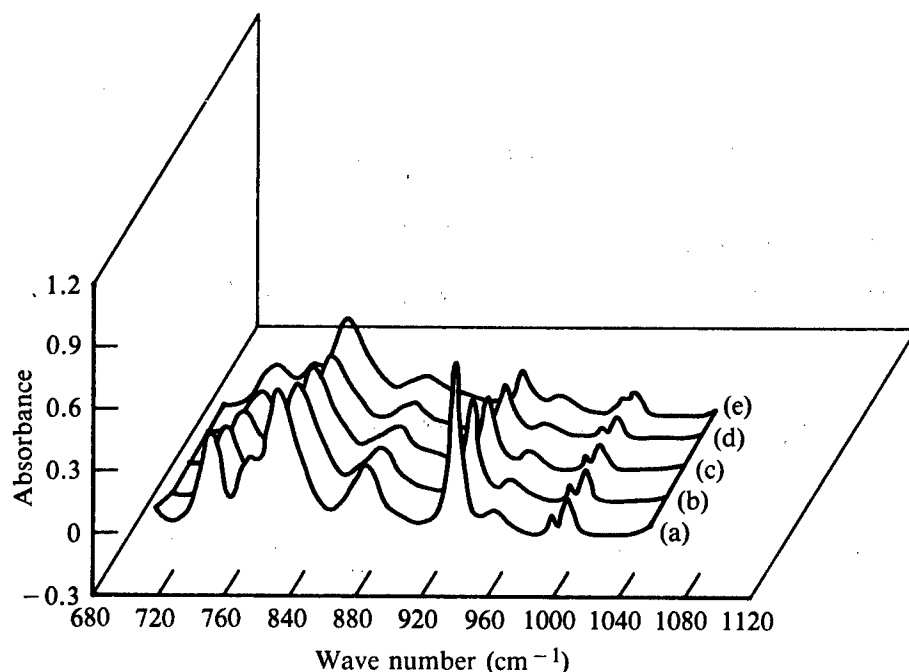


Figure 29. Superimposed FT-IR spectra of the 941 cm^{-1} acetylene-band region of ATS in different stages of cure at 423 K (302°F); (a) 0 min cure, (b) 40 min cure, (c) 70 min cure, (d) 100 min cure, and (e) 150 min cure.

net cure-induced changes between two consecutive stages of ATS cure are shown in Figure 30. In addition to the expected negative acetylenic band at 941 cm^{-1} which reflects the consumption of acetylene groups, these difference spectra exhibit spectral profiles indicative of frequency shifts for some of the bands. A typical difference spectrum intensity profile for a frequency-shifted IR band is shown in Figure 34. Such a profile provides a greatly amplified record for small and otherwise difficult-to-measure frequency shifts.¹⁸ The peak-to-peak intensity, μ , is related to $\Delta\nu$ and can thus be used for measuring of small frequency shifts.¹⁸

Frequency shifts are observed in IR spectra of stressed polymers¹⁹ due to deformed geometry of chains caused by molecular strain. Phenomena other than stress, i.e., change in the mass of the substituents or the intermolecular interactions which take place during cure, can also induce frequency shifts.

The difference FT-IR spectra between consecutive stages of curing (Figure 30) show that the frequency shifts of the 1250 cm^{-1} band, which originates in the aryl-ether C-O stretch vibration, are the most pronounced spectral change observed during the later stages of cure. Cure-induced molecular strain is one possible mechanism that contributes to the frequency shift of the 1250 cm^{-1} band. The comparison between the changes in the frequency of the band

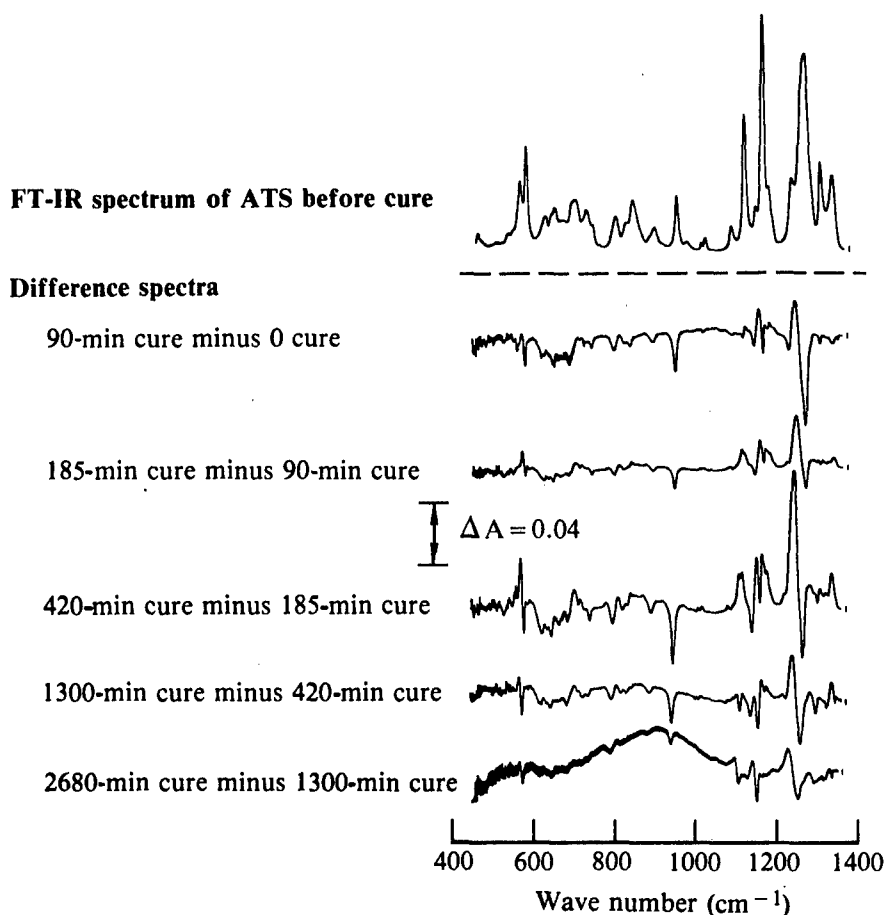


Figure 30. Superimposed difference FT-IR spectra of 400 - 1400 cm^{-1} region that represent the net spectral differences between consecutive stages of ATS cure at 403 K (266°F), showing that the most pronounced changes in later stages of cure are a result of band frequency shifts.

maxima as a function of degree of cure for isothermal cure at 453 K and at 403 K, as shown in Figure 35, indicates that at 453 K there is no significant shift up to a degree of cure of 35%, while at 403 K substantial shift occurs. If the increase in the mass of the substituents which accompanies curing was the mechanism responsible for the frequency shift and not molecular strain, then there should be no difference between the 403-K and 452-K cures. The difference between the 403-K and 453-K cures can, however, be explained in terms of cure-induced molecular strain. The higher chain mobility occurring during cure at 453 K permits relaxation of molecular strain up to $\approx 35\%$ degree of cure (DOC), while such relaxation is not facilitated during the 403 K cure. A number of other IR bands also undergo cure-induced frequency shifts. The band frequencies of the aromatic band at 1572 cm^{-1} and

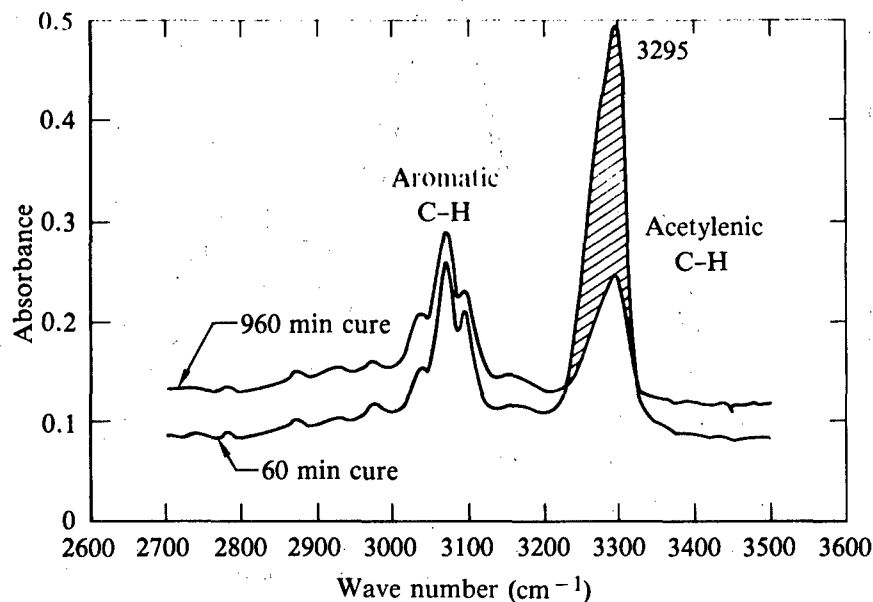


Figure 31. Superimposed FT-IR spectra of the 3295 cm^{-1} acetylene-band region of ATS recorded after 60 min and 960 min cure at 423 K (302°F) showing the consumption of terminal acetylenic moiety during cure and the extent of unreacted groups. The shaded area is proportional to the acetylenic groups consumed in the curing reactions.

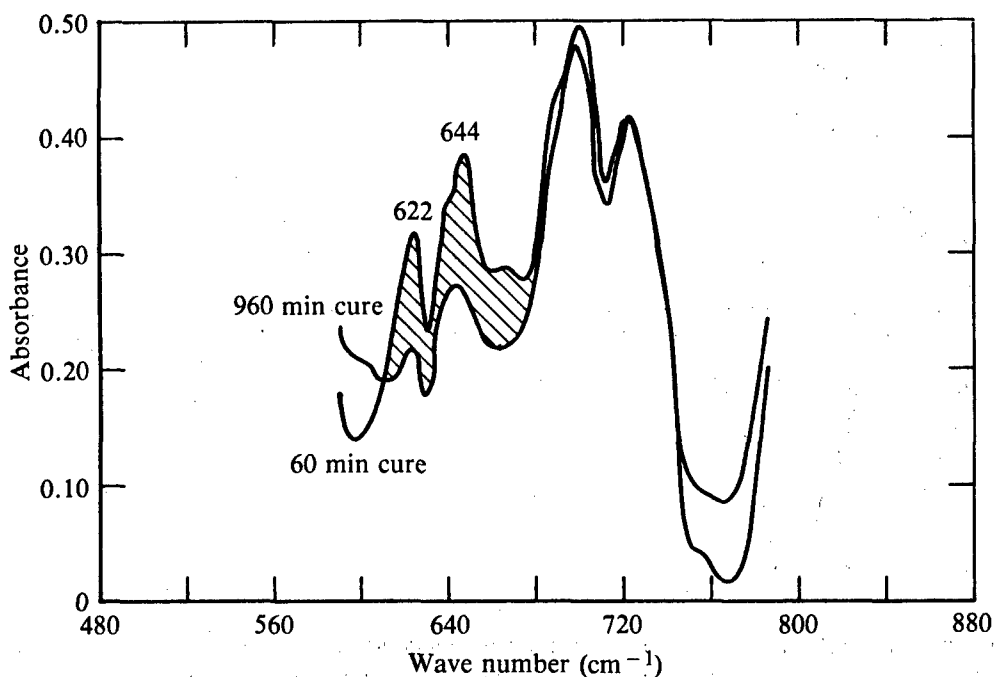


Figure 32. Superimposed FT-IR spectra of the $550 - 750\text{ cm}^{-1}$ region of ATS recorded after 60 min and 960 min cure at 423 K (302°F) showing the changes in the acetylenic-hydrogen wagging vibration (644 cm^{-1}). The shaded area accentuates the cure-induced changes in the spectra.

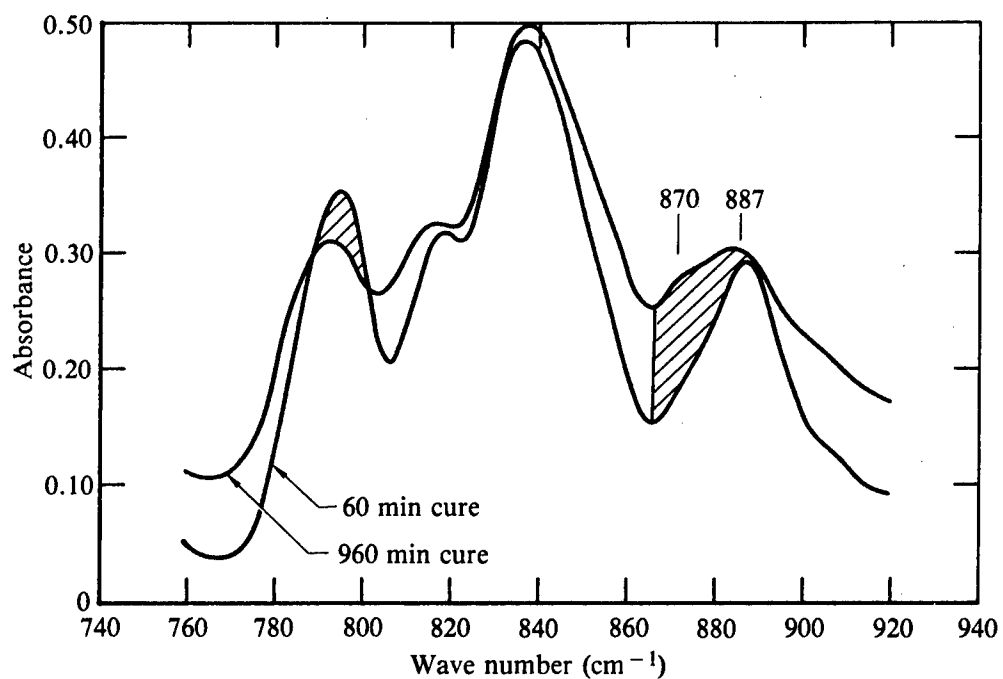


Figure 33. Superimposed FT-IR spectra of the 750 - 950 cm^{-1} region of ATS recorded after 60 min and 960 min cure at 423 K (302°F) showing the small changes in bands representing nonreactive moieties (aromatic hydrogen wag). The shaded areas accentuate the cure-induced changes in the spectra.

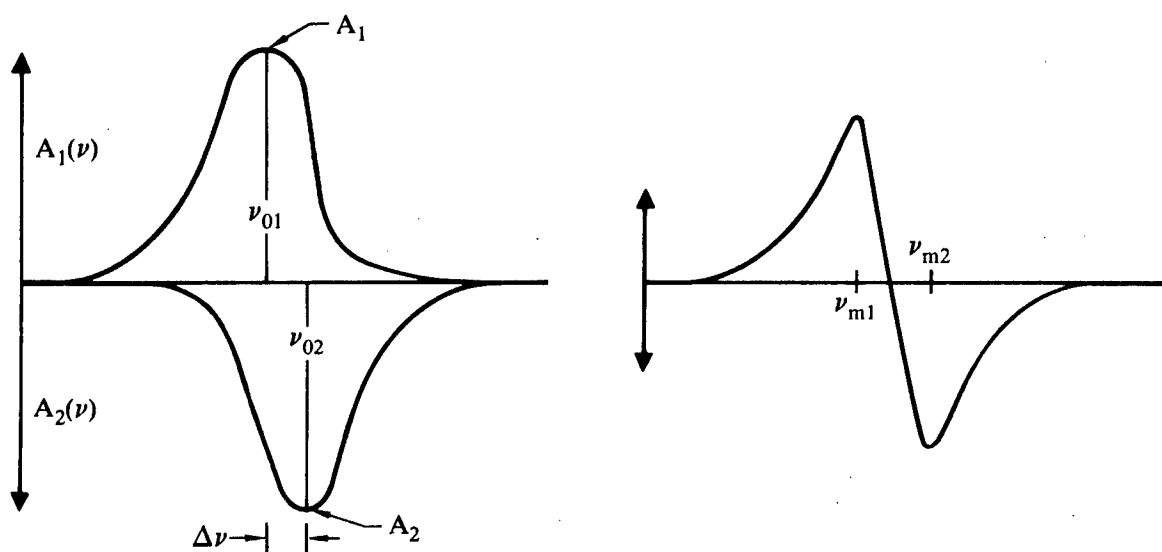


Figure 34. Schematic illustration of a frequency-shifted band; $A_1(\nu)$, $A_2(\nu)$, and the resulting spectral profile observed in its difference spectrum, $\Delta A(\nu)$.

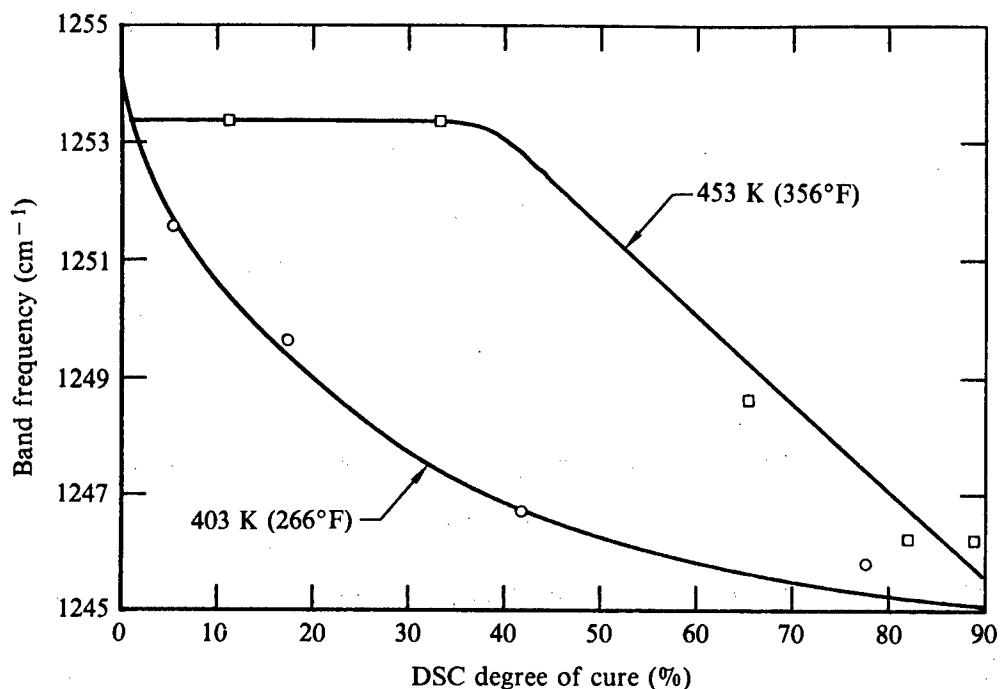


Figure 35. Band frequency of the aryl-ether band at 1250 cm^{-1} as a function of the ATS degree of cure for isothermal cure at 453 K (356°F) and 403 K (266°F).

the sulfone scissoring mode band at 575 cm^{-1} as a function of the degree of cure are shown in Figures 36 and 37. However, the potential of these shifts as parameters for characterization of ATS cure states was not investigated further.

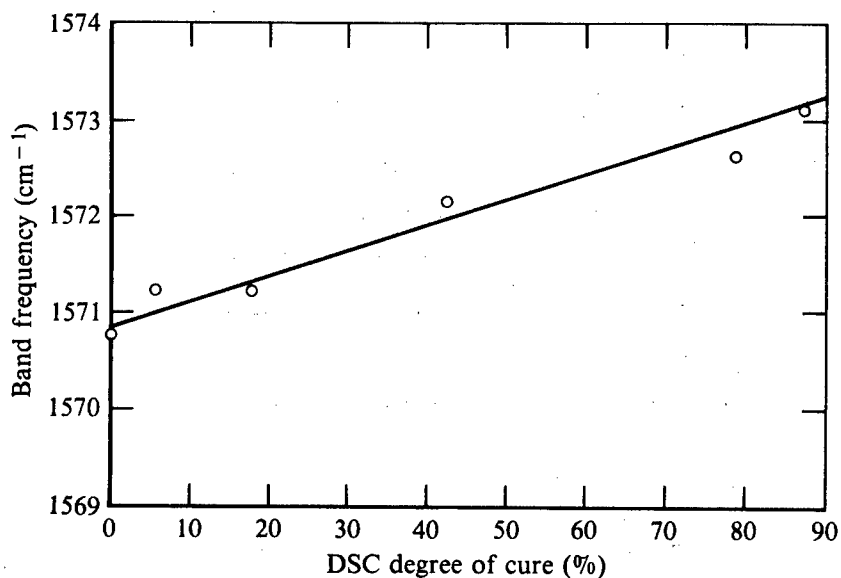


Figure 36. Band frequency as a function of degree of cure at 403 K (266°F) for the 1572 cm^{-1} band.

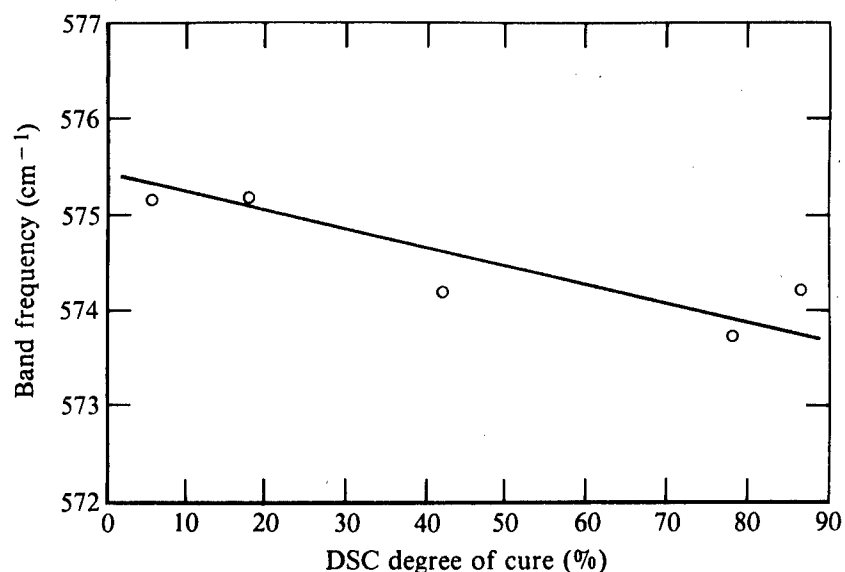


Figure 37. Band frequency as a function of degree of cure at 403 K (266°F) for the 575 cm⁻¹ band.

Band Ratios

As part of the search for sensitive IR parameters which characterize ATS cure states, all possible band ratios were plotted as function of the degree of cure. A typical band ratio as a function of degree of cure plot is shown in Figure 38 for the ratio of the 1489 and 1572 cm⁻¹ bands. This band ratio exhibits significant change up to DOC of approximately 35%, but little change for higher degrees of cure. Most other band ratios exhibited similar behavior and, therefore are not considered suitable for use as sensitive cure state parameters.

Spectral evidence that supports the intramolecular cyclization (IMC) mechanism¹⁷ can be found in the decrease of the 794/834 band ratio as a function of the degree of cure. The 794 cm⁻¹ band originates in the out-of-plane hydrogen wag for three adjacent hydrogen atoms in 1,3 disubstituted benzene rings, and the postulated IMC reaction would eliminate one of these three hydrogens. Since the decrease in the 794/834 band ratio is detectable from the beginning of the cure cycle, it can be concluded that the IMC reaction takes place during the early stages of the cure cycle.

Enyne Linkages

Experiments designed to investigate cure-induced spectral changes occurring in the very weak acetylene band at 2108 cm⁻¹ yielded some valuable information on the formation and consumption of enyne linkages. Transmission

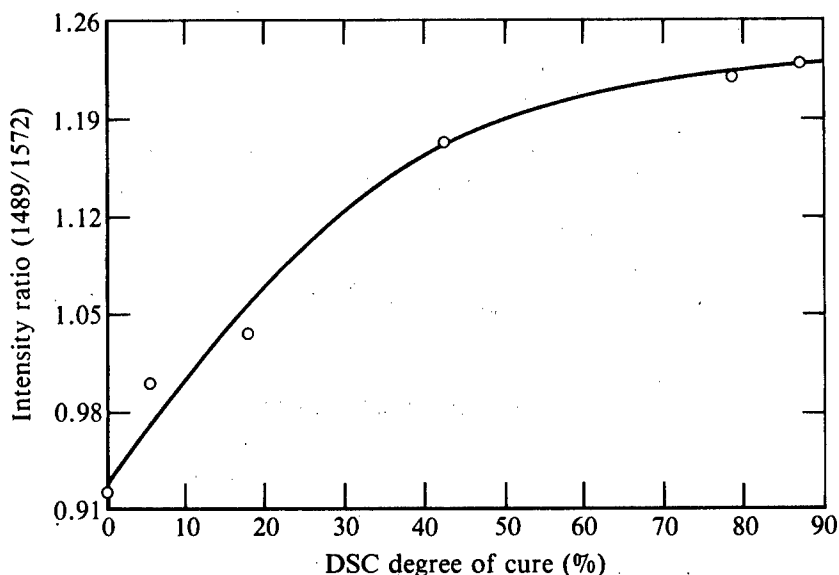


Figure 38. IR band ratios representing nonreactive ATS moieties as a function of the degree of cure for isothermal cure at 403 K (266°F).

FT-IR spectra of a relatively thick (0.4 mm) ATS oligomer film deposited between two KBr plates were recorded after 0, 60, 330, and 460 min of cure at 423 K (302°F). The use of a relatively thick ATS specimen permits observation of the 1900–2500 cm^{-1} region of the spectrum where a number of weak and overtone bands appear whereas all other IR bands reach saturation absorbances.

The superimposed FT-IR spectra recorded after 0, 60, 330, and 460 min of cure at 423 K (302°F) are shown in Figure 39. The observed decrease of the 2108 cm^{-1} band intensity corresponds to the consumption of the terminal acetylene groups. The intensity of the 2334 cm^{-1} band, which we tentatively assign to the chain (enyne) acetylene, initially increases (after 60 min cure) reflecting formation of enyne linkages. Following this initial stage, the concentration of enyne linkages appears to remain almost constant, possibly reflecting the consumption of enyne linkages in intramolecular cycloaddition (IMC) reactions¹⁷.

The superimposed difference spectra representing the 60-min cure minus before cure, the 330-min cure minus before cure, and the 460-min cure minus before cure (Figure 40) show the net cumulative change of the terminal acetylene and enyne acetylene during the different stages of cure. The superimposed difference spectra representing 60-min cure minus before-cure, 330-min cure minus 60-min cure, and 460-min cure minus 330-min cure (Figure 41) show

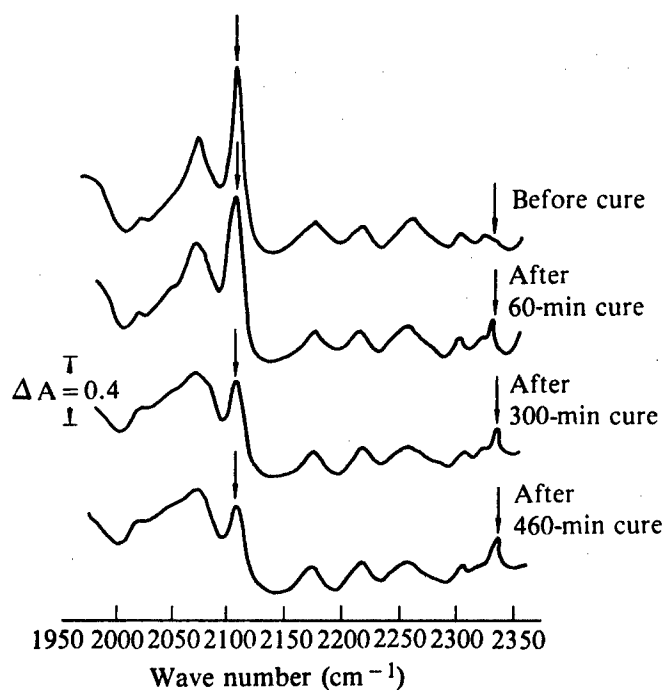


Figure 39. Superimposed FT-IR spectra of the 2000 - 2400 cm^{-1} region of ATS recorded before cure and after 60, 330, and 460 min of cure at 423 K (302°F) showing the consumption of terminal acetylene moiety (2108 cm^{-1}) and the appearance of the enyne moiety at 2334 cm^{-1} .

the net changes occurring during each stage of curing. The results shown in Figures 40 and 41 illustrate the steady-state concentration of enyne linkages following the initial stage of enyne formation.

ATS Degrees of Cure Derived from IR Data

The terminal acetylene groups of the ATS monomer react during cure via a number of simultaneous routes.² Thus, consumption of the terminal acetylene groups, which is directly reflected in the absorbance decreases of the acetylene bands at 3295 cm^{-1} and 941 cm^{-1} , can be used as a basis for determining the degree of cure. The three different methods for calculating DOC from IR absorbances are:

- (1) from normalized band areas of the acetylene band at 3295 cm^{-1} using $R_t(5) = (A_0 - A_t)/A_0 \times 100$, where R_t is the degree of isothermal cure after curing for a given period (t), A_0 is the band-area cure, and A_t is the band area after curing for a given period.
- (2) from normalized band areas of the acetylene band at 941 cm^{-1} plus the same expression for R_t , and

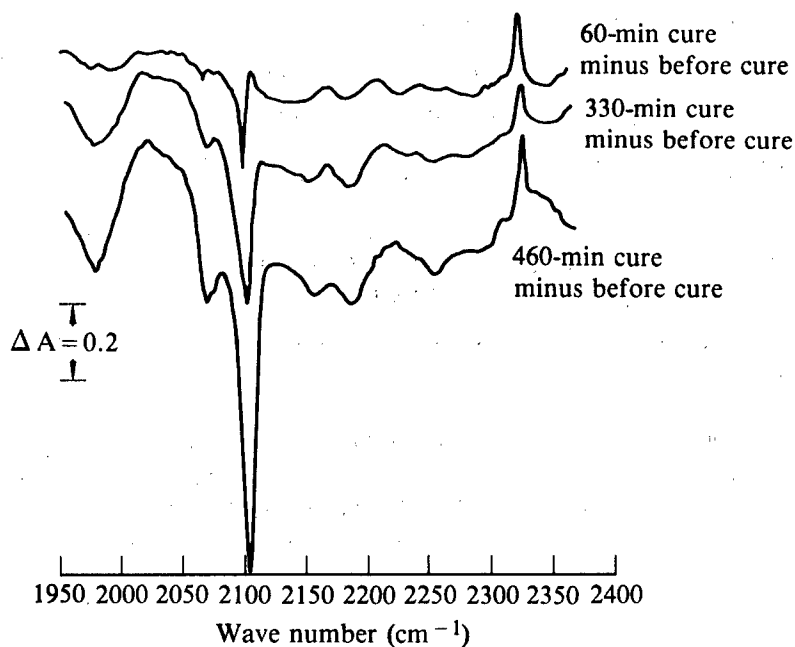


Figure 40. Superimposed difference FT-IR spectra of the 2000 - 2400 cm^{-1} region that represent the observed cumulative changes in consecutive stages of ATS curing at 423 K (302°F), showing the consumption of terminal acetylene 2108 cm^{-1} and the appearance of an enyne band at 2334 cm^{-1} .

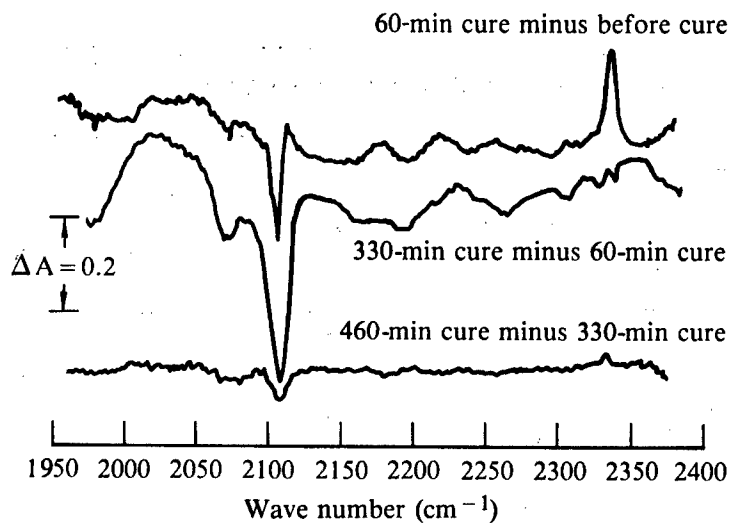


Figure 41. Superimposed difference FT-IR spectra of the 2000 - 2400 cm^{-1} region that represent the observed net changes between consecutive stages of ATS cure, showing that the enyne moiety formed in the initial stage does not increase, probably because of its consumption via intramolecular cyclization.

(3) from normalized band intensities (absorbance value at band maximum of the acetylene band at 3295 cm^{-1}).

The IR-derived DOC values determined for isothermal curing by the three different methods were compared with the DOC values derived by differential scanning calorimetry (DSC)¹³; the results are given in Tables 3-6.

TABLE 3.
IR BAND AREAS AS A FUNCTION OF CURE AT 403 K (266°F) FOR
NONREACTIVE MOIETIES OF ATS.

| Cure time (min) | DOC from IR 3295 cm^{-1} band area (%) | Aliphatic double bond 965 cm^{-1} | Aromatic C-H $3040\text{-}3210\text{ cm}^{-1}$ | Aromatic ring 1580 cm^{-1} | Aromatic ring $1460\text{-}1485\text{ cm}^{-1}$ |
|-----------------|---|--|--|-------------------------------------|---|
| 0 | 0 | 0.16 | 1.9 | 15.8 | 11.1 |
| 90 | 11.3 | 0.18 | 1.8 | 16.4 | 11.7 |
| 185 | 20.4 | 0.20 | 1.9 | 17.3 | 11.9 |
| 420 | 48.2 | 0.26 | 2.2 | 18.8 | 13.5 |
| 1300 | 62.1 | 0.27 | 2.4 | 19.0 | 14.0 |
| 2680 | 68.5 | 0.28 | 2.8 | 18.8 | 14.1 |

TABLE 4.
IR BAND AREAS AS A FUNCTION OF CURE AT 423 K (302°F) FOR
NONREACTIVE MOIETIES OF ATS.

| Cure time (min) | DOC derived from 3295 cm^{-1} acetylene band (%) | Aliphatic double bond 965 cm^{-1} | Aromatic ring $1460\text{ - }1485\text{ cm}^{-1}$ | Aromatic ring 1580 cm^{-1} | Aromatic C-H $3040\text{ - }3120\text{ cm}^{-1}$ |
|-----------------|---|--|---|-------------------------------------|--|
| 0 | 0 | 0.84 | 33.5 | 41.2 | 4.9 |
| 20 | 6.4 | 0.97 | 30.3 | 37.9 | 4.9 |
| 40 | 10.9 | 0.86 | 33.1 | 41.3 | 4.6 |
| 51 | 15.9 | 0.92 | 31.3 | 39.9 | 4.5 |
| 60 | 17.6 | 0.98 | 31.9 | 39.9 | 4.8 |
| 70 | 18.9 | 1.00 | 30.1 | 38.0 | 4.6 |
| 80 | 20.0 | 1.01 | 29.9 | 38.8 | 4.6 |
| 120 | 28.2 | 1.08 | 32.7 | 40.4 | 4.9 |
| 180 | 62.3 | 0.80 | 29.3 | 35.7 | 3.7 |
| 240 | 65.3 | 0.72 | 38.4 | 47.9 | 4.1 |
| 320 | 76.2 | 0.7 | 38.1 | 48.1 | 3.9 |
| 420 | 73.5 | 0.76 | 37.1 | 46.9 | 4.7 |
| 780 | 81.7 | 0.79 | 37.4 | 46.9 | 4.0 |
| 960 | 83.8 | 0.99 | 37.5 | 48.3 | 4.1 |

TABLE 5.
COMPARISON OF DOC VALUES DERIVED BY DIFFERENT
METHODS FOR ATS CURE AT 403 K (266°F).

| Cure time (min) | DSC (%) | DOC derived by 3295 cm ⁻¹ band area (%) | DOC from IR 941 cm ⁻¹ band area (%) | DOC from IR 3295 cm ⁻¹ band maximum (%) |
|-----------------------|------------|--|--|--|
| 0 | 0 | 0 | 0 | 0 |
| 90 | 5.5 | 11.3 | 13.4 | 16.7 |
| 185 | 17.5 | 20.4 | 22.8 | 22.2 |
| 420 | 41.9 | 48.2 | 51.0 | 55.6 |
| 1300 | 78.0 | 62.1 | 64.9 | 66.7 |
| 2680 | 86.3 | 68.5 | 69.8 | 72.2 |

TABLE 6.
COMPARISON OF DOC VALUES DERIVED BY DIFFERENT
METHODS FOR ATS CURE AT 453 K (356°F).

| Cure time (min) | DOC derived by DSC (%) | DOC from IR 941 cm ⁻¹ band area (%) | DOC from IR 3295 cm ⁻¹ band area (%) |
|-----------------------|---------------------------------|--|---|
| 0 | 0 | 0 | 0 |
| 5 | 11.2 | 17.7 | 26.4 |
| 10 | 33.7 | 31.1 | 33.9 |
| 20 | 65.5 | 47.0 | 49.4 |
| 30 | 82.3 | 59.7 | 62.1 |
| 40 | 89.1 | 66.2 | 66.6 |
| 60 | 91.2 | 72.3 | 71.4 |

The three different IR values for DOC (Table 5) are in fair agreement, and the two sets of values based on the band areas are in good agreement. The considerably higher DOC values derived by DSC (Tables 5-6) could possibly be attributed to secondary curing reactions other than those that involve the acetylene groups, i.e., the intramolecular cycloaddition (IMC) reaction¹⁷ as illustrated in Figure 42.

A comparison of DOC values for cure at 453 K (Table 6) shows a discrepancy between the DSC and the IR values. The extent of discrepancy for the advanced stages of curing is significant; the differences are greater at higher cure temperatures, possibly reflecting the greater extent of IMC¹⁷ and other nonacetylenic reactions that can occur at elevated temperatures.

The degrees of cure determined from the average of the DOC values derived from the 941 cm^{-1} and the 3295 cm^{-1} acetylene band areas is plotted as function of the cure times for the three isothermal cures in Figure 43.

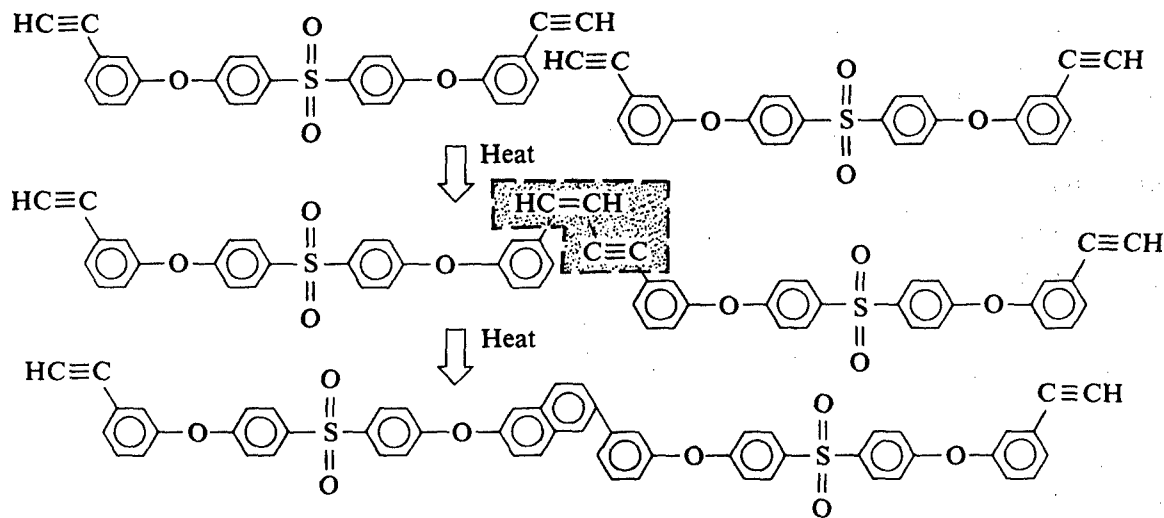


Figure 42. Postulated cure reactions of ATS resin indicating formation of enyne linkages as an intermediate step to intramolecular cyclization.

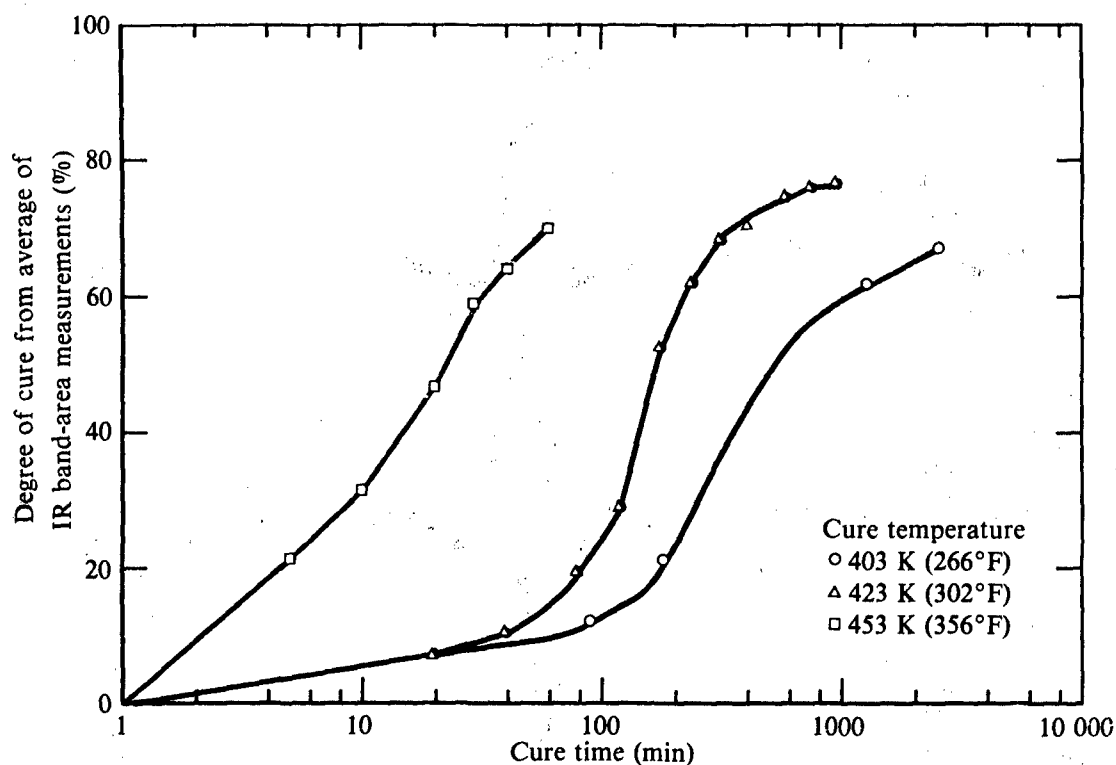


Figure 43. Degree of cure determined from the average of 941 cm^{-1} and 3295 cm^{-1} IR band-area measurements for the three different isothermal cures of ATS samples.

2. POSTCURE RESULTS

a. NMR Postcure Results

Postcure studies of ATS samples incompletely cured at 423 K (302°F) and 453 K (356°F) have been performed, as shown in Table 1. Magic-angle spinning ^{13}C NMR spectra were obtained and analyzed, as shown in Figures 44 and 45. The spectra of the samples before postcuring show the decrease in intensity of the upfield acetylene resonance peak as the curing time is increased. The relative areas beneath the acetylene peaks are in agreement with previous measurements. The spectra of the postcured samples do not contain the acetylene resonance peak. Analysis of the spectra of the postcured ATS samples cured and postcured at different temperatures have revealed no significant differences. This implies there were no significant differences in the chemical structures of the postcured ATS samples for the cure times and the postcure temperatures used in these experiments.

It was observed that ATS samples that were postcured without prior curing at low temperature contained numerous voids, presumably the result of rapid outgassing.

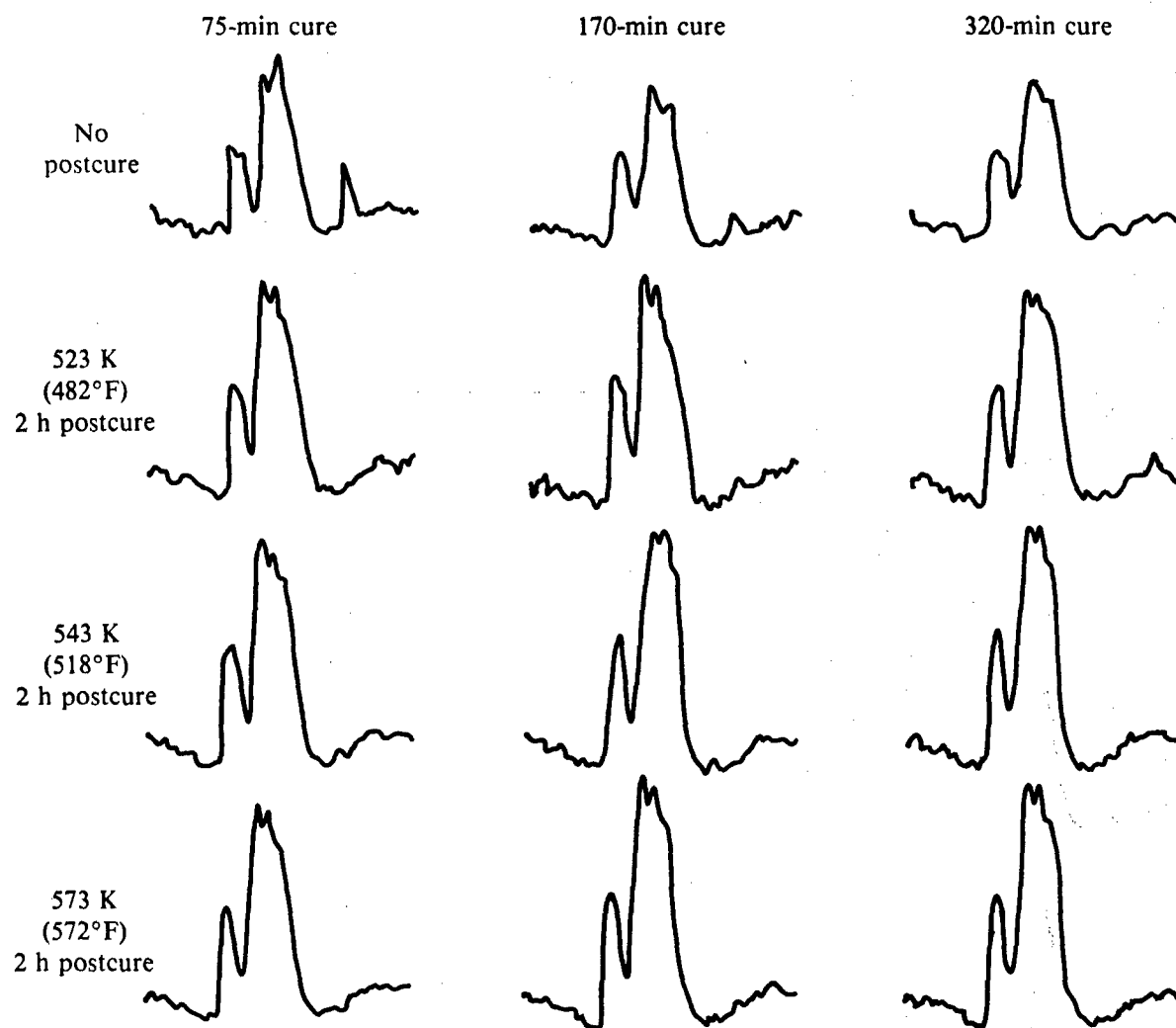


Figure 44. ^{13}C NMR spectra of ATS resin samples cured at 423 K (302°F) for the indicated times followed by a postcure for 2 h at the indicated temperatures.

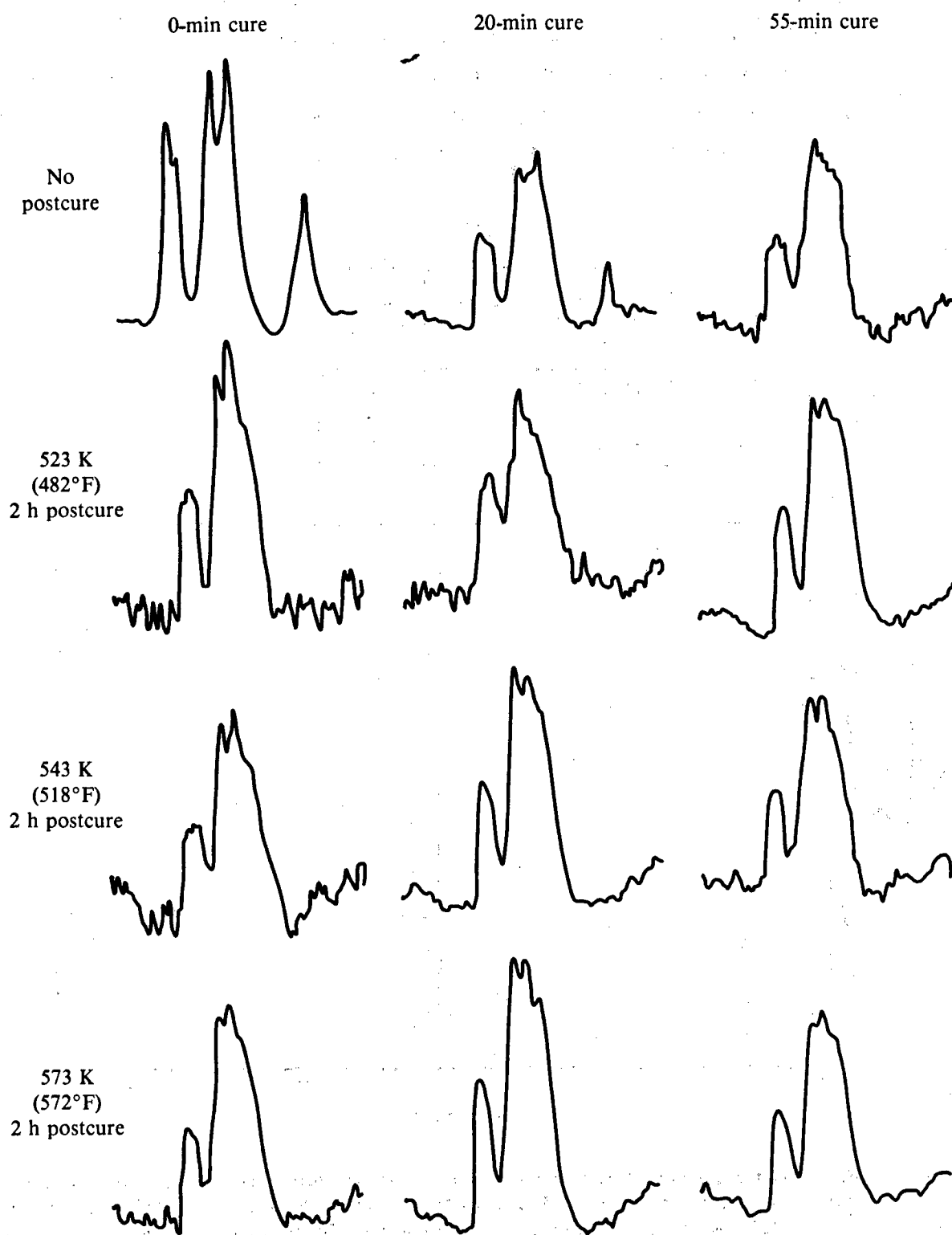


Figure 45. ^{13}C NMR spectra of ATS resin samples cured at 453 K (356°F) for the indicated times followed by a postcure for 2 h at the indicated temperatures.

b. EPR Postcure Results

In addition to the EPR studies of isothermally cured of ATS, studies of postcured samples were initiated. The samples examined were cured and postcured according to the schedule shown in Table 1. Spectral intensities were recorded both prior to and following postcuring. The results for the samples postcured at 523 K (482°F) and 543 K (518°F) are shown in Figures 46 and 47, respectively.

| Cure temperature [K (°F)] | Before postcure | After postcure |
|------------------------------|--------------------|-------------------|
| 403 (266) | ○ | ● |
| 423 (302) | △ | ▲ |
| 453 (356) | □ | ■ |

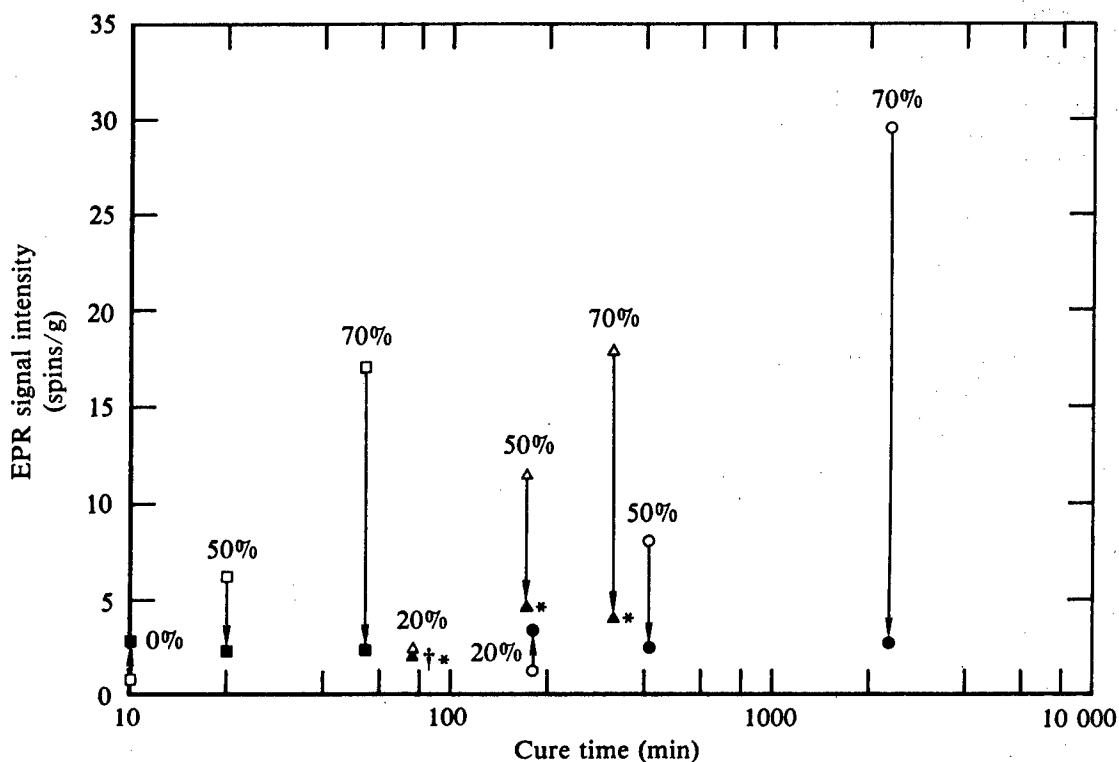


Figure 46. Radical concentrations of cured ATS samples before and after postcuring at 523 K (482°F). Cure temperatures and percents of cure (as determined by IR) are as indicated. The samples cured to 50% or above lose intensity upon postcuring. The uncured sample (0%) should have a higher value for radical concentration following postcure; however, it could not be determined because much of the sample was outside the EPR cavity. (†) sample broke open during postcuring; (*) these samples were not postcured in flowing nitrogen.

| Cure temperature [K (°F)] | Before postcure | After postcure |
|---------------------------|-----------------|----------------|
| 403 (266) | ○ | ● |
| 423 (302) | △ | ▲ |
| 453 (356) | □ | ■ |

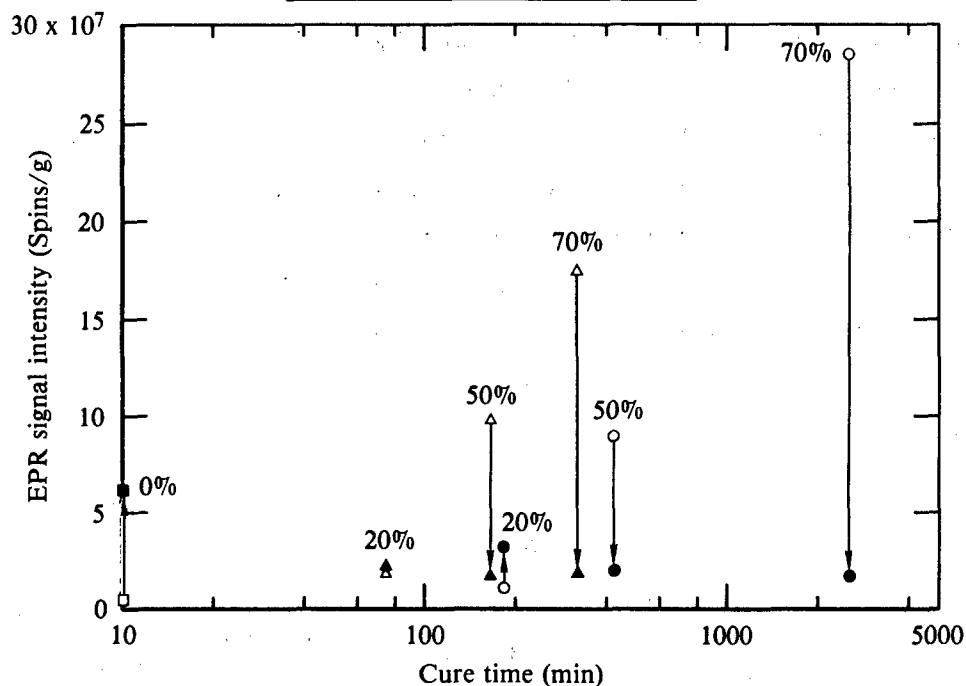


Figure 47. Radical concentrations of cured ATS samples before and after postcuring at 543 K (518°F). Cure temperatures and percents of cure (as determined by IR) are as indicated. The samples cured to 50% or above lose intensity upon postcuring, whereas the samples cured to 20% or below gain intensity. In particular, the uncured sample (0%) showed a significant increase in intensity (to more than $\sim 6 \times 10^{17}$ spins/g) upon postcuring.

Prior to postcuring, the EPR spectral intensities were consistent with the data obtained during the isothermal curing studies, i.e., the data fell on or near the curves shown in Figures 21 and 22. The spectral intensities of samples cured to $> 50\%$ of full cure decreased in intensity upon postcuring to a spin concentration value of $\sim 5 \times 10^{17}$ spins/g. In contrast to this, EPR signals from the samples cured to $< 20\%$ of full cure increased in intensity following postcuring; moreover, the samples having the lowest radical concentration prior to postcuring had the greatest radical concentration following postcuring (6×10^{17} spins/g).

It appears, therefore, that there is a complicated process involving competition between radical production and destruction at the postcure tem-

peratures, and that the number of radicals remaining in a sample following postcuring may depend on the extent of network development prior to postcuring.

The EPR linewidths of all samples decreased as a result of the postcuring process, and some samples produced spectra that appeared to be superpositions of two separate component spectra having different linewidths (see Figure 48). Thus, for example, the linewidths of samples that had attained at least 50% cure at 403K (266°F) or 453 K (356°F) were typically 1.2-1.4 mT prior to postcuring and about 1 mT following postcuring at 523 K (482°F). An uncured sample subjected to postcuring at 523 K (482°F) produced an EPR spectrum having a linewidth of 0.69 mT, and a sample cured 20% at 403K (266°F) changed in linewidth from 1.16 mT to 0.81 mT upon postcuring at 523 K (482°F). The latter spectrum appeared to be a superposition of two separate component spectra, one having a linewidth on the order of 0.7 mT and the other on the order of 1.0-1.2 mT.

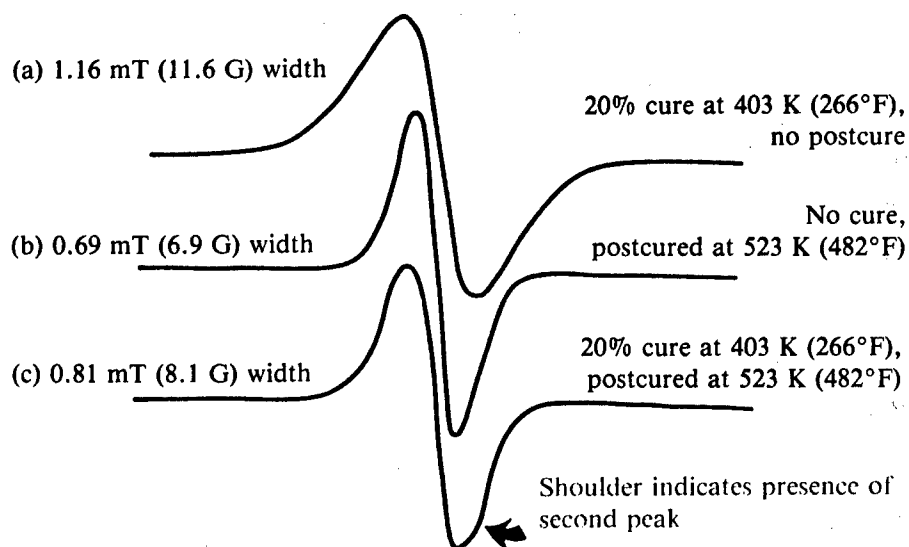


Figure 48. EPR spectra observed during curing/postcuring of selected ATS samples. Uncured and unpostcured samples have a background signal with a linewidth of ~ 1.05 mT. Curing causes linewidth to increase with increasing radical concentration: 20% cure at 403 K (266°F) produces a 1.16 mT line, (a). High-temperature curing (523 K, 482°F) produces a much narrower line (~ 0.69 mT), (b). Spectra from samples cured to $\sim 20\%$ at low temperature and subsequently postcured at high temperatures show the presence of two superimposed spectral components of different linewidth, (c).

Therefore, some of the postcured samples produced both the broad spectrum that is normally observed upon postcuring and an additional narrow line. Two types of radical species thus seem to be present in some postcured samples. The species may differ in environment or structure.

The anomalous narrow line 0.7 mT (~ 7 G) cannot be explained exclusively in terms of reduced electron-electron dipolar interactions resulting from reduced overall radical concentrations in the samples in question; ATS samples having even lower radical concentrations can produce EPR spectra having linewidths of over 1 mT. Possible sources of differences in linewidths in samples having the same radical concentrations include radical clustering and differences in electron delocalization, or the number of magnetic nuclei encountered by electrons for a given delocalization.

c. IR Postcure Results

Several series of experiments were performed to obtain IR parameters from ATS specimens subjected to postcure heating. The specimens used in these series of experiments were the same specimens used for deriving NMR parameters which are described in Section III 2(a). Three distinctly different postcure schemes were studied. The main FT-IR results for the three postcure series are individually summarized in Tables 7-9. It is apparent from these measurements that postcure heating leads to an almost total consumption of the acetylenic moieties, which yields apparent degrees of cure close to or greater than 98.5%.

In a search for other IR parameters which could aid the characterization of network features of postcured ATS specimens, we examined the variability of band area ratios as a function of postcuring. These ratios, given in Table 8, show that no significant changes in the relative band intensities of the aromatic, aryl ether, and sulfone moieties occur as a result of postcure heating.

TABLE 7.
FT-IR RESULTS OF 453 K (356°F) CURE OF ATS FOLLOWED BY 120 MIN
POSTCURE AT 523 K (482°F), 543 K (518°F), AND 573 K (572°F).

| Sample no. | Cure time at 453 K (356°F) (min) | Postcure temp [K (°F)] | Acetylene band area 3295 cm ⁻¹ | Degree of cure (%) | Aromatic C-H stretch 3040-3120 cm ⁻¹ |
|------------|----------------------------------|------------------------|---|--------------------|---|
| 25 | 0 | 523 (482) | 0.20* | 98.5* | 2.2 |
| 26 | 0 | 543 (518) | 0.20* | 98.5* | 2.2 |
| 27 | 0 | 573 (572) | 0.20* | 98.5* | 2.2 |
| 28 | 20 | — | 3.41 | 55.5 | 1.9 |
| 29 | 20 | 523 (482) | 0.30 | 97.0 | 1.9 |
| 30 | 20 | 543 (518) | 0.20* | 98.5* | 2.2 |
| 31 | 20 | 573 (572) | 0.20* | 98.5* | 2.1 |
| 32 | 55 | — | 1.80 | 76.5 | 2.1 |
| 33 | 55 | 523 (482) | 0.20* | 98.5* | 2.0 |
| 34 | 55 | 543 (518) | 0.20* | 98.5* | 2.2 |
| 35 | 55 | 573 (572) | 0.20* | 98.5* | 1.9 |

*Band area < 0.2; DOC > 98.5%

TABLE 8.
FT-IR RESULTS OF 423 K (302°F) CURE AT VARIOUS TIMES FOLLOWED BY A
120 MIN POSTCURE AT 523 K (482°F), 543 K (518°F), AND 573 K (572°F)

| Sample no. | Cure time (min) | Postcure temperature [K (°F)] | Acetylene band area 3295 cm ⁻¹ | DOC % derived from 3295 cm ⁻¹ | Band area ratios | | | |
|------------|-----------------|-------------------------------|---|--|--|--------------------|---|---|
| | | | | | Sulfone Aromatic 1495 cm ⁻¹ | Sulfone Aryl ether | Aromatic 1495 cm ⁻¹ / Aromatic 1595 cm ⁻¹ | Aromatic 1495 cm ⁻¹ / 833 cm ⁻¹ |
| 12 | 75 | none | 6.2 | 19.5 | 1.3 | 0.64 | 1.07 | 2.62 |
| 13 | 75 | 523 (482) | 0.3 | 96.2 | 1.2 | 0.80 | 1.17 | 2.34 |
| 14 | 75 | 543 (518) | 0.1 | 98.6 | 1.3 | 0.77 | 1.14 | 1.96 |
| 15 | 75 | 573 (572) | 0.2 | 97.8 | 1.4 | 0.78 | 1.06 | 2.53 |
| 16 | 170 | none | 2.8 | 56.6 | 1.3 | 0.81 | 1.21 | 2.27 |
| 17 | 170 | 523 (482) | 0.2 | 97.8 | 1.3 | 0.81 | 1.17 | 2.30 |
| 18 | 170 | 543 (518) | 0 | 100.0 | 1.3 | 0.80 | 1.14 | 2.26 |
| 19 | 170 | 573 (572) | 0 | 100.0 | 1.3 | 0.79 | 1.11 | 2.50 |
| 20 | 320 | none | 1.7 | 76.2 | 1.3 | 0.81 | 1.19 | 2.55 |
| 21 | 320 | 523 (482) | 1.2 | 84.0 | 1.4 | 0.83 | 1.11 | 2.74 |
| 22 | 320 | 543 (518) | 0 | 100.0 | 1.3 | 0.82 | 1.17 | 2.30 |
| 23 | 320 | 573 (572) | 0 | 100.0 | 1.4 | 0.81 | 1.17 | 2.58 |

TABLE 9.
ATS 573 K (572°F) POSTCURE SERIES NORMALIZED IR BAND AREAS AS A FUNCTION
OF CURE TIME AND TEMPERATURE (DEGREE OF CURE).

| Cure time (min) | Cure temperature [K (°F)] | Postcure temperature [K(°F)] | Degree of cure from 3295 cm ⁻¹ (%) | Aliphatic double bond 965 cm ⁻¹ | Aromatic ring 1460-1485 cm ⁻¹ | Aromatic ring 1580 cm ⁻¹ | Aromatic C—H 3040-3120 cm ⁻¹ |
|-----------------------|---------------------------------|------------------------------------|--|--|--|---|---|
| 0 | — | — | 0 | 0.53 | 22.9 | 28.4 | 2.9 |
| 50 | 453(356) | None | 79.7 | 0.66 | 24.5 | 31.2 | 3.2 |
| 50 | 453(356) | 573(572) | 100 | 1.23 | 22.0 | 28.7 | 3.0 |
| 800 | 423(302) | None | 86.3 | 0.81 | 22.8 | 29.6 | 3.2 |
| 800 | 423(302) | 573(572) | 100 | 1.24 | 22.1 | 28.7 | 2.9 |
| 7200 | 403(266) | None | 85.5 | 0.58 | 23.7 | 30.2 | 3.5 |
| 7200 | 403(266) | 573(572) | 100 | 1.04 | 21.7 | 28.6 | 3.2 |

IV. CURE-STATE PARAMETERS

1. SELECTION OF SPECTROMETRIC CURE-STATE PARAMETERS

The various spectrometric parameters that were obtained from ATS samples in various stages of cure were examined for their utility in characterizing the cure state of ATS. First, the parameters were compared to test for their independence. Second, the parameters that were not independent were eliminated from further consideration; from a group of dependent parameters, the ones eliminated were those subject to the greatest measurement errors or most difficult to measure. In some cases, in particular the IR parameters, two dependent parameters were averaged to obtain a parameter having less measurement error.

Figures 49-52 show how the independence of the parameters was determined. In these figures, one parameter is plotted against the other for the three isothermal cures. Figure 49 shows ^{13}C NMR parameters and EPR parameters and it clearly demonstrates their independence. While both parameters are related to the cure process, they have a different dependence because the ^{13}C parameter measures the concentration of acetylene carbons (or carbons associated with a triple bond), whereas the EPR parameter measures the free radical concentration. The data clearly show that the acetylene carbon concentration is not a simple, single-valued function of the free radical concentration; it is also a function of the cure temperature. Thus, if the constant time lines had been plotted in Figure 49, it would be possible to determine both the cure time and temperature from the independent ^{13}C NMR and EPR cure parameters. A similar independence is shown in Figure 50 for the ^{13}C NMR and IR parameters; Figure 51 shows the independence of the IR and EPR parameters. The IR parameters plotted in Figures 50 and 51 are averages of the degree of cure obtained from two acetylene bands, 941 cm^{-1} and 3295 cm^{-1} .

Figure 52 illustrates two parameters that are not sufficiently independent to justify retaining them both as independent cure-state parameters. The reason for the dependence of the ^1H NMR spin-lattice relaxation time, T_1 , and the EPR free radical concentration was discussed in Section III 1.a.

Two other parameters were examined for independence in Section III 1.b., the EPR intensity and EPR derivative linewidth (Figure 26). Because the linewidth increased linearly with intensity, it was determined that these two parameters were not independent. However, postcure studies discussed in

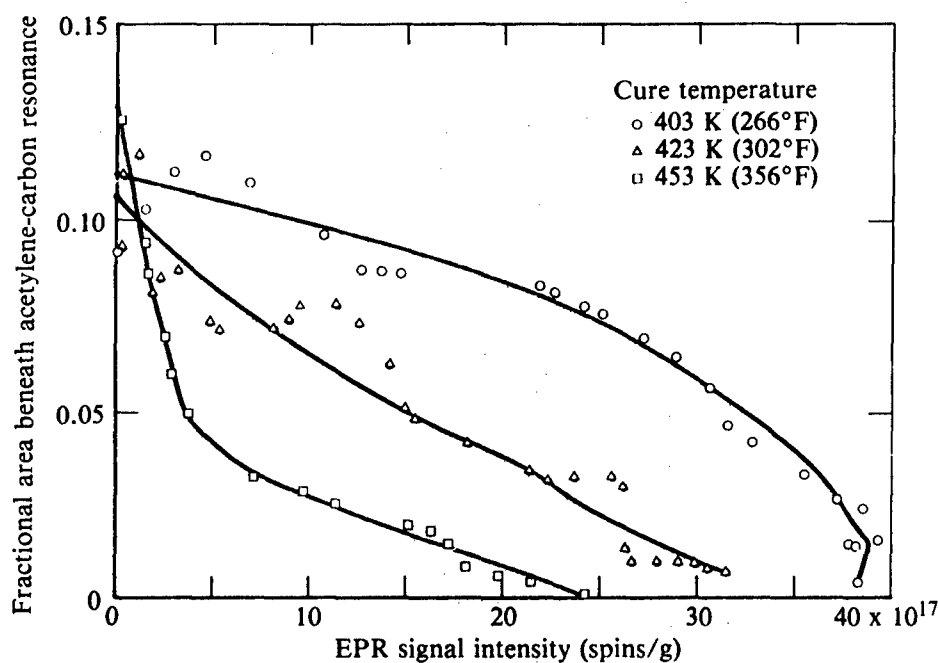


Figure 49. Comparison showing independence of ^{13}C NMR and EPR parameters. The data for samples cured at different temperatures follow different curves, indicating that these parameters are independent. Thus, for any particular degree of cure determined by NMR, the EPR signal intensity is different for different cure temperatures.

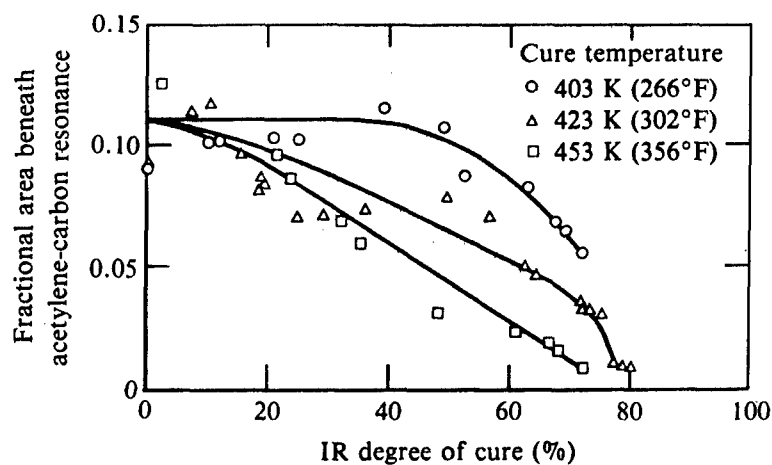


Figure 50. Comparison between ^{13}C NMR and IR parameters.

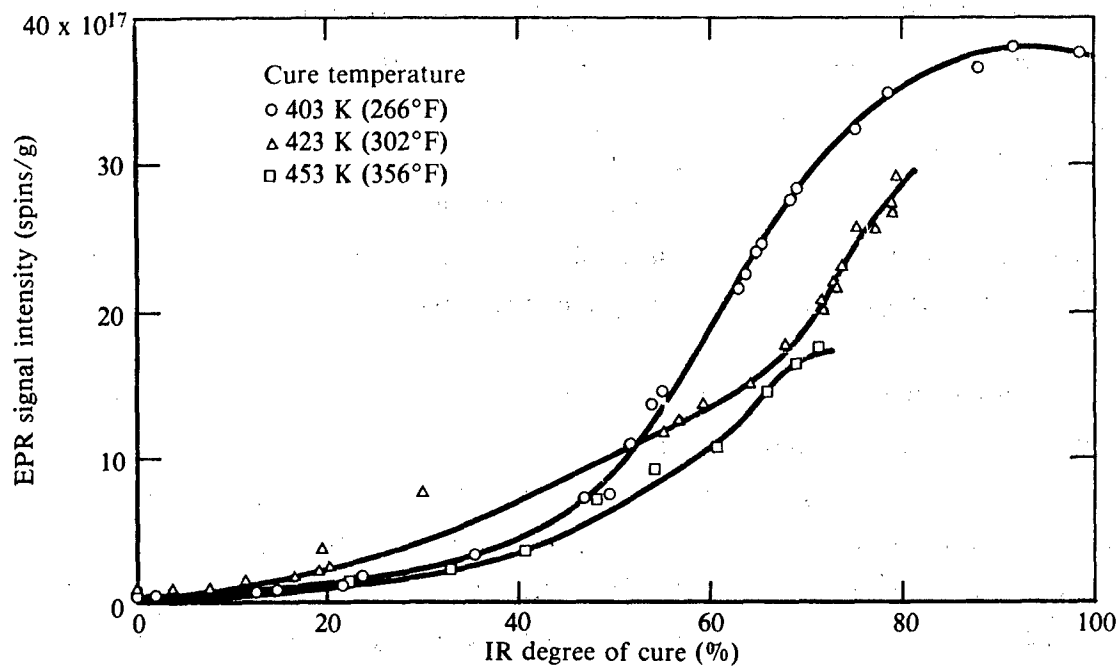


Figure 51. EPR signal intensity (spins/g) as a function of degree of cure as determined by IR acetylene-band intensities. EPR and IR data for different cure temperatures follow separate curves above $\sim 70\%$ cure.

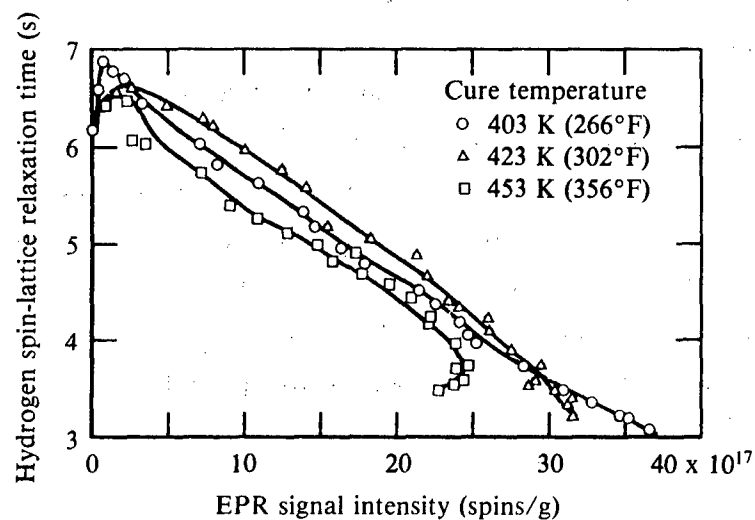


Figure 52. Comparison showing that ^1H spin-lattice relaxation and EPR signal intensity are closely related. Early in the cure process, when the radical concentration is low, T_1 increases because of increasing sample viscosity. Later, as the radical concentration increases, T_1 becomes shorter.

Section III 2.b. have shown that the linewidth can be an independent parameter that is sensitive to conditions just prior to postcuring.

Thus, the primary cure-state parameters are:

- (1) the ^{13}C NMR acetylene relative area,
- (2) the EPR signal intensity, and
- (3) the IR acetylene-band degree-of-cure measurements.

The EPR linewidth constitutes an additional parameter whose utility is being studied for characterizing postcured samples.

2. COMPARISON BETWEEN THE SPECTROMETRIC CURE STATE PARAMETERS AND THE MECHANICAL AND THERMAL PROPERTIES

The tensile strengths at 296 K (73°F),²⁰ the fracture energies at 296 K (73°F),²¹ and glass transition temperatures²¹ of ATS resin at various stages of isothermal cures at 403 K (266°F), 423 K (302°F), and 453 K (356°F) were plotted as a function of ^{13}C NMR, ^1H NMR, EPR, and FT-IR cure-state parameters, as shown in Figures 53-64. In these figures, it was intended to construct the iso-time lines, but because the curing at these three isothermal temperatures occurred in virtually nonoverlapping time periods, this was not done. Instead, the cure times are shown on the curves as running parameters; the reader can construct individual iso-time curves by connecting the iso-time points where time overlaps occur.

As previously noted, the EPR signal intensity and ^1H NMR spin-lattice relaxation time measurements are not independent. If one were to compare Figures 54 and 55, 58 and 59, and 62 and 63 by placing the pairs of figures face to face and viewing them with backlighting, the corresponding curves would be seen to very nearly fall on top of one another. This proves the accuracy of these two measurements and supports our decision to terminate the ^1H NMR measurements because they provided insignificant additional information.

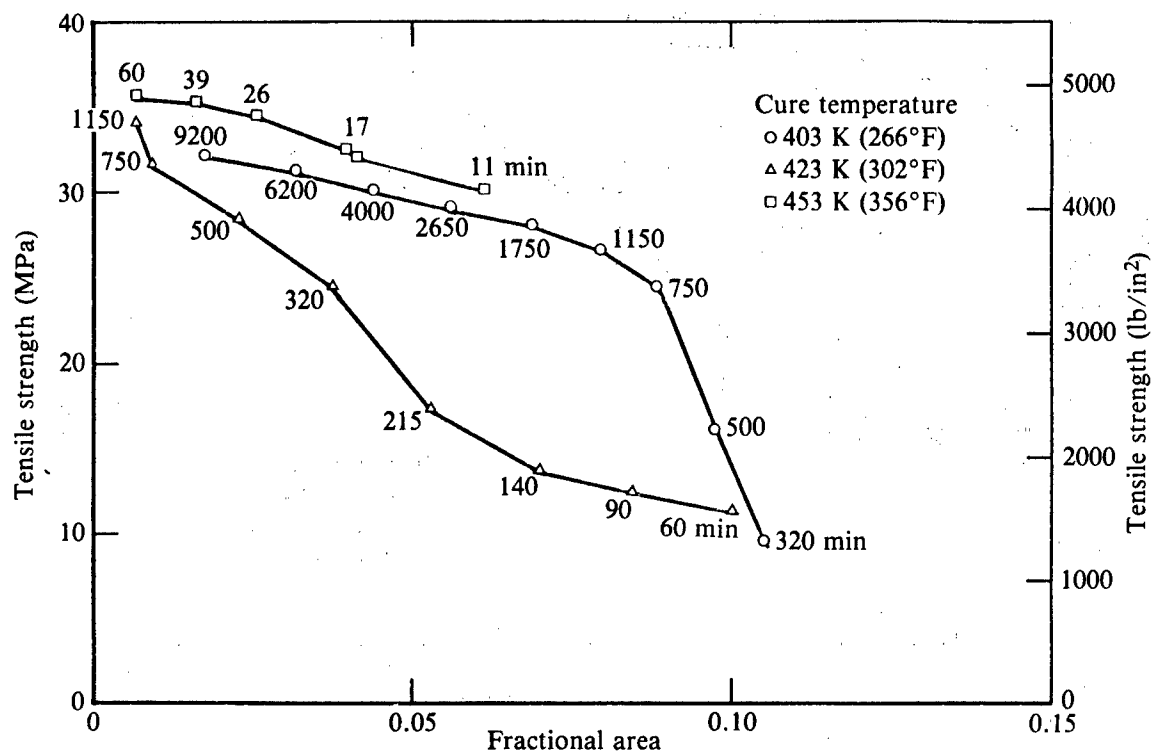


Figure 53. Tensile strength of ATS at 23°C as a function of ^{13}C NMR parameter (area beneath acetylene peak) for three different isothermal cures. Cure times are indicated.

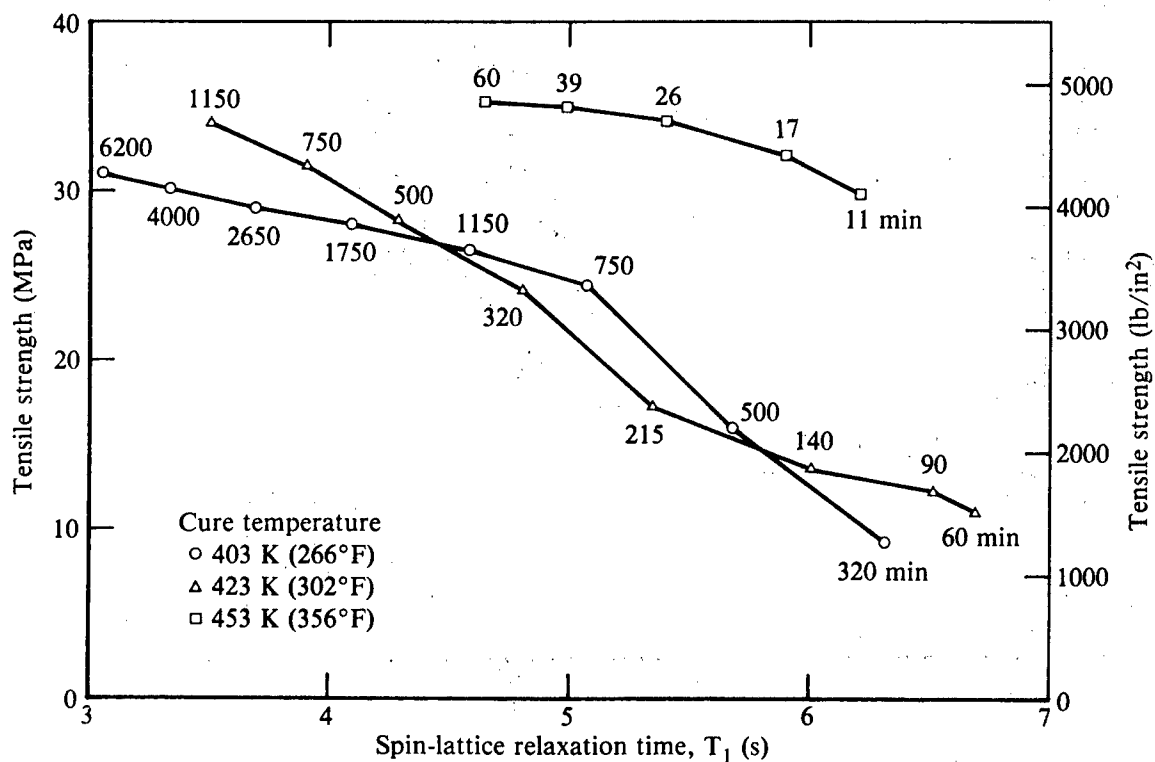


Figure 54. Tensile strength of ATS at 23°C as a function of ^1H NMR parameter (spin-lattice relaxation time) for three different isothermal cures. Cure times are indicated.

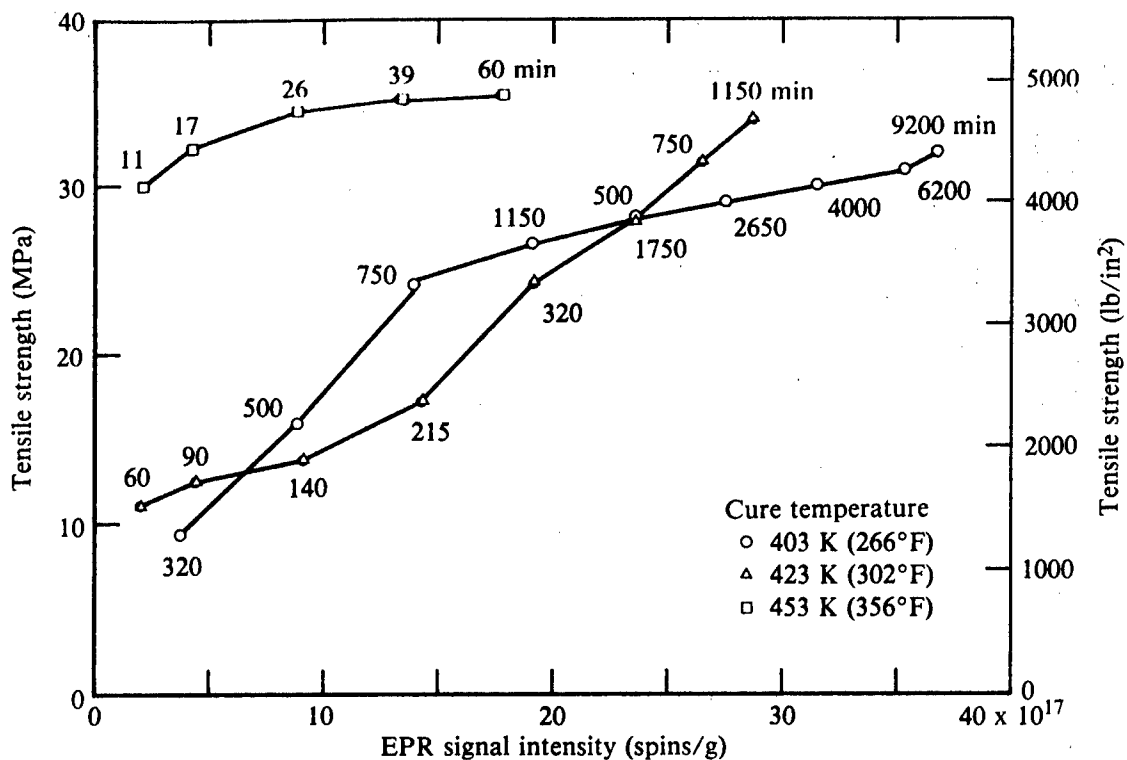


Figure 55. Tensile strength of ATS at 296 K (73°F) as a function of EPR parameter (signal intensity) for three different isothermal cures. Cure times are indicated.

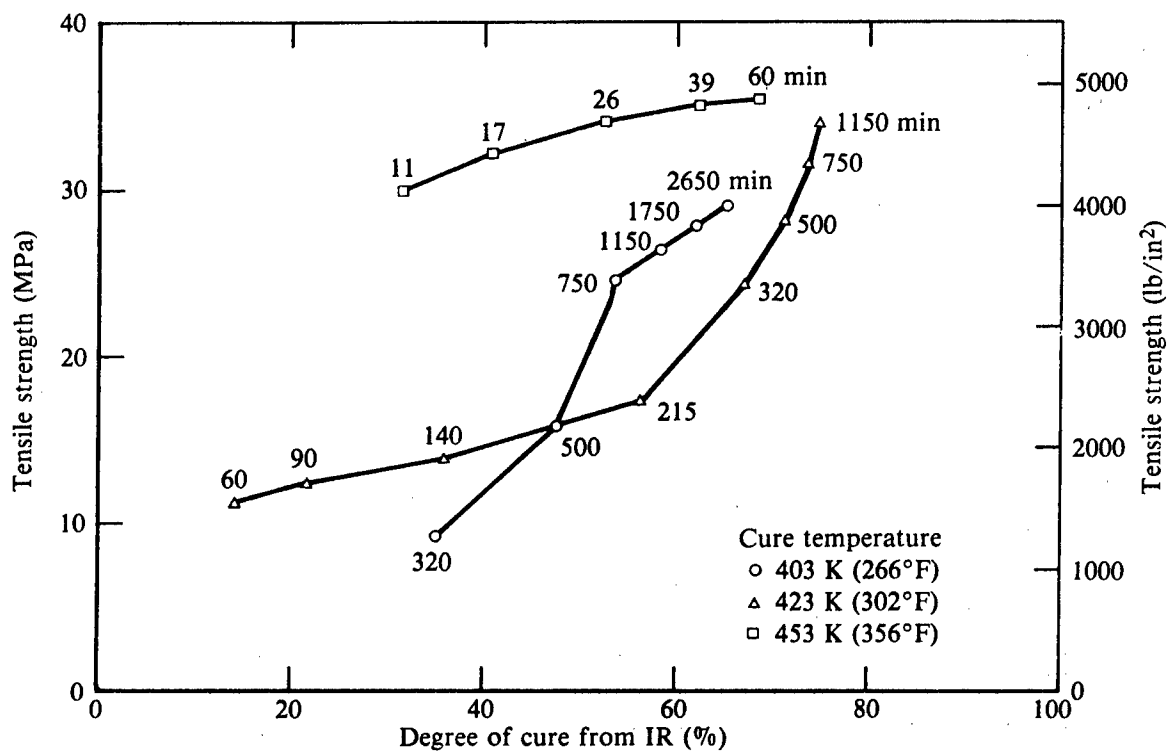


Figure 56. Tensile strength of ATS at 23°C as a function of IR parameter (degree of cure) for three different isothermal cures. Cure times are indicated.

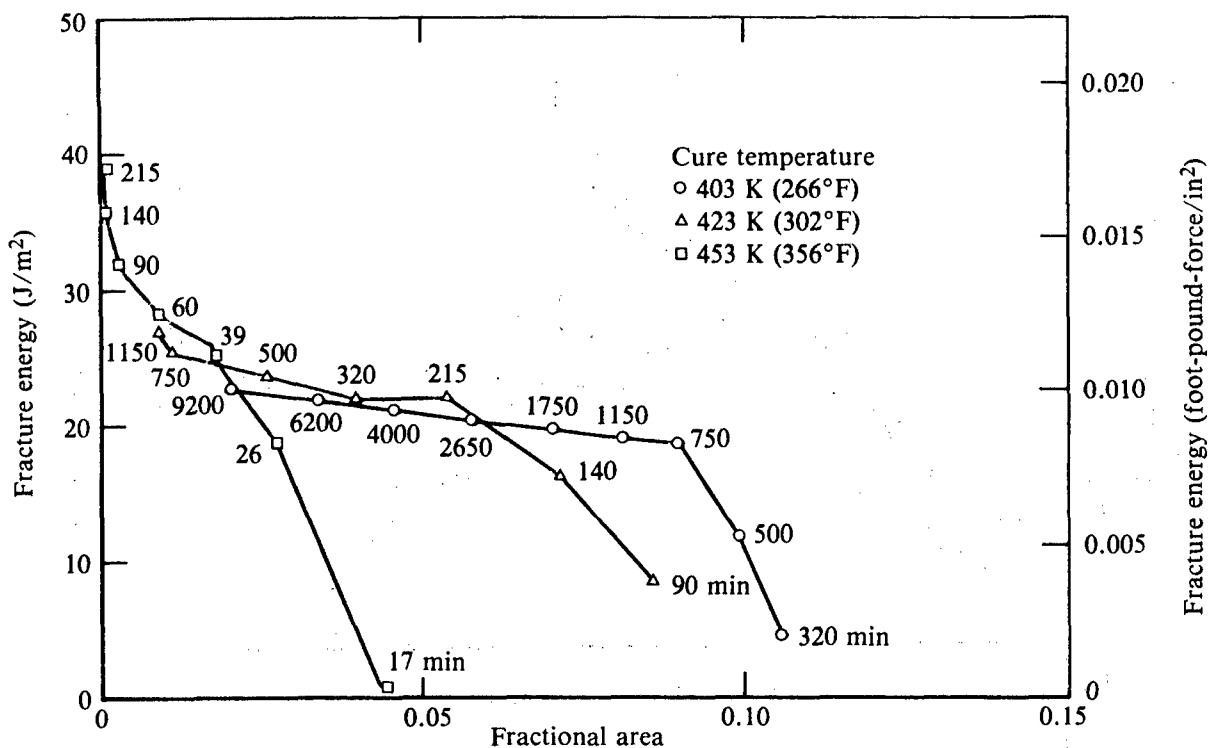


Figure 57. Fracture energy of ATS at 296 K (73°F) as a function of ^{13}C NMR parameter (area beneath acetylene peak) for three different isothermal cures. Cure times are indicated.

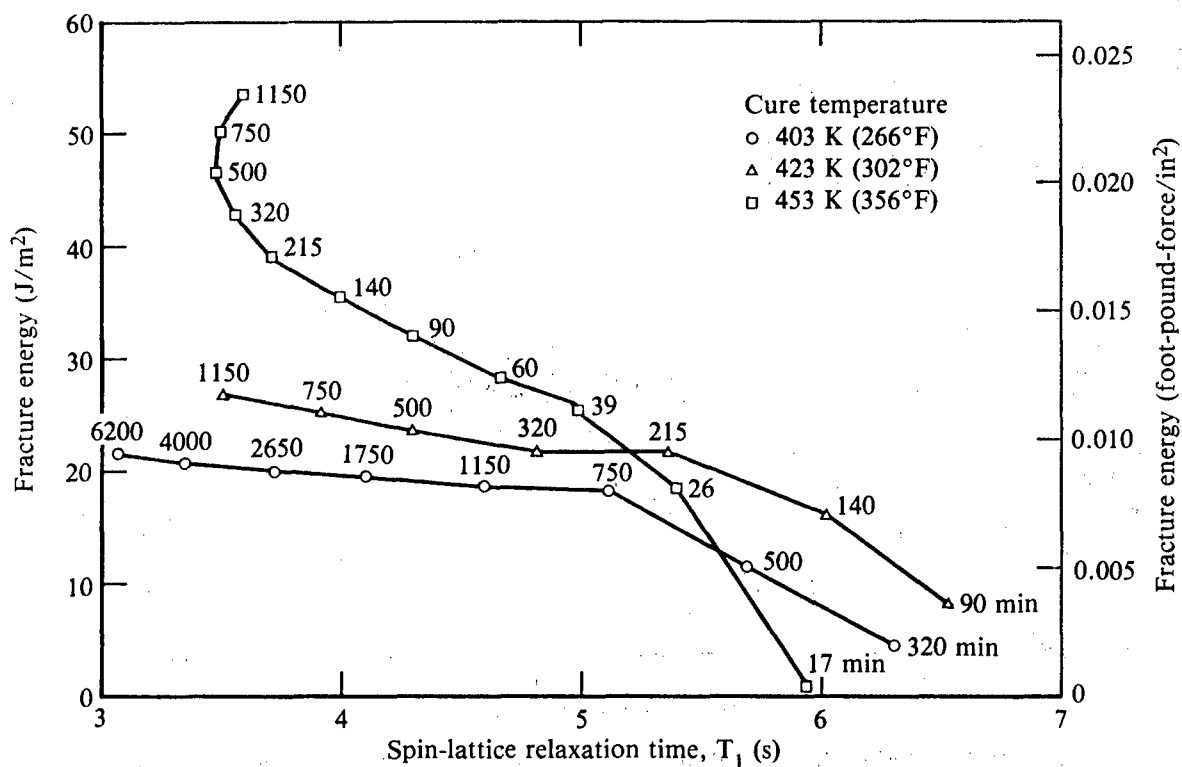


Figure 58. Fracture energy of ATS at 296 K (73°F) as a function of ^1H NMR parameter, (spin-lattice relaxation time) for three different isothermal cures. Cure times are indicated.

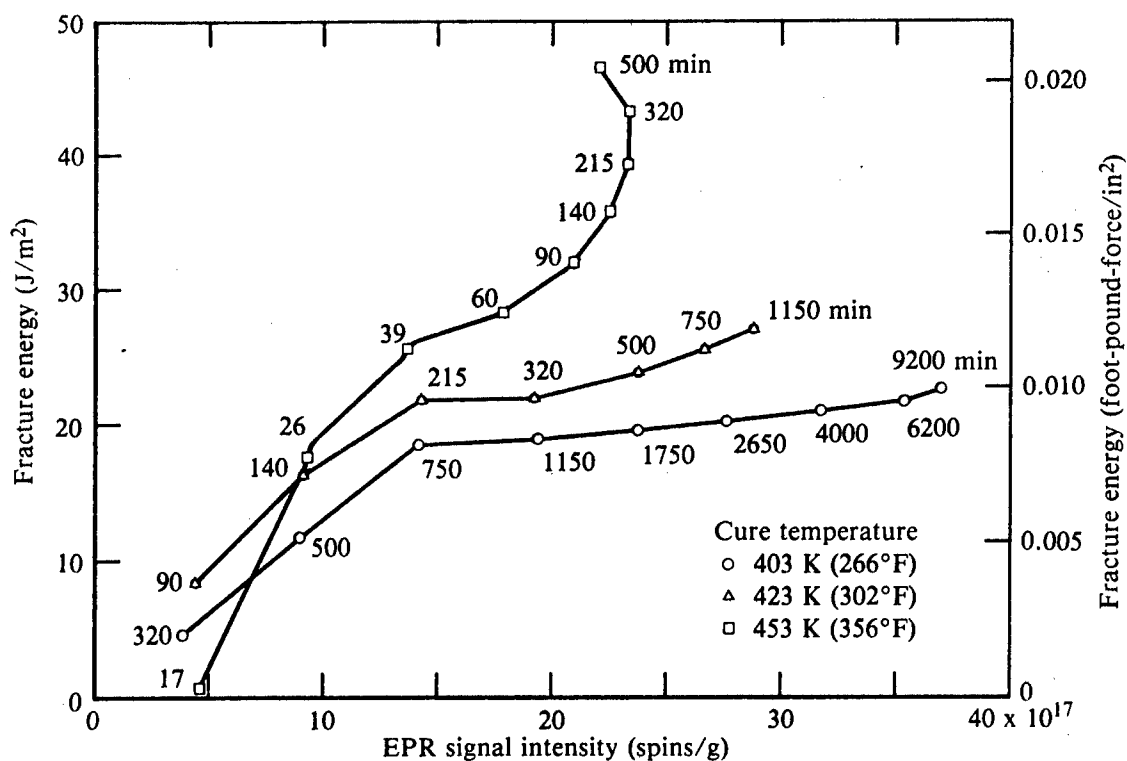


Figure 59. Fracture energy of ATS at 296 K (73°F) as a function of EPR parameter (signal intensity) for three different isothermal cures. Cure times are indicated.

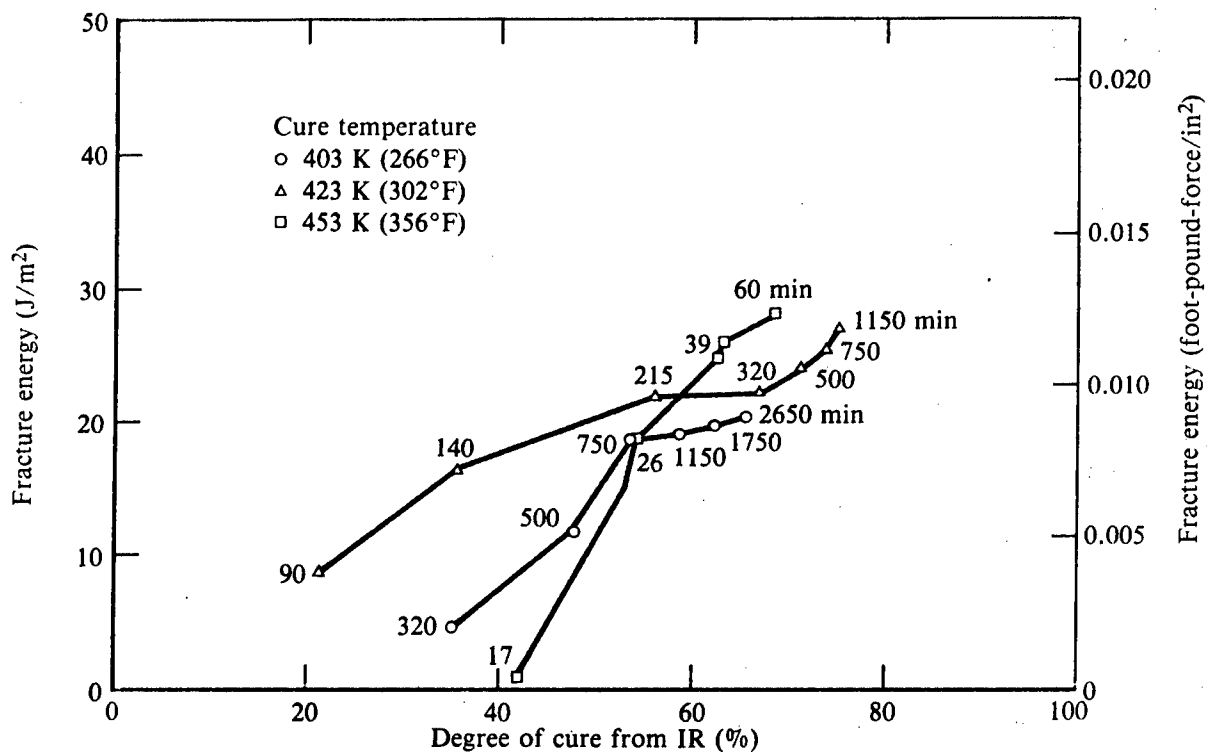


Figure 60. Fracture energy of ATS at 23°C as a function of IR parameter (degree of cure) for three different isothermal cures. Cure times are indicated.

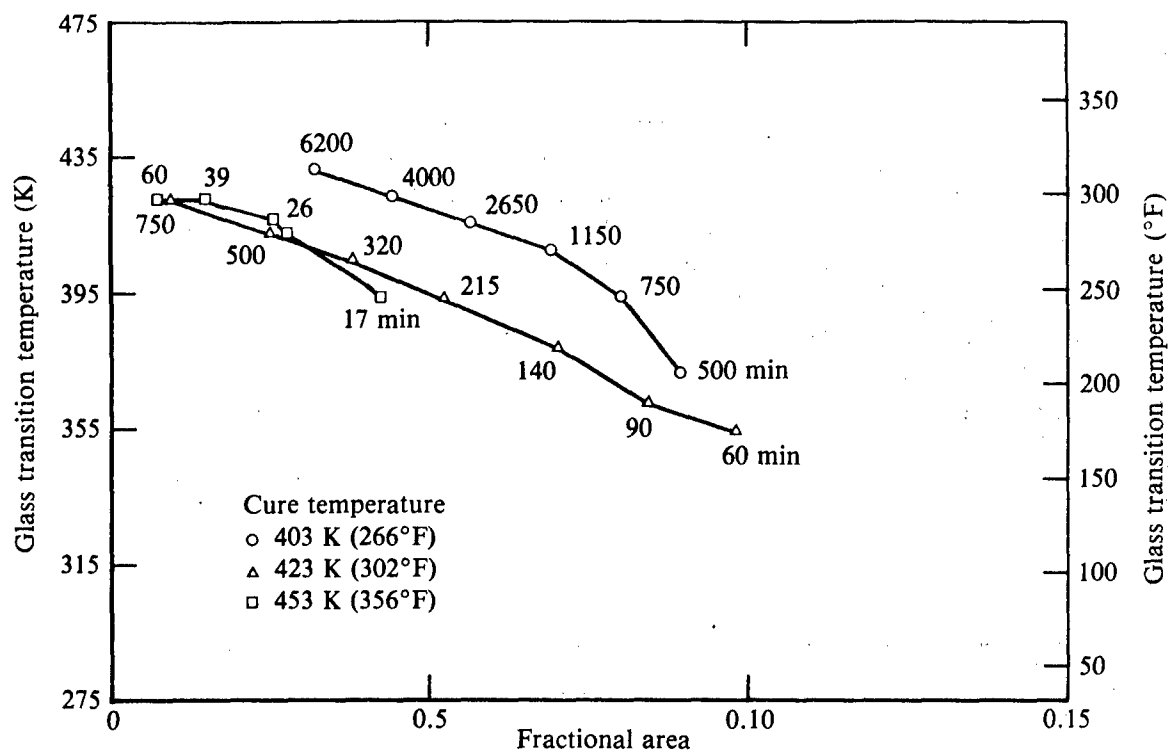


Figure 61. Glass transition temperature of ATS as a function of ^{13}C NMR parameter (area beneath acetylene peak) for three different isothermal cures. Cure times are indicated.

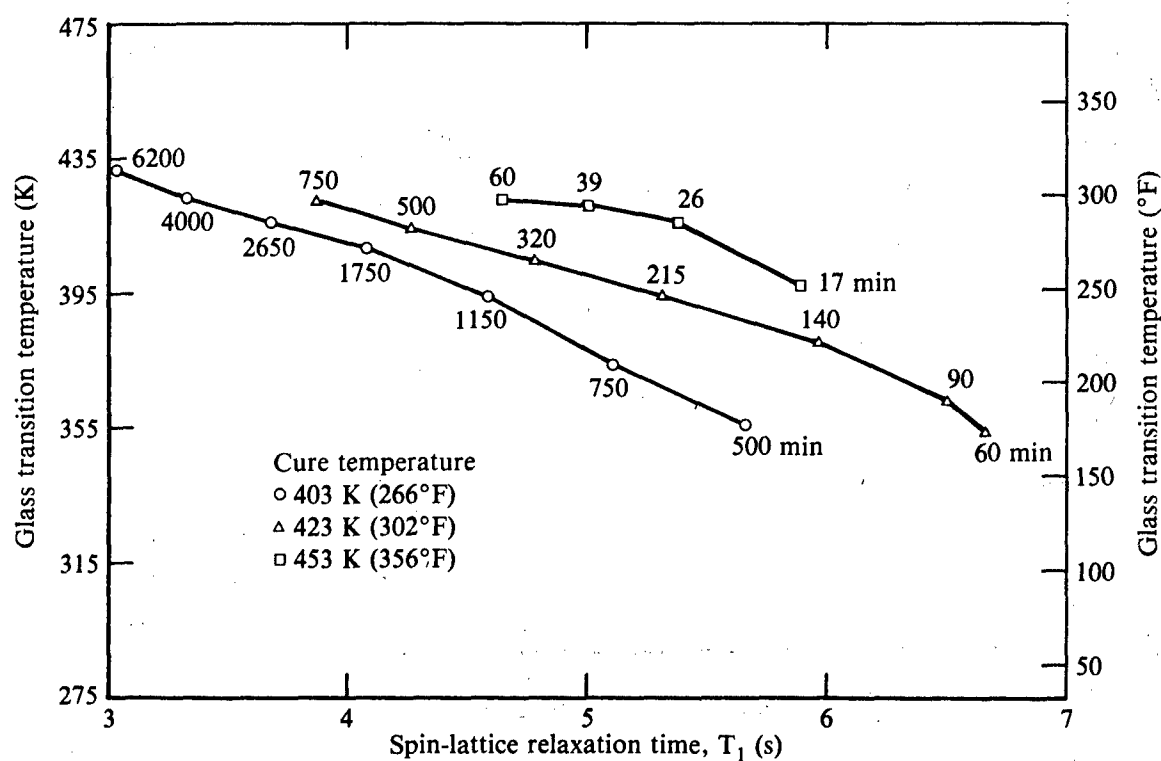


Figure 62. Glass transition temperature of ATS as a function of ^1H NMR parameter (spin-lattice relaxation time) for three different isothermal cures. Cure times are indicated.

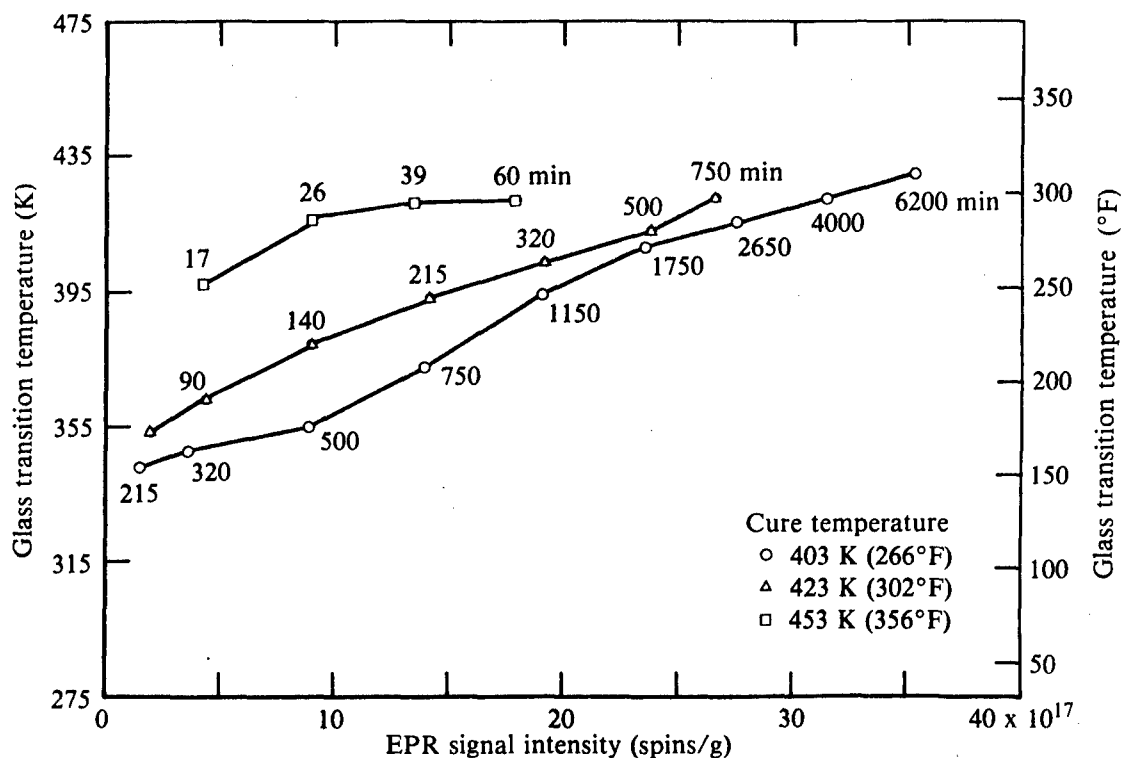


Figure 63. Glass transition temperature of ATS as a function of EPR parameter (signal intensity) for three different isothermal cures. Cure times are indicated.

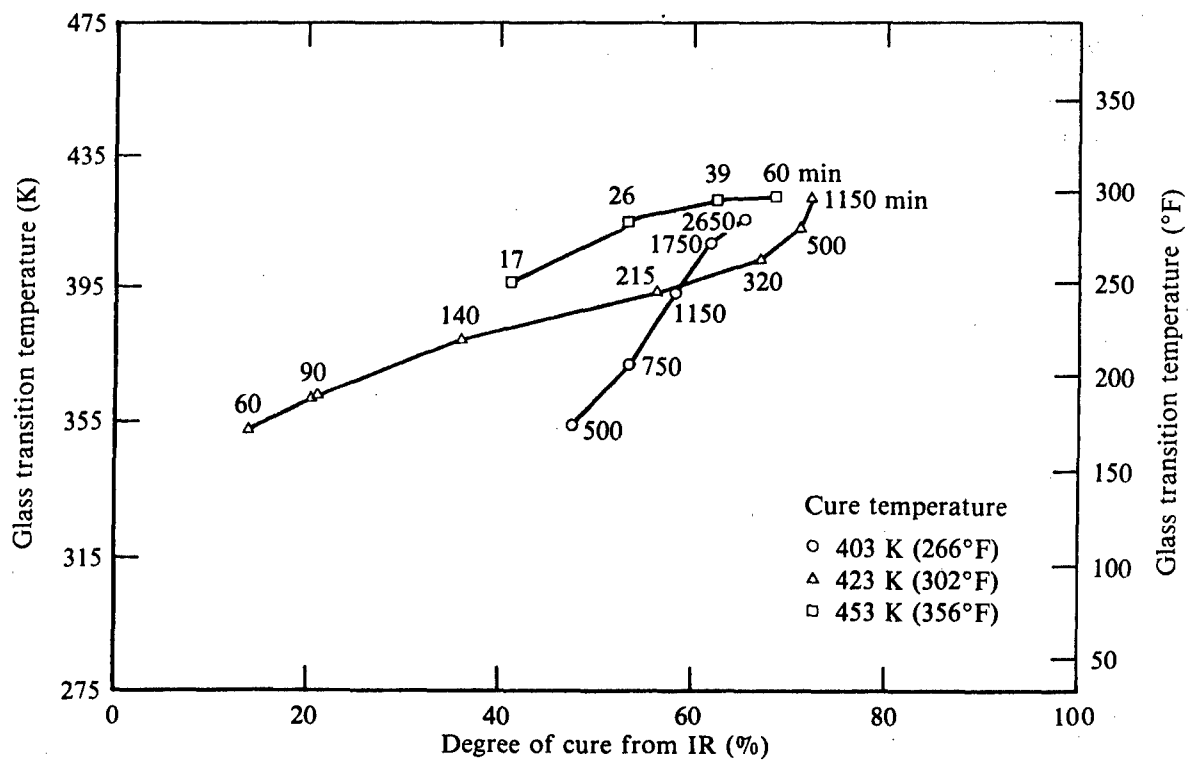


Figure 64. Glass transition temperature of ATS as a function of IR parameter (degree of cure) for three different isothermal cures. Cure times are indicated.

V. CONCLUSIONS

The major conclusions of this work are summarized below. Some of these conclusions have been published²²⁻²⁵ during the course of this contract.

- (1) The relative area beneath the acetylene resonance in the solid-state ^{13}C NMR spectra is a valid independent cure-state parameter.
- (2) The relative area beneath the acetylene IR bands constitutes a valid independent cure-state parameter.
- (3) The EPR signal intensity and the ^1H NMR spin-lattice relaxation time are both valid cure-state parameters, but they are not independent because they both measure free-radical concentration.
- (4) Because of the independence of these cure-state parameters, it is possible to uniquely determine the cure time and isothermal cure temperature of an unknown sample.
- (5) The EPR signal intensity and linewidth are sensitive to cure conditions, even after postcuring at elevated temperatures.
- (6) IR band ratios of nonreactive moieties did not provide unique information, nor are they sensitive to small changes in the cure state.
- (7) Cure-induced shifts represent a novel method for characterization of cure states, particularly applicable when the shifts occur in a band that originates from the vibrations of a main-chain backbone.
- (8) IR results show that postcure heating leads to almost total consumption of acetylene groups.
- (9) 3×10^{16} free radicals per gram exist in the uncured resin.
- (10) As many as 3.8×10^{18} free radicals per gram are generated during isothermal curing.
- (11) The radicals are delocalized in the cured ATS oligomers.

REFERENCES

1. R. F. Kovar, G. F. L. Ehlers, and F. E. Arnold, J. Polym. Sci., Chem. Ed. 15, 1081 (1977).
2. J. M. Pickard, E. G. Jones, and I. J. Goldfarb, Macromolecules 12, 895 (1979).
3. E. T. Sabourin, AFWAL-TR-80-4151, Oct 1980.
4. W. J. Price, Sample Handling Techniques, in Laboratory Methods in Infrared Spectroscopy, R. G. Miller and B. C. Stace eds. (Hayden and Son, London, 1972), p. 118.
5. J. Schaefer and E. O. Stejskal, J. Am. Chem. Soc. 98, 1031 (1976).
6. A. Pines, M. G. Gibby, and J. S. Waugh, J. Chem. Phys. 59, 569 (1973).
7. J. M. Pickard, S. C. Chattoraj, G. A. Loughran, and M. T. Ryan, Macromolecules 13, 1289 (1980).
8. M. D. Sefcik, E. O. Stejskal, R. A. McKay, and Jacob Schaefer, Macromolecules 12, 423 (1979).
9. M. Goldman and L. Shen, Phys. Rev. 144, 321 (1966).
10. R. A. Assink, Macromolecules 11, 1233 (1978).
11. A. C. Lind, Polymer Preprints 21 (2), 241 (1980).
12. A. C. Lind, Polymer Preprints 22 (2), 333 (1981).
13. C. L. Leung, ACS Org. Coat. Plast. Chem. Prep. 46, 322 (1982).
14. Unpublished data, McDonnell Douglas Research Laboratories, St. Louis, MO.
15. C. C. Kuo and C. Y.-C. Lee, AFWAL-TR-82-4037 (1982).
16. D. Bloor, R. J. Kennedy, and D. N. Batchelder, J. Poly. Sci., Phys. Ed. 17, 1355 (1979).
17. B. A. Reinhardt and F. E. Arnold, Polymer Preprints 20 (1), 211 (1979).
18. R. L. Levy and R. P. Wool, Polymer Preprints 20 (2), 239 (1980).
19. R. L. Levy, Polymer Preprints 21 (2), 263 (1980).
20. C. Leung, Acetylene Terminated Resin Mechanical Characterization, Interim Technical Report No. 3, AFWAL/ML Contract F33615-80-C-5142, June 1982.
21. C. Leung, Acetylene Terminated Resin Mechanical Characterization, Interim Technical Report No. 2, AFWAL/ML Contract F33615-80-C-5142, January 1982.
22. A. C. Lind and C. Y.-C. Lee, Polymer Preprints 23 (2), 183 (1982).
23. R. L. Levy and C. Y.-C. Lee, Polymer Preprints 23 (2), 181 (1982).
24. T. C. Sandreczki and C. Y.-C. Lee, Polymer Preprints 23 (2), 185 (1982).
25. R. L. Levy, A. C. Lind, and T. C. Sandreczki, Proceedings of 15th Nat. SAMPE Conf. 15, 21 (1983).